学　位　論　文

Studies of roles of *NLRC5* expression in cancers on antigen presentation and host anti-cancer immunity

(癌の抗原提示とホストの抗癌免疫における *NLRC5* 発現の役割の研究)

２０２４年３月

北海道大学

Sun Xin（スン　シン）

学　位　論　文

Studies of roles of *NLRC5* expression in cancers on host anti-cancer immunity and tumor growth

(癌の抗原提示とホストの抗癌免疫における *NLRC5* 発現の役割の研究)

２０２４年３月

北海道大学

Sun Xin（スン　シン）

Table of Contents

List of Publications and Presentations

This study is not yet published on journal articles.

Part of this study is presented in the following conference.

1. Xin Sun, Toshiyuki Watanabe, Ning An, Hideo Yagita, Koichi Kobayashi. *NLRC5* confers to immune response upon cancer ICI therapy and serves as a prediction biomarker. The 51st Annual Meeting of the Japanese Society for Immunology; 2022, Kumamoto
2. Xin Sun, Toshiyuki Watanabe, Ning An, Hideo Yagita, Koichi Kobayashi. *NLRC5* confers to immune response upon cancer ICI therapy and serves as a prediction biomarker. The 8th Hokkaido University Cross-Departmental Symposium; 2022, Hokkaido

Summary

【**Background and Objectives**】NLRC5 (NLR Family CARD Domain Containing 5), also known as CITA (Class I transactivator), is identified as transcription activator for MHC class I and related genes. CD8+ T cells recognize antigens presented by MHC class I and consist of a critical part of anti-cancer immunity. Although a data mining study has identified *NLRC5* as a target for immune evasion in cancer, its role in regulating cancer antigen presentation and anti-cancer immunity is not well experimentally characterized. In this study, we investigated the role of *NLRC5* expression in cancer in modulating antigen presentation, host anti-cancer immunity, and efficacy of immune checkpoint blockade (ICB) treatment (anti-PD-1 treatment). We sought to enhance our understanding of the interactions involving NLRC5, cancer, and the immune system, which eventually aimed to help the development of novel cancer therapy.

【**Materials and methods**】To investigate the roles of NLRC5 in host anti-cancer immunity, we induced genomic deletion of *Nlrc5* in mouse melanoma B16F10 and mouse breast cancer E0771 cell lines. Furthermore, to investigate whether *NLRC5* is a viable target for development of novel immunotherapy, we developed a CRISPR/dCas9-TET1cd based targeted demethylation and activation (TDMa) system to enhance *Nlrc5/NLRC5* expression in mouse melanoma B16F10 and human breast cancer MCF7 cell lines. QRT-PCR and RNA-Seq were performed to determine the mRNA expression levels of MHC class I and related genes after knockout of *Nlrc5* or *Nlrc5/NLRC5* activation. Bisulfite sequencing was performed to determine *Nlrc5* promoter methylation levels. Flow cytometry were performed to determine cancer cell immunogenicity. Subsequently, mouse cell lines were subcutaneously implanted *in vivo* to observe tumor growth. Flow cytometry and immunohistochemistry were performed using *in vivo* tumors to characterize tumor infiltrating lymphocytes (TILs) and tumor cells.

【**Results**】We found that genomic deletion of *Nlrc5* specifically downregulated MHC class I and related genes expression levels in B16F10 and E0771 cells. *Nlrc5* deletion promoted E0771 tumor growth *in vivo* by inhibiting CD8+ T cell infiltration and activation through MHC class I. On the other hand, due to its low baseline MHC class I expression levels, *Nlrc5* deletion did not affect B16F10 tumor growth without stimulation. However, we found that *Nlrc5* is required for response to anti-PD-1 therapy in B16F10 tumor transplantation model. Based on these results, we performed transcriptome screening and generated the optimal prediction model for prediction of

response to anti-PD-1 therapy in melanoma. Furthermore, we induced targeted demethylation and activation of *Nlrc5* promoter in B16F10 and MCF7 cell lines using CRISPR/dCas9 based system (Targeted demethylation (TDM) and Targeted demethylation and activation (TDMa) system). Although targeted demethylation of *Nlrc5* promoter (TDM system) alone induced only modest augmentation of MHC class I expression and tumor immunogenicity, we found that the expression of MHC class I is robustly augmented by combination of targeted demethylation activation of *Nlrc5* (TDMa system). RNA-Seq analysis showed that TDMa system robustly induced specific augmentation of *Nlrc5* and dependent MHC class I expression. OT-I co-culture analysis showed that the immunogenicity of B16F10 were augmented by targeted demethylation and activation of *Nlrc5*. *In vivo* implantation of B16F10-TDMa cells showed that tumor growth is impaired by targeted demethylation and activation of *Nlrc5* in C57BL/6 mice. Adaptive immune system is required for tumor suppression *in vivo* as we did not observe significantly different tumor growth when TDMa cells were implanted in NUDE mice. CD8+ T cell infiltration and activation was augmented by targeted demethylation and activation of *Nlrc5* in B16F10 tumors, but not in CD4+ T cells. Moreover, immunohistochemistry analysis showed that targeted demethylation and activation of *Nlrc5* in B16F10 not only increased the number of TILs, but it also promoted concentration of CD8+ T cells into the tumor center. Furthermore, we showed that targeted demethylation and activation of *Nlrc5* sensitized the response to anti-PD-1 treatment in B16F10. Similarly, we showed that CD8+ T cell infiltration and activation were specifically enhanced by anti-PD-1 treatment, but not in CD4+ T cell.

【**Discussion**】The expression levels of NLRC5 is abundant in cells related with immune system, therefore, most of the investigations were focused its role as MHC class I transactivator in the immune system. The roles of NLRC5 as MHC class I transactivator in cancer cells are largely unexplored. MHC class I is of high priority as target for cancer treatment and our research addressed a key molecule to regulate its expression. Here, using both genomic deletion, and targeted demethylation and activation approach, we systemically illustrated the role of *Nlrc5* in modulating immunogenicity through MHC class I and host anti-cancer immunity in melanoma and breast cancer. For genomic deletion of *Nlrc5*, consistent with the previous investigations using *Nlrc5* knockout mice, we found that *Nlrc5* deletion downregulated MHC class I expression levels with or without mIFN-γ stimulation. To our knowledge, our study is the first to characterize the effect of *Nlrc5* in MHC class I antigen presentation pathway in cancer. On the contrary, we also induced targeted demethylation and activation of *Nlrc5/NLRC5* in B16F10 and MCF7 using the TDMa system. Our results further confirmed that activation of *Nlrc5* enhanced the expression

of MHC class I and host anti-cancer immunity. In addition, we found that targeted demethylation and activation of *Nlrc5* promoted concentration of CD8+ T cell into the tumor center. Previous studies observed that aggravation of CD8+ T cell into tumor center is correlated with a better prognosis, however the mechanism is left unexplored. We identified that expression of surface MHC class I in cancer is one of the factors that promote CD8+ T cell infiltration into tumor center. Furthermore, we found that targeted demethylation and activation of *Nlrc5* sensitized response of B16F10 to anti-PD-1 treatment. Previous studies have identified that surface MHC class I levels and *NLRC5* expression levels correlates with a good response to immune checkpoint blockade therapy. However, the underlying mechanisms are not well studied. Our results indicate that CD8+ T cell mediated anti-cancer immunity were exclusively and synergistically activated by anti-PD-1 treatment and targeted demethylation and activation of *Nlrc5*. These results highlighted *Nlrc5* as a therapeutic target to synergistically enhance the efficacy of anti-PD-1 treatment.

【Conclusion】 In conclusion, our research deepened our understanding of the role of *Nlrc5* in host anti-cancer immunity. Our strategy to induce and genotyping genomic deletion is solid and can be applied to other genes and cell lines. We show that the CRISPR/dCas9 mediated targeted demethylation and activation strategy of *Nlrc5* is a viable and novel immunotherapy approach to enhance cancer immunogenicity. For future study, optimization of delivery system to effectively induce targeted demethylation and activation *in vivo* could contribute to development of novel immunotherapy.

List of Abbreviations

- NLRC5: NLR Family CARD Domain Containing 5.
- NLR: NOD like receptor.
- NOD: Nucleotide oligomerization domain.
- TDM: Targeted demethylation.
- TDMa: Targeted demethylation and activation.
- CITA: Class I transactivator.
- IFN-γ: Interferon gamma.
- QRT-PCR: Quantitative real-time PCR.
- FACS: Fluorescence-activated cell sorting.
- MHC: Major histocompatibility complex.
- ICB: Immune checkpoint blockade.
- PD-1: Programmed death 1.
- CRISPR: Clustered regularly interspaced short palindromic repeats.
- SgRNA: Single guide RNA.
- HIRA: Histone cell cycle regulator
- TET1cd: Tet methylcytosine dioxygenase 1 catalytic domain.
- HSF1: Heat shock factor 1.
- VP64: Herpes simplex viral protein 16.
- TCGA: The cancer genome atlas.
- SKCM: Skin cutaneous melanoma.
- BRCA: Breast invasive carcinoma.

Introduction

Antigen presentation through MHC class I is critical for recognition and eradication of malignant tumors by host CD8+ T cell mediated anti-cancer immunity. MHC class I antigen presentation pathway is composed of both MHC class I and other key elements, including proteasome, transporter, and MHC class I subunit B2M. Genes encoding these components are mostly transcriptionally co-activated by CITA (MHC class I transactivator), also known as NLRC5. NLRC5 associate with multiple transcription factors on MHC class I promoters to form the MHC class I enhanceosome complex, which transactivates the expression of MHC class I and related genes. Therefore, NLRC5 is important to maintain MHC class I expression. Numerous studies utilizing *Nlrc5* knockout mouse have well demonstrated that Nlrc5 functions as CITA in normal tissues (Biswas *et al.*, 2012, Robbins *et al.*, 2012, Staehli *et al.*, 2012, Yao *et al.*, 2012), however, the role of *Nlrc5* in cancer cells are not well studied. Here, we utilized loss of function and gain of function approach to elucidate the function of *Nlrc5* in cancer.

Title of Chapter 1: Elucidating the role of *Nlrc5* in cancer by genomic deletion of *Nlrc5*.

Chapter 1: Introduction

Previous studies have shown that overexpression of *NLRC5* in cancer cell lines increased MHC class I levels and inhibited tumor growth by activating CD8+ T cell-dependent host anti-cancer immunity (Rodriguez *et al.*, 2016, Zhan *et al.*, 2022). But the role of *NLRC5* for immune evasion in cancer is poorly studied.

The expression of *NLRC5* is silenced by mechanisms such as promoter hypermethylation in multiple types of human cancers (Yoshihama *et al.*, 2016). *NLRC5* silencing is correlated with reduced cytotoxic immune signatures and poor prognosis (Yoshihama *et al.*, 2016), however, the specific mechanisms underlying host anti-cancer immunity suppression following *NLRC5* silencing remains unknown. Therefore, it is necessary to investigate whether *NLRC5* silencing induce cancer immune evasion through downregulation of MHC class I antigen presentation in cancer and host CD8+ T cell mediated anti-cancer immunity.

Immune checkpoint blockade (ICB) therapy, including anti-PD-1 therapy, has emerged as a promising strategy for treating patients with various cancers (Pardoll, 2012, Sharma *et al.*, 2015), but not all patients respond to ICB therapy (Postow *et al.*, 2015, Swart *et al.*, 2016). Defects in MHC class I antigen processing and presentation pathway in cancer cells has been identified as one of the factors that correlate with resistance to ICB therapy (Liu *et al.*, 2019). Given that NLRC5 transactivates the expression MHC class I and related genes, *NLRC5* silencing could contribute to resistance to ICB therapy. Furthermore, *NLRC5* expression has been identified as a biomarker for predicting patient responses and combining expression level of *NLRC5* and other genes has shown to increase prediction efficacy (Yoshihama *et al.*, 2021). Transcriptome screening for the best partner marker of *NLRC5* and utilization of larger cohorts for prediction model establishment and validation by independent external cohorts could provide a widely applicable prediction model that may contribute to real-world applications.

In this study, to investigate the effect of *Nlrc5* silencing MHC class I antigen presentation pathway in cancer and anti-cancer immunity, we induced genomic deletion of *Nlrc5* in E0771 and B16F10 cell lines. *Nlrc5* deletion suppressed the expression of MHC class I and related genes and CD8+ T cell-mediated anti-cancer immunity. Interestingly, response to anti-PD-1 treatment was diminished in B16F10 model following deletion of *Nlrc5*. Furthermore, the expression of *NLRC5* is enriched in melanoma patients who responded to anti-PD-1 therapy, therefore, we performed transcriptome screening and identified combination of *NLRC5* + *HIRA* generated response prediction models of the highest prediction accuracy by validation internally

and externally. Our results showed that *NLRC5* silencing cause immune evasion from CD8+ T cell mediated anti-cancer immunity, which is associated with reduced expression levels of MHC class I and related genes. Furthermore, our results revealed important role of *NLRC5* in controlling and predicting response to anti-PD-1 therapy.

Chapter 1: Methods

Cells

E0771 cell line was purchased from American Type Culture Collection (ATCC, Manassas, VA, USA, cat. CRL-3461, RRID:CVCL_GR23). B16F10 cell was purchased from RIKEN Bio BRC (Tsukuba, Japan, cat. RCB2630, RRID:CVCL_0159). B16F10 and E0771 cell line were maintained in Dulbecco's modified Eagle's medium (DMEM, Nacalai, Kyoto, Japan, cat. 08458-16) supplemented with 10% fetal bovine serum (FBS; Nichirei, Kyoto, Japan, cat. 175012) at 37 °C with 5% CO_2 in a humidified incubator. Cells were used for no more than 30 passages and no longer than 3 months. Cells were tested negative for Mycoplasma by PCR, once a year (Salio *et al.*, 2000).

Nlrc5 +/− and *Nlrc5* −/− E0771 cells, and *Nlrc5* −/− B16F10 cells were generated by CRISPR/Cas9. Briefly, paired single guide RNAs (sgRNAs) insert were amplified by PCR using pScaffold-H1 donor (Addgene, Watertown, NY, USA, #118152) as a template and cloned into px458-GFP (Addgene, #48138), as described previously (Ran *et al.*, 2013, Miguel-Escalada *et al.*, 2019). The paired sgRNAs were designed to target two introns surrounding (at 5′ and 3′ ends of) *Nlrc5* exon that encodes NATCH domain. Subsequently, the construct was transfected into B16F10 and E0771 cells. GFP+ cells were sorted by FACSAria III (BD, San Jose, CA, USA) to acquire single cell colonies with successful transfection. *Nlrc5* +/− B16F10 cells and *Nlrc5* +/− E0771 cells were identified by genotyping and Sanger sequencing. The sequence of sgRNA used in this study is described in Table 1.

Next, to generate *Nlrc5* −/− B16F10 cells and *Nlrc5* −/− E0771 cells, *Nlrc5* +/− B16F10 cells and *Nlrc5* +/− E0771 cells were transfected with px458-GFP that express a 2nd pair of sgRNAs, which target the surrounding (5′ and 3′ ends of) region that encodes NLRC5 NATCH domain at inner location compared with 1st pair of sgRNAs. Genotypes of single cell colonies were screened by PCR using specific genotyping primers and the genomic DNA of corresponding single cell colonies as templates. The genotype of corresponding single cell clones was determined by size of PCR product on agarose gel. Successful *Nlrc5* deletion was verified by Sanger sequencing of PCR product. All experiments involving recombinant DNA were approved by Hokkaido University Safety Committee on Genetic Recombination Experiments (Approval number: 2018-037).

Mice

Wild-type C57BL/6JJcl (RRID:MGI:3055581) mice were purchased from CLEA Japan, Inc. (Tokyo, Japan), bred, and housed in Institution for Animal Experimentation

at Hokkaido University Graduate School of Medicine under specific pathogen free conditions. Male and female mice aged 7–10 weeks were used in subsequent experiments. All animal experiments were conducted according to guidelines of Hokkaido University Animal Experiment Implementation Manual and approved by Institutional Animal Care and Use Committee of Hokkaido University Graduate School of Medicine (approval no.: 19-0134).

Orthotopic E0771 breast cancer model

Approximately 1×10^6 *Nlrc5* +/− E0771 and *Nlrc5* −/− E0771 cells in 100 μL phosphate buffered saline (PBS; Nacalai, Kyoto, Japan, 14249-24) were subcutaneously injected into right and left fourth mammary fat pads of female C57BL/6J mice. Tumor size was measured every other day since day 5 using a digital caliper. Tumor volume was estimated using following formula: Tumor Volume (mm3) = length × width × width /2 (Faustino-Rocha *et al.*, 2013). Mice were euthanized on day 19 and resected tumors were subjected to flow cytometry analysis.

Subcutaneous B16F10 melanoma model

C57BL/6J mice were subcutaneously injected with approximately 5×10^5 *Nlrc5* +/+ B16F10 or *Nlrc5* −/− B16F10 cells in 100 μL PBS into left lateral flank. Subsequently, mice with *Nlrc5* +/+ B16F10 or *Nlrc5* −/− B16F10 were randomly divided into PBS (control) and PD-1 groups. 250 μg/100 μL of anti-PD-1 antibody (RMP1-14), generated in our laboratory as previously described (Yamazaki *et al.*, 2005), was intraperitoneally injected into the mice in PD-1 groups every other day since day 5, for total 5 times. The same volume of PBS was injected into PBS groups. Tumor size was measured daily from day 5 using a digital caliper, and tumor volume was estimated in the same manner as E0771 tumors. Mice were euthanized on day 16 and the resected tumors were subjected to flow cytometry analysis.

qRT-PCR

To quantify mRNA levels, approximate 1×10^5 cells were plated on one well in 12-well plate on day 0. From day 1, cells were stimulated with 20 ng/mL of mouse interferon-γ (IFN-γ; BioLegend, San Diego, CA, USA, cat. 575302) for 24 hours. Subsequently, total RNA was isolated from cells using Sepasol (Nacalai, Kyoto, Japan, cat. 09379-55) according to manufacturer's instruction. cDNA was synthesized using ReverTra Ace qPCR RT Master Mix (Toyobo, Osaka, Japan, cat. FSQ-301), and then quantitative PCR was performed on StepOne RT-qPCR instrument (Thermo Fisher Scientific, Waltham, MA, USA) with THUNDERBIRD SYBR qPCR Mix reagent

(Toyobo, Osaka, Japan, cat. QPS-201). Mouse *Nlrc5, H2-kb, Lmp2, B2m, Ciita*, and *Gapdh* were amplified using specific primers. *Gapdh* was used as internal reference gene for between-sample comparisons by ΔCt method. The sequence of primers used for qRT-PCR in this study is described in Table 1.

Flow cytometry

To assess the effect of *Nlrc5* deletion on cell surface MHC class I levels, approximate 5×10^4 cells were plated on one well in 12-well plate (day 0). From day 1, cells were stimulated with 20 ng/mL IFN-γ for 48 hours. On day 3, cells were harvested, resuspended in FACS buffer (2% FBS in PBS), and then stained with 100μL 1:100 FACS buffer diluted antibodies (all from BioLegend): FITC H2-K^b/D^b (cat. 114605, RRID:AB_313596), and PE PD-L1 (cat. 124308, RRID:AB_2073556) for 30 min on ice.

To characterize tumor-infiltrating lymphocytes (TILs), tumors were fragmented by scissors and were further dissociated by grinding with slide glasses. Single-cell suspension was prepared by filtering through a 48 μm filter net (SANSYO, Tokyo, Japan, cat. 91-1189), followed by red blood cell lysis for 5 min on ice in 1 mL ammonium-chloride-potassium (ACK) lysis buffer (Thermo Fisher Scientific, Waltham, USA, cat. A1049201).

To distinguish dead cells, 3×10^6 isolated tumor cells were stained by 100 μL Zombie Violet Fixable Viability dye (1:1000 dilution in PBS) (BioLegend, cat. 423113) at 25℃ for 15 min. Subsequently, tumor cells were aliquoted into two tubes for subsequent analysis of TILs (2×10^6) or tumor cells (1×10^6).

To characterize TILs, Zombie dye-stained cells were further stained with the following antibodies (all from BioLegend, 1:100 dilution): APC-Cy7 CD45.2 (cat. 109824, RRID:AB_830789), FITC CD4 (cat. 100405, RRID:AB_312690), APC CD8a (cat. 100712, RRID:AB_312751), and PE IFN-γ (cat. 505808, RRID:AB_315402). Cells were incubated with antibodies for surface markers in 100 μL FACS buffer on ice for 30 min. Subsequently, cells were fixed by incubating with 4% PFA for 15 min on ice, and then permeabilized with 1× intracellular staining permeabilization wash buffer (BioLegend, San Diego, USA, cat. 420801) according to manufacturer's instructions. Subsequently, cells were incubated with anti-IFN-γ antibody in 100 μL 1× intracellular staining buffer for 30 min on ice.

To study MHC class I levels in tumor cells *in vivo*, 1×10^6 Zombie dye-stained cells were further stained with APC-Cy7 CD45.2, FITC H-2K^b/D^b, and PE PD-L1, in the same manner as TILs surface marker staining.

Stained cells were detected using a FACSCanto II (BD, Becton, USA). Collected

data were analyzed using FlowJo v10.6.2. (BD, Becton, USA).

RNA-Seq data acquisition and processing

RNA-seq transcriptome profile of before anti-PD-1 therapy from studies by Gide et al. (*n*=73) (Gide *et al.*, 2019a), Hugo et al. (*n*=28) (Hugo *et al.*, 2016), and Riaz et al. (*n*=25) (Riaz *et al.*, 2017) were collected from Sequence Read Archive (Leinonen *et al.*, 2011) (accession numbers ERP105482, ERP105482, and SRP094781). RNA-seq gene expression matrix from study by TCGA SKCM (The Cancer Genome Atlas, skin cutaneous melanoma) (*n*=473) (Cancer Genome Atlas, 2015) or Miao et al. (*n*=16) (Miao *et al.*, 2018) was obtained from UCSC XENA (Goldman *et al.*, 2020) or TIDE (Fu *et al.*, 2020).

For FastQ files obtained from Gide et al. (Gide *et al.*, 2019a), Hugo et al. (Hugo *et al.*, 2016), and Riaz et al. (Riaz *et al.*, 2017), paired-end reads were examined to trim low-quality bases and adaptor sequences using fastp (Chen *et al.*, 2018). Filtered reads were mapped to GRCh38 cDNA using Salmon (Patro *et al.*, 2017) to generate transcription-level estimates. A gene-level count matrix was generated using tximport (Soneson *et al.*, 2015). For TCGA SKCM data, gene-level count matrix was downloaded from UCSC XENA (Cancer Genome Atlas, 2015, Goldman *et al.*, 2020). Gene-level count matrix was normalized for between-sample comparisons using DESeq2 (Love *et al.*, 2014). Normalized count matrix was $\log_2$(count+1) transformed and Z-score matrix for each dataset was generated by formular Z-score = (Observed expression of target gene – Mean expression of target gene) / Standard deviation of target gene expression. Z-score normalized data was used in establishment and validation of Random Forest (RF) prediction model, visualization, gene set enrichment analysis (GSEA), and survival analysis (Tin Kam, 1995, Subramanian *et al.*, 2005). For gene expression data from Miao et al. (Miao *et al.*, 2018), where only transcript per million (TPM) was accessible, expression levels were log2(TPM+1) transformed, and Z-scores were calculated and used for validation, visualization, and GSEA.

Gene set enrichment analysis

GSEA was used to assess differential expression of NLRC5 dependent MHC class I gene set between response and non-response groups to anti-PD-1 therapy. The tested gene set of NLRC5 and MHC class I antigen presentation pathways was based on knowledge of related literatures (Yoshihama *et al.*, 2021).

Anti-PD-1 therapy response prediction model establishment and validation

RF approach from caret package was used to identify gene with the top prediction

performance in combination with NLRC5 (Kuhn, 2015). Prediction models in this study were generated using data from Gide et al. (Gide *et al.*, 2019b). Genes with a mean DESeq2 normalized count of >1 were included in screening process. This screening process was repeated 5 times and mean 5-fold cross-validated accuracy for models generated from each combination was calculated. Prediction models with a mean prediction accuracy >0.7 were selected as candidate to be validated by Hugo et al. cohort (Hugo *et al.*, 2016). Validation was repeated for 5 times, and the candidate with the highest mean accuracy in validation step was identified as ideal prediction model. A clear cell renal cell carcinoma (ccRCC) cohort from Miao et al. (Miao *et al.*, 2018) was used as an additional validation step to investigate whether identified model can be applied to ccRCC.

Patient response data

The clinical response data of patients that received anti-PD-1 therapy were classified based on clinical information provided by TIDE (Fu *et al.*, 2020). Patients without clear response/nonresponse information were classified using RECIST categories, with "PR", "CR" indicating "response", and "SD", "PD" indicating "nonresponse".

Survival analysis

All overall survival (OS) time data of melanoma patients were obtained from TIDE (Fu *et al.*, 2020). High group was defined as patients who had a high gene expression compared with mean (Z-score > 0), and remaining patients were defined as low group (Z-score ≤ 0). To normalize differences between total follow up time within each cohort, patients whose OS time exceeding 1825 days (5 years) were removed from survival analysis after definition of high/low groups. Hazard ratio was calculated using low/high. Two patients with either missing or duplicated survival data in Hugo et al. were excluded from survival analysis (Hugo *et al.*, 2016).

Pathway enrichment map

Correlations between HIRA expression and pathway enrichment were analyzed using the Z-score normalized transcriptome matrix for TCGA SKCM cohort (Cancer Genome Atlas, 2015). Patients expressing HIRA level above mean level (Z-score > 0) were included in "high" group while remaining (Z-score ≤ 0) were included in "low" group. Differentially expressed genes were evaluated using DESeq2, and a pathway enrichment map was generated using clusterProfiler (Yu *et al.*, 2012).

Statistical analysis

For *in vivo* tumor growth analysis, significance was analyzed using 2-way ANOVA test. For survival analysis, significance was analyzed using log-rank and Wilcoxon test. For others, significance was analyzed using two-tailed unpaired Student's t-test. A *p*-value of less than 0.05 was regarded as statistically significant. Error bars represents mean values ±SEM. All analyses were performed using GraphPad Prism software (v9.3.1).

Data availability statement

Data analyzed in this study were obtained from Sequence Read Archive at https://www.ncbi.nlm.nih.gov/sra (ERP105482, SRP070710, and SRP094781) or from UNSC XENA at https://xenabrowser.net/datapages/ or at Miao et al. or from TIDE at http://tide.dfci.harvard.edu/ (Miao *et al.*, 2018, Fu *et al.*, 2020, Goldman *et al.*, 2020). Code and processed transcriptome and clinical data generated in this study are publicly available at Github.

Table 1 Sequence of PCR primers and sgRNAs used in Chapter 1

Names	Purpose	Sequence (5'-3', without NGG)
*Nlrc5*_Fw	qRT-PCR; Mouse	CTTCCCGCCTCTCCTTCCACAAT
*Nlrc5*_Re	qRT-PCR; Mouse	CTCCACCTGCCCACATCCTACCA
*H2-K^b*_Fw	qRT-PCR; Mouse	GGCAATGAGCAGAGTTTCCGAG
*H2-K^b*_Re	qRT-PCR; Mouse	CCACTTCACAGCCAGAGATCAC
*Lmp2*_Fw	qRT-PCR; Mouse	CATGAACCGAGATGGCTCTAGT
*Lmp2*_Re	qRT-PCR; Mouse	TCATCGTAGAATTTTGGCAGCTC
*Tap1*_Fw	qRT-PCR; Mouse	GACTCCTTGCTCTCCACTCAGT
*Tap1*_Re	qRT-PCR; Mouse	AACGCTGTCACCGTTCCAGGAT
*B2m*_Fw	qRT-PCR; Mouse	ACAGTTCCACCCGCCTCACATT
*B2m*_Re	qRT-PCR; Mouse	TAGAAAGACCAGTCCTTGCTGAAG
*Ciita*_Fw	qRT-PCR; Mouse	CCCTGCGTGTGATGGATGTC
*Ciita*_Re	qRT-PCR; Mouse	ATCTCAGACTGATCCTGGCAT
Nlrc5_R1_Fw	sgRNA; Genomic deletion	CTACATCACCTGTATTGACCTGG
Nlrc5_R1_Re	sgRNA; Genomic deletion	GTTACGTATTACTTCCCTTAAGG
Nlrc5_R2_Fw	sgRNA; Genomic deletion	CCCATAGCAGCCACTTATGCAGG
Nlrc5_R2_Re	sgRNA; Genomic deletion	GGATTTTGACGGCTGCCCACTGG
Genotype_*Nlrc5*_WT_Fw	WT *Nlrc5* Genotyping	CCCATAGATGTTGCAAAACAAA
Genotype_*Nlrc5*_KO_Fw	KO *Nlrc5* Genotyping	ATCCAGGATCTCTTCAGCTTCA
Genotype_*Nlrc5*_Re	WT/KO *Nlrc5* Genotyping	CATGAGTCTGTCTTGATCCTGC

Chapter 1: Results

- **Application of dual-sgRNA CRISPR/Cas9 mediated genomic deletion of *Nlrc5* in B16F10 and E0771**

Detection of mouse Nlrc5 protein is challenging as the specific antibodies are still not available. Therefore, it is necessary to use an alternative method to induce Nlrc5 knockout that can be validated without detection of protein. To this end, we used dual-sgRNA CRISPR/Cas9 system to induce genomic deletion of *Nlrc5* (Figure 1a). Dual-sgRNA system is more suitable for our purpose compared with the more commonly used single sgRNA system because dual-sgRNA system can induce genomic deletion while single sgRNA system can only induce indels. Genomic deletion can be easily validated by genotyping while confirmation of homozygous of intel is difficult.

The efficacy of genomic deletion is negatively associated with length of expected to be deleted fragment (Canver *et al.*, 2014). We targeted to delete a 2,500 bp long region. We genotyped total of 78 clones and found 16 clones to be heterozygous knockout (Figure 1b). The deletion efficacy was 10%. Since mouse genome has a pair of alleles, the probability of obtaining homozygous knockout would be about 1%, which is too low. Therefore, we utilized two-step dual-sgRNA knockout strategy (Figure 1a, e). After second genotyping, we found that out of 52 clones, 4 of them were homozygous knockout. Genotyping using both WT and KO primers obtained bands of expected length (Figure 1c, d). Successful KO was further confirmed by sanger sequencing of PCR product. Similar approach was perfromed to induce Nlrc5 deletion in E0771 breast cancer cell line.

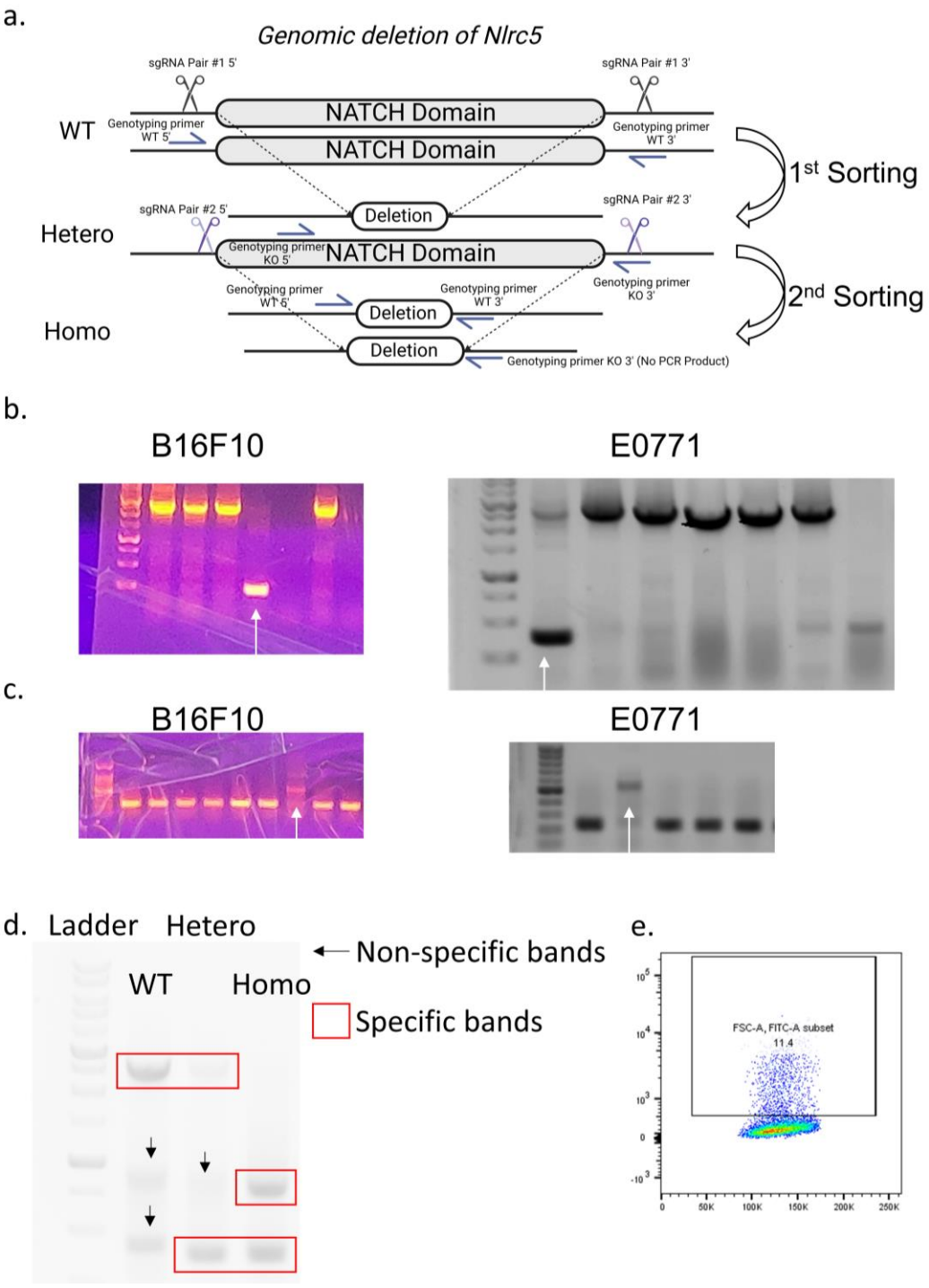

Figure 1 Generating genomic deletion of *Nlrc5* using dual-sgRNA CRISPR/Cas9 system in B16F10.

(a) Schematic of genomic deletion of *Nlrc5*. Plasmid encoding Cas9, GFP, and paired sgRNA flanking exon of *Nlrc5* encoding NATCH domain was transfected into wild type B16F10. GFP+ cells were sorted by flow cytometry and single cell clones were generated. Heterozygous KO clones were screened using WT genotyping primer, with WT clones having long 2,500 bp band and heterozygous clones having short

250 bp band. Next, a heterozygous clone was transfected with plasmid encoding Cas9, GFP, and a second pair of sgRNA, which targets NATCH domain at inner part compared with the first paired sgRNA. Similarly, homozygous KO clones were screened using KO genotyping primer, with heterozygous clones having short 250 bp band and homozygous clones having no specific bands. (b) Genotyping results to screen for heterozygous KO clones using WT genotyping primer in B16F10 and E0771 cells. White arrow indicates heterozygous clones. (c) Genotyping results to screen for homozygous KO clones using KO genotyping primer in B16F10 and E0771 cells. White arrow indicates homozygous KO clones. (d) Confirmation of genomic deletion of *Nlrc5* using WT genotyping primers in B16F10 cells. Black arrow indicates non-specific bands. Red box indicates specific bands. (e) GFP+ cells (FITC+) were sorted to generate single cell clones.

- **Genomic deletion of *Nlrc5* specifically downregulates MHC class I gene expression in E0771 cells.**

To investigate the effect *NLRC5* silencing in NLRC5 dependent MHC class I and related genes, homozygous Nlrc5 genomic deletion cell line (*Nlrc5*−/−) of E0771 cells were established using CRISPR/Cas9 system. Expression levels of *Nlrc5*, *H2-K*^{b}, and *B2m* were significantly reduced in *Nlrc5*−/− E0771 cells compared with *Nlrc5*+/− E0771 cells in absence or presence of IFN-γ stimulation (Figure 2a). Similarly, *Lmp2* expression level was significantly decreased in the presence of IFN-γ stimulation (Figure 2a). In contrast, no significant difference in the expression levels of *Ciita*, an unrelated gene to NLRC5 dependent MHC class I antigen presentation pathway, was found in *Nlrc5*+/− and *Nlrc5*−/− E0771 cells treated with or without IFN-γ (Figure 2a).

To study the effect of *Nlrc5* deletion on surface expression levels of MHC class I in E0771, surface H2-K^{b}/D^{b} levels were quantified using flow cytometry (Figure 3a). Baseline and IFN-γ-induced H2-K^{b}/D^{b} levels were decreased in *Nlrc5*−/− E0771 cells compared with *Nlrc5*+/− E0771 cells (Figure 2b). Comparison of PD-L1 expression in *Nlrc5*+/− and *Nlrc5*−/− E0771 cells treated with IFN-γ revealed unimpaired response to IFN-γ stimulation (Figure 2b). In addition, to investigate whether *Nlrc5* deletion affect cell growth, we compared proliferation rate of *Nlrc5*+/− and *Nlrc5*−/− E0771 cells by counting total cell number, and no significant difference was found (Figure 2c). Taken together, these results indicate that *Nlrc5* deletion induced specific decrease in transcription of MHC class I and related genes, and in surface MHC class I levels, but did not affect cell proliferation rate in E0771 cell line.

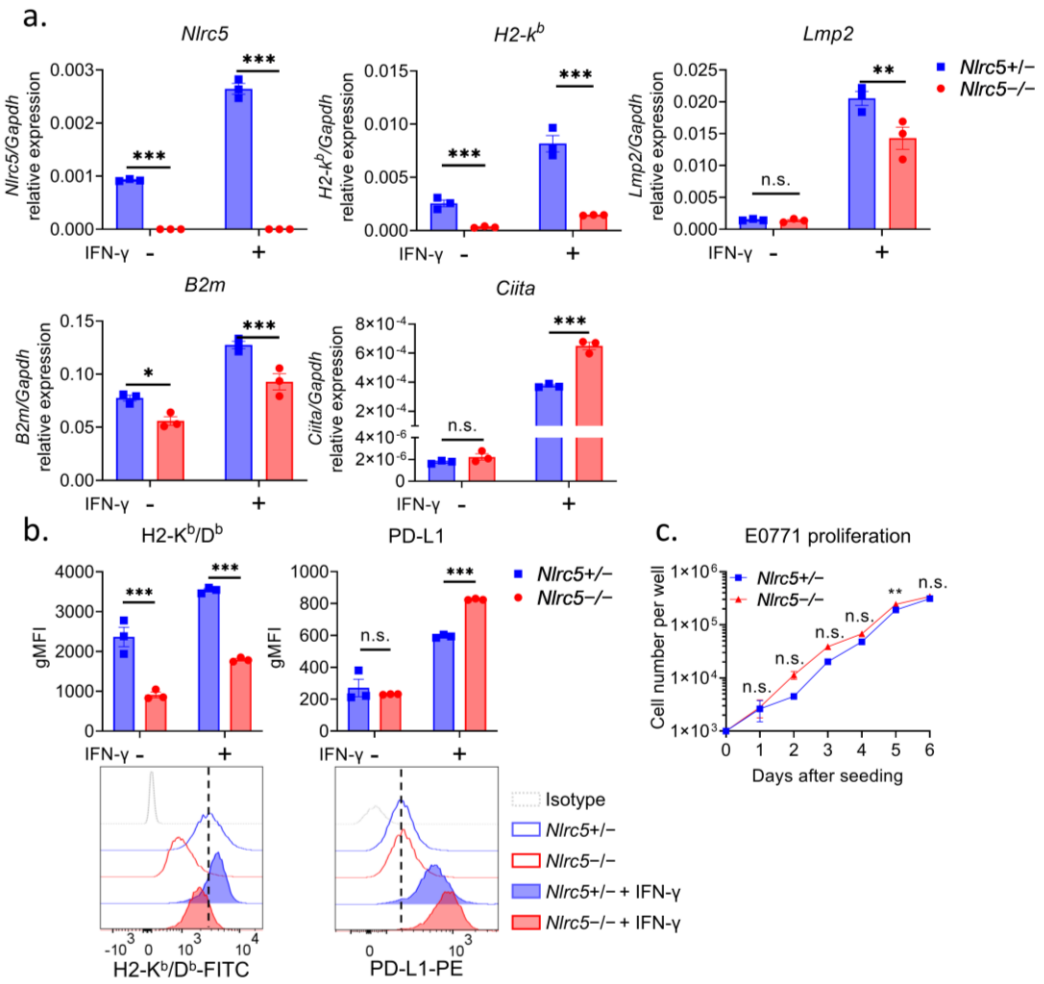

Figure 2 The expression of MHC class I genes is impaired in the *Nlrc5*-deficient E0771 breast cancer cell line.

(a) The mRNA expression levels of *Nlrc5*, *H2-K^b*, *Lmp2, B2m* and *Ciita* in *Nlrc5*+/− and *Nlrc5*−/− E0771 cells in the absence or presence of IFN-γ stimulation were determined by qRT-PCR. Relative gene expression levels were determined by ΔCT method using Gapdh as a reference gene. (a,b) *n*=3; (c) *n*=4 for each genotype. (b) Surface H2-K^b/D^b and PD-L1 expression levels in *Nlrc5*+/− and *Nlrc5*−/− E0771 cells in the absence or presence of IFN-γ stimulation. (c) Proliferation rate of E0771 cells *in vitro*. *n*=4; '*n*' indicates the number of biological replicated sample size. Data shown are representative of at least 3 independent experiments. Values shown are mean ±SEM. Statistical significance was determined by unpaired two-sided student's *t*-test. n.s., not significant; * $p < 0.05$; ** $p < 0.01$; *** $p < 0.001$.

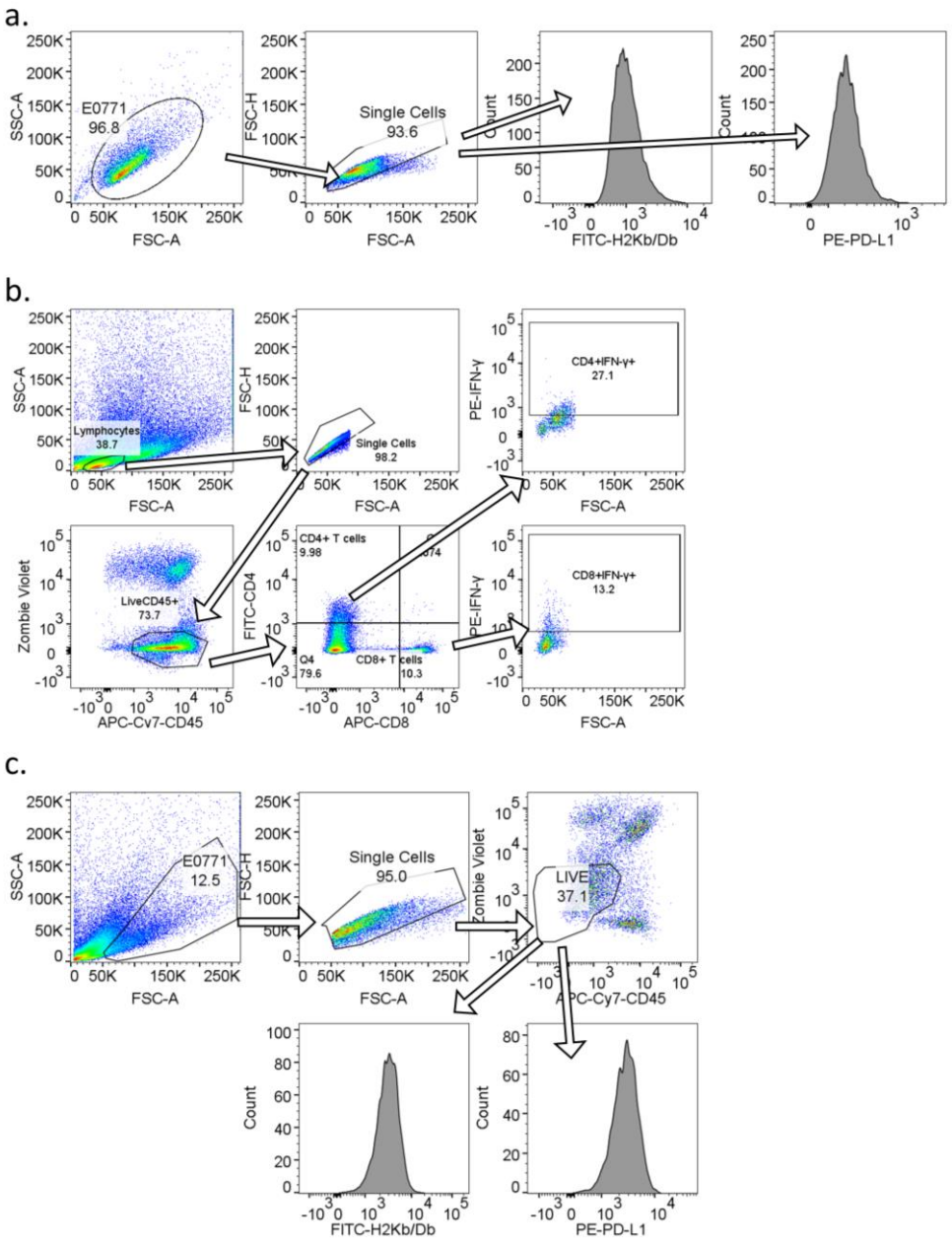

Figure 3 Gating strategy of flow cytometry.

(a) Gating strategy for quantification of surface MHC class I and PD-L1 levels in cultured cell lines, corresponding to Figure 2b and Figure 6b. Cell debris were excluded and followed by single cell selection by FSC-A and SSC-H. (b) Gating strategy for quantification and characterization of tumor infiltrating lymphocytes, corresponding to Figure 4e and Figure 7e. Single live nucleated hematopoietic cells were gated based on FSC-A, SSC-A, SSC-H, zombie−, and CD45+ signals. Subsequently, CD4+ or CD8+ T cells were gated by CD4+ or CD8+, followed by IFN-γ+ cells to identify activated lymphocytes. (c) Gating strategy for quantification of MHC Class I and PD-L1 levels in transplanted E0771 and B16F10 tumors.

Corresponding to Figure 4f, Figure 7f. Cell debris were excluded by FSC-A and SSC-A, followed by single cell selection by FSC-A and SSC-H. Subsequently, live tumor cells were gated by zombie– and CD45–.

- ***Nlrc5* deletion promotes E0771 tumor growth *in vivo* by inhibiting CD8+ T cell infiltration and activation through MHC class I**

Because *Nlrc5* deletion induced decrease in MHC class I levels of E0771 cells, the effect of *Nlrc5* deletion on immune evasion was investigated *in vivo* using orthotopic E0771 transplantation model (Figure 4a). *Nlrc5*−/− E0771 cells showed a significant increase in tumor growth compared with *Nlrc5*+/− E0771 cells (Figure 4b,c,d). Characterization of TILs showed that CD45+ leukocyte and CD8+ T cell infiltration, and infiltrated CD8+/CD4+ T cell ratio in *Nlrc5*−/− E0771 tumors were significantly reduced compared with *Nlrc5*+/− E0771 tumors, but not in CD4+ T cell infiltration (Figure 4e,a). Similarly, proportion of activated IFN-γ+ CD8+ T cells was decreased in *Nlrc5*−/− tumor tissue, but not IFN-γ+ CD4+ T cells (Figure 4e,b,c). We hypothesized that decrease in CD8+ T cell infiltration and activation was associated with reduced MHC class I level. Therefore, H2-K^b/D^b levels on tumor cells *in vivo* were quantified by flow cytometry (Figure 3c). H2-K^b/D^b levels were significantly decreased in *Nlrc5*−/− E0771 *in vivo* (Figure 4f, d), while a significant decrease in PD-L1 levels was also observed (Figure 4f,d). These results suggest that *Nlrc5* deletion in E0771 induced decrease in MHC class I expression, resulting in cancer immune evasion through inhibiting CD8+ T cell infiltration and activation.

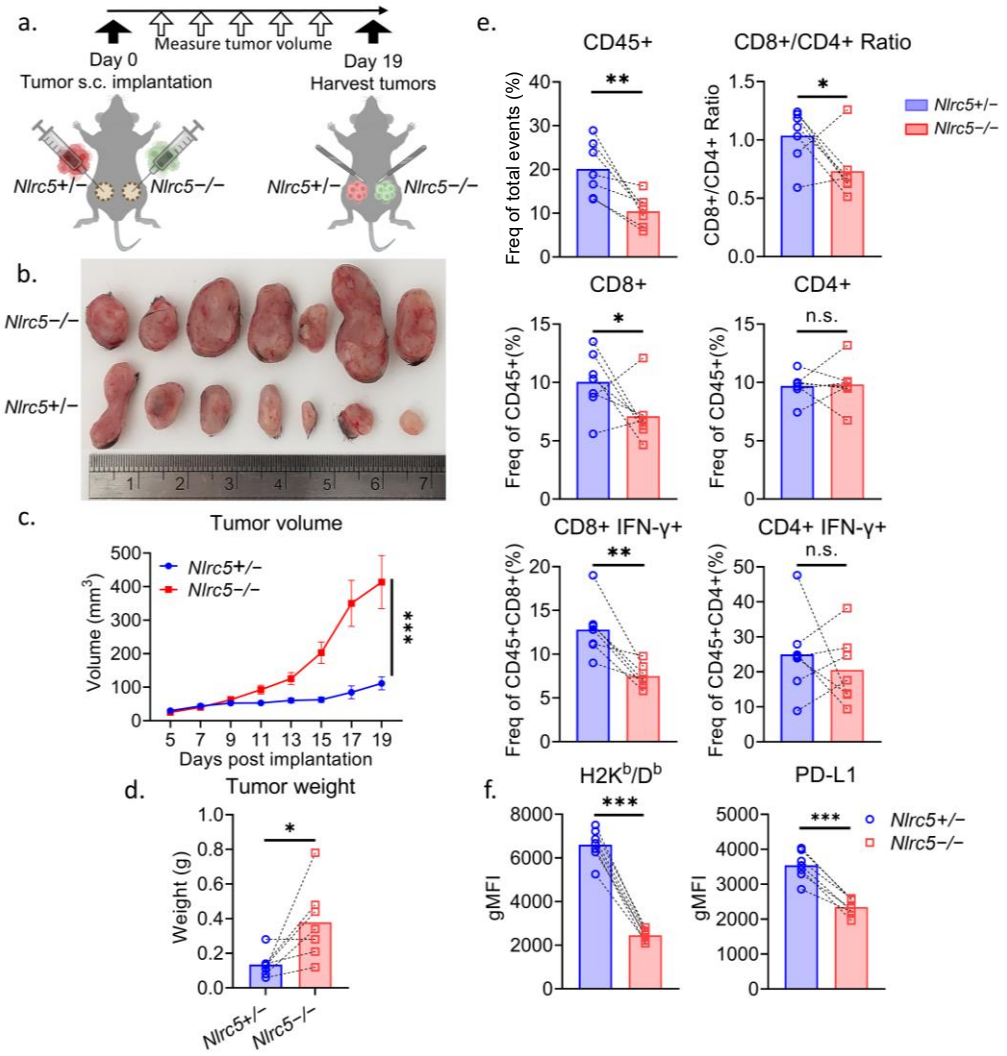

Figure 4 Genomic deletion of *Nlrc5* leads to immune evasion of E0771 cell line.

(a) A schematic illustration of orthotopic E0771 breast cancer model transplanted into syngeneic C57BL/6 mice. (b-f) n=7 for each genotype. (b) A picture of *Nlrc5*+/− and *Nlrc5*−/− transplanted E0771 tumors harvested on day 19. Each vertically aligned tumor was from the same mouse. (c, d) Tumor growth was quantified by (c) tumor volume and (d) weight. (e) Tumor infiltrating lymphocytes in E0771 tumors. Proportion of CD45+, CD4+, CD8+ and IFN-γ+ cells in their corresponding parent population, and infiltrated CD8+/CD4+ T cell number ratio were determined by flow cytometry. (f) Surface expression of H2-K^b/D^b and PD-L1 on E0771 cells were analyzed by flow cytometry. Dots connected by dashed line in bar graphs indicate tumors harvested from the same mouse. Data shown are representative of at least 2 independent experiments. Values shown are mean ±SEM. Statistical significance was tested by a two-way ANOVA test for (c) and unpaired two-sided student's t-test were

performed for (d-f). n.s., not significant; * $p < 0.05$; ** $p < 0.01$; *** $p < 0.001$.

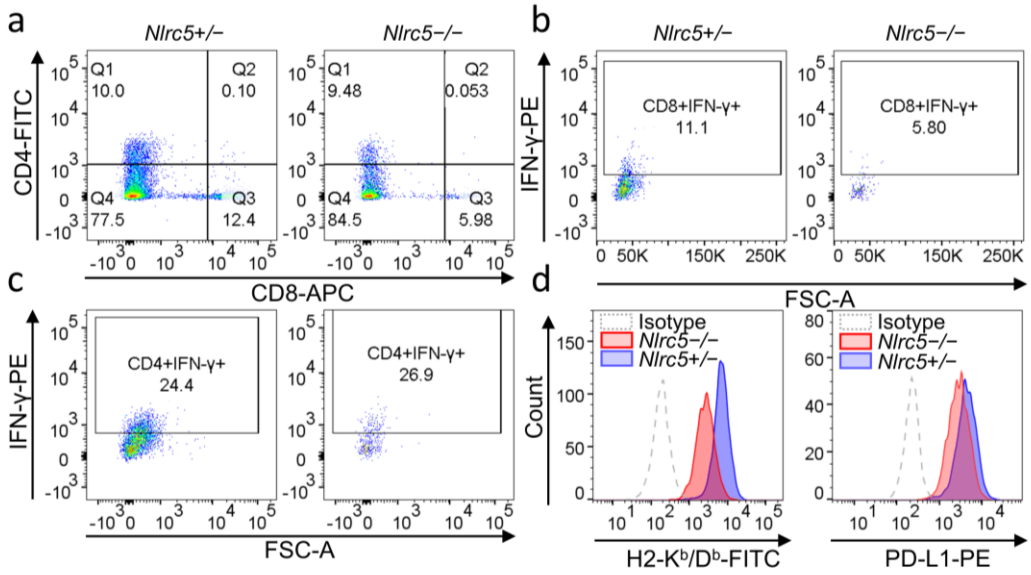

Figure 5 *Nlrc5* deletion in E0771 cell line resulted in impaired CD8+ T cell infiltration and activation *in vivo*.

(a-c) Representative scatter plot of (a) CD4+ and CD8+, (b) IFN-γ+CD8+, and (c) IFN-γ+CD4+ T cells that infiltrated into *Nlrc5*+/− and *Nlrc5*−/− E0771 tumors, corresponding to Figure 4e. Single live nucleated hematopoietic cells were gated based on FSC-A, SSC-A, SSC-H, zombie−, and CD45+ signals. Subsequently, CD4+ or CD8+ T cells were gated by CD4+ or CD8+, followed by IFN-γ+ cells to identify activated lymphocytes. (d) Representative histogram of the surface H2-K^b/D^b and PD-L1 level in *Nlrc5*+/− and *Nlrc5*−/− E0771 cells *in vivo*, corresponding to Figure 4f. Cell debris were excluded by FSC-A and SSC-A, followed by single cell selection by FSC-A and SSC-H. Subsequently, live tumor cells were gated by zombie– and CD45–.

- ***Nlrc5* deletion specifically downregulates MHC class I gene expression in B16F10 cells**

While orthotopic E0771 transplantation model is immunogenic (Le Naour *et al.*, 2020), we next sought to investigate the effect of *Nlrc5* silencing on immune evasion in the poorly immunogenic B16F10 model by inducing genomic deletion of Nlrc5 (Chen *et al.*, 2015, Pan *et al.*, 2018). The mRNA expression of *H2-k*^{b} at baseline level, and IFN-γ treatment induced *H2-k*^{b}*, Lmp2,* and *B2m* mRNA expression levels were significantly decreased in *Nlrc5*−/− B16F10 cells compared with *Nlrc5*+/+ B16F10 cells (Figure 6a). Moreover, baseline and IFN-γ-induced *Ciita* expression level were not significantly different in *Nlrc5*+/+ and *Nlrc5*−/− B16F10 (Figure 6a), indicating that *Nlrc5* deletion induced specific decrease in the expression levels of MHC class I and related genes in B16F10 cells.

To study the effect of *Nlrc5* deletion on surface expression level of MHC class I in B16F10, surface levels of H2-K^{b}/D^{b} in *Nlrc5*+/+ and *Nlrc5*−/− B16F10 cells were compared using flow cytometry (Figure 3a). No significant decrease in baseline of H2-K^{b}/D^{b} was found. On the other hand, mean fluorescence intensity of IFN-γ-induced H2-K^{b}/D^{b} and PD-L1 in *Nlrc5*−/− B16F10 cells was decreased to 13% and 92% relative to *Nlrc5*+/+ cells, respectively (Figure 6b). In addition, to investigate whether *Nlrc5* deletion affect cell proliferation, we compared proliferation rate of *Nlrc5*+/+ and *Nlrc5*−/− B16F10 cells by counting total cell number and did not observe significant difference (Figure 6c).

These results suggest that *Nlrc5* deletion in B16F10 impaired IFN-γ-induced MHC class I surface expression through downregulating the transcription of MHC class I and related genes, without affecting cell proliferation.

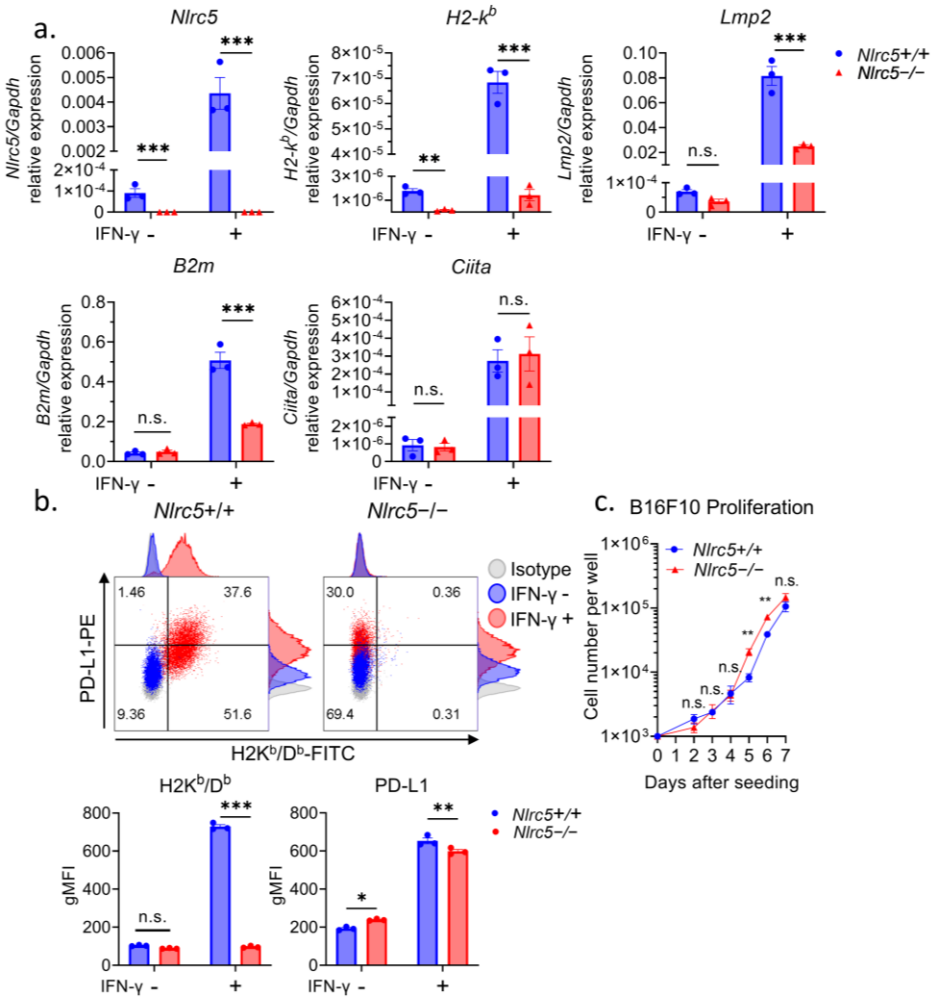

Figure 6 The expression of MHC class I genes is impaired in *Nlrc5*-deficient B16F10 melanoma cell line.

(a) The mRNA expression levels of *Nlrc5*, *H2-k*^{b}, *Lmp2*, *B2m* and *Ciita* in *Nlrc5*+/+ and *Nlrc5*−/− B16F10 cells in the absence or presence of IFN-γ stimulation were determined by qRT-PCR. Relative gene expression level was calculated by ΔCT method, using *Gapdh* as a reference gene (a,b) n=3; (c) n=4 for each genotype. (b) Surface expression of H2-K^b/D^b and PD-L1 on *Nlrc5*+/+ and *Nlrc5*−/− B16F10 cells in the absence or presence of IFN-γ stimulation was determined by flow cytometry. (c) Proliferation rate of *Nlrc5*+/+ and *Nlrc5*−/− B16F10 cells *in vitro*. Data shown are representative of at least 3 independent experiments. Values shown are mean ±SEM. Statistical significance was determined by unpaired two-sided student's *t*-test. n.s., not significant; * $p < 0.05$; ** $p < 0.01$; *** $p < 0.001$.

- ***Nlrc5* is required for response to anti-PD-1 therapy in B16F10 tumor transplantation model**

ICB therapies, such as anti-PD-1 therapy, activate cytotoxic T cells by blocking inhibitory signaling from immunosuppressive tumor microenvironment. Activated cytotoxic T cells produce IFN-γ to sensitize cancer cells to T cell killing, partially through upregulation of MHC class I antigen presentation in cancer (Jorgovanovic *et al.*, 2020). Since *Nlrc5* deletion inhibited IFN-γ-induced MHC class I in *Nlrc5*−/− B16F10 cells (Figure 6a,b), effect of NLRC5-MHC class I axis on immune evasion was further studied in anti-PD-1 antibody treated B16F10 model mouse.

C57BL/6J mice with *Nlrc5*+/+ or *Nlrc5*−/− B16F10 cells were treated with anti-PD-1 antibody or PBS (Figure 7a). Consistent with previous reports, tumor growth of *Nlrc5*+/+ B16F10 cells was significantly inhibited by anti-PD-1 antibody treatment but not by PBS treatment (Figure 7b,c,d) (Pi *et al.*, 2022). However, no significant decrease in tumor growth was observed in *Nlrc5*−/− B16F10 cells treated with anti-PD-1 antibody compared with treatment with PBS (Figure 7b,c,d). Tumor volume of *Nlrc5*−/− B16F10 cells was not significantly altered compared with *Nlrc5*+/+ B16F10 cells either under PBS or anti-PD-1 antibody treatment (Figure 7b,d).

Characterization of TILs showed that under anti-PD-1 antibody treatment, *Nlrc5*−/− B16F10 tumors showed significant decrease in infiltration of CD45+ leukocytes, CD8+ T cells, IFN-γ+ CD8+ T cell, and ratio of infiltrated CD8+/CD4+ T cell compared with *Nlrc5*+/+ B16F10 tumors, but not under PBS treatment (Figure 7e, Figure 3b, Figure 8a,b). While a significant increase in infiltration of CD8+ T cell and IFN-γ+ CD8+ T cell was observed in in *Nlrc5*+/+ B16F10 tumors treated with anti-PD-1 antibody, this induction was not detected in *Nlrc5*−/− B16F10 tumors treated by anti-PD-1 (Figure 7e, Figure 8a,b). *Nlrc5* deletion and anti-PD-1 treatment did not alter CD4+ T cell and IFN-γ+ CD4+ T cell infiltration (Figure 7e, Figure 8a,b).

Decrease in CD8+ T cell infiltration and activation by *Nlrc5* deletion prompted us to investigate MHC class I levels in B16F10 cells *in vivo* (Figure 3c). H2-K^b/D^b expression in *Nlrc5*+/+ B16F10 tumors tended to be induced by anti-PD-1 treatment (Figure 7f, Figure 8c). *Nlrc5* deletion significantly inhibited increase in H2-K^b/D^b expression, which was found in *Nlrc5*+/+ B16F10 tumor treated with anti-PD-1 antibody (Figure 7f, Figure 8c). In contrast, no difference of PD-L1 expression was found in all groups. Taken together, we found that *Nlrc5* deletion depleted response to anti-PD-1 treatment in B16F10 model. *Nlrc5* deletion impaired cytotoxic CD8+ T cell infiltration through decreasing MHC class I inducibility in B16F10 cells upon anti-PD-1 treatment.

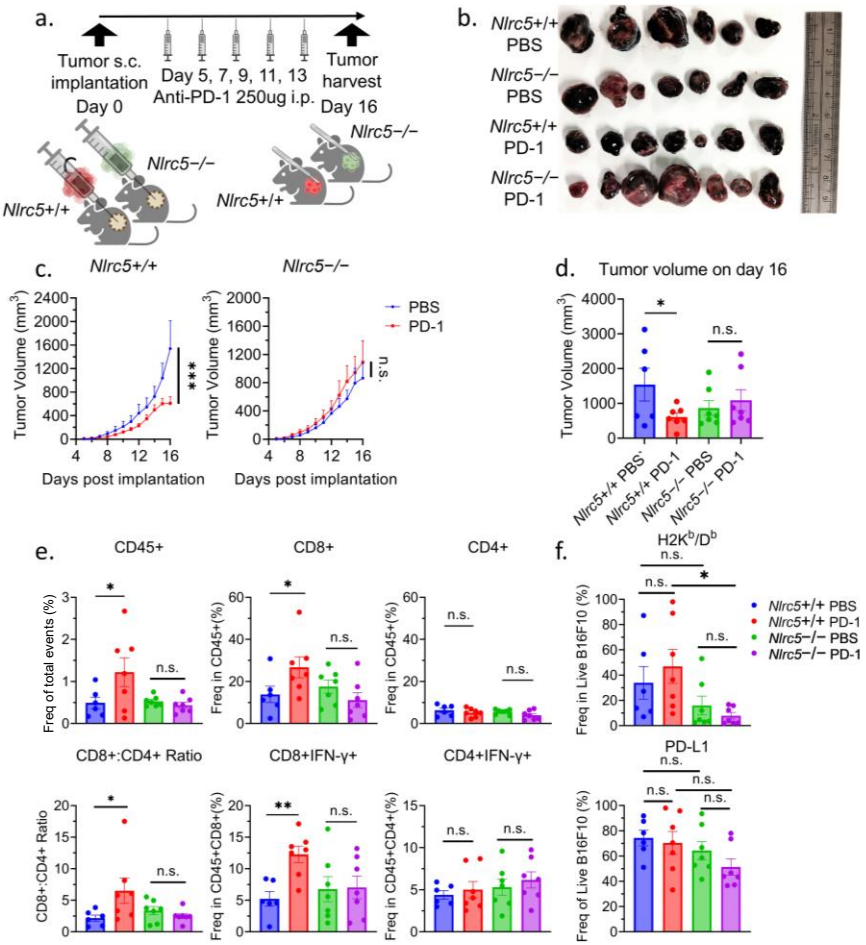

Figure 7 *Nlrc5* deficiency in B16F10 melanoma diminish effectiveness of anti-PD-1 therapy.

(a) Schematic illustration of B16F10 melanoma model subcutaneously implanted into syngeneic C57BL/6 mice and treated with anti-PD1 or PBS alone as indicated. (b) A picture of *Nlrc5*+/+ and *Nlrc5*−/− transplanted B16F10 melanoma harvested on day 16. One tumor in *Nlrc5*+/+ PBS group had grown excessively and were excluded from day 12. (b, d, e, f) *n*=6 for *Nlrc5*+/+ B16F10 treated with PBS mouse group; *n*=7 for other groups. (c) Tumor growth curves of *Nlrc5*+/+ and *Nlrc5*−/− B16F10 melanoma by measuring the volume. *n*=7 for each group. (d) Tumor volume on day 16. (e) Tumor infiltrating lymphocytes in resected B16F10 tumors. Proportion of CD45+, CD4+, CD8+, IFN-γ+ cells, and infiltrated CD8+/CD4+ T cell number ratio were determined by flow cytometry. (f) Surface expression levels of H2-K^b/D^b and PD-L1 on B16F10 cells in resected B16F10 tumors were analyzed by flow cytometry. Data shown are representative of at least 2 independent experiments. Values shown are mean ±SEM. Statistical significance was determined by a two-way ANOVA test

for (c,f.) and by Fisher's LSD test for (d,e.). n.s., not significant; * $p < 0.05$; ** $p < 0.01$; *** $p < 0.001$.

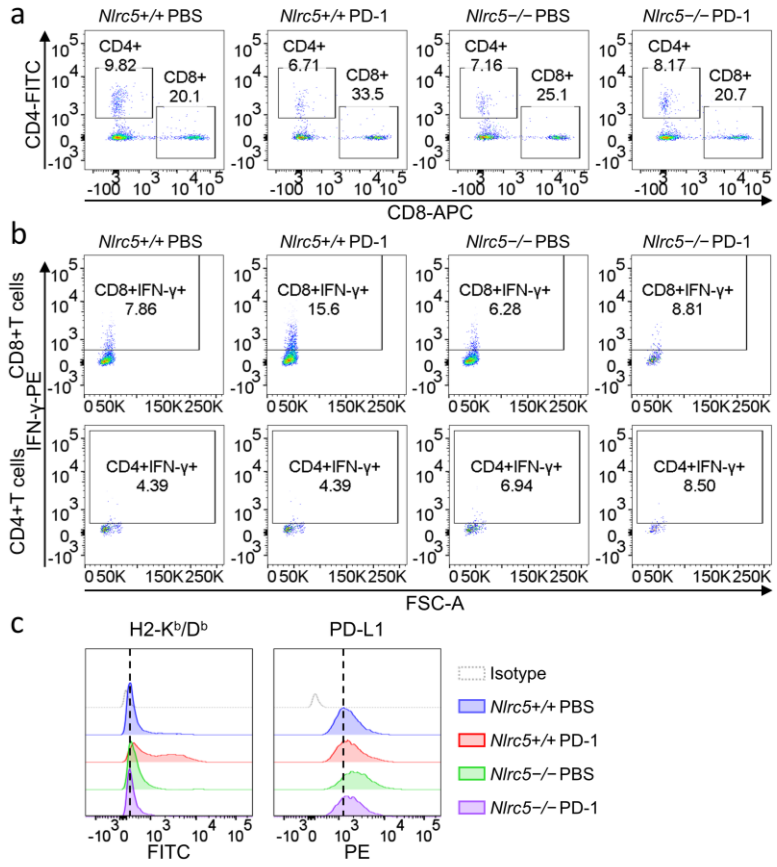

Figure 8 Anti-PD-1 treatment induced CD8+ T cell infiltration and activation in B16F10 *Nlrc5*+/+, but not in B16F10 *Nlrc5*−/− melanoma model.

(a-b) Representative scatter plots of (a) CD4+ and CD8+, (b) IFN-γ+CD8+ and IFN-γ+CD4+ T cells that infiltrated into *Nlrc5*+/+ and *Nlrc5*−/− B16F10 tumor treated with PBS or anti-PD-1 antibody. Corresponding to Figure 7e. Single live nucleated hematopoietic cells were gated based on FSC-A, SSC-A, SSC-H, zombie−, and CD45+ signals. Subsequently, CD4+ or CD8+ T cells were gated by CD4+ or CD8+, followed by IFN-γ+ cells to identify activated lymphocytes. (c) Representative histograms for the surface H2-K^b/D^b and PD-L1 expression levels in *Nlrc5*+/+ and *Nlrc5*−/− B16F10 tumors treated with PBS or anti-PD-1 antibody. Corresponding to Figure 7f. Cell debris were excluded by FSC-A and SSC-A, followed by single cell selection by FSC-A and SSC-H. Subsequently, live tumor cells were gated by zombie– and CD45–.

- ***NLRC5* expression is correlated with patient response to anti-PD-1 therapy**

Since *Nlrc5* is required for response to anti-PD-1 treatment in B16F10 model and *NLRC5* has been identified as marker to predict response to anti-PD-1 therapy in patients with melanoma in limited cohorts (Yoshihama *et al.*, 2021), we hypothesized that *NLRC5* could widely function as prediction marker in various melanoma cohorts, and applicable even in other types of cancer. Therefore, we generated aggregated transcriptome profile (referred to as combined cohort) of pre-anti-PD-1 therapy melanoma biopsies from independent sources (Hugo *et al.*, 2016, Riaz *et al.*, 2017, Gide *et al.*, 2019a).

We first characterized expression profile of *NLRC5* and NLRC5 dependent MHC class I genes in combined cohort. Heatmap visualization, GSEA and comparison of expression levels of each genes showed that expression levels of *NLRC5* and its dependent MHC class I genes in combined cohort was elevated in group who benefitted from anti-PD-1 therapy (responders) compared with group who did not benefit from anti-PD-1 therapy (non-responders) (Figure 9a,b,c), indicating that *NLRC5* and NLRC5 dependent MHC class I genes expressions were elevated in responders across multiple cohorts in melanoma.

To extend this finding, the expression levels of *NLRC5* and NLRC5 dependent MHC class I genes were analyzed in ccRCC patients (Miao *et al.*, 2018). We observed enriched expression of *NLRC5*, MHC class I and related genes in responders by heatmap Figure 10a), GSEA (Figure 10b) and expression levels of individual genes (Figure 10c), indicating that elevated expression of *NLRC5* and its dependent MHC class I genes was found in anti-PD-1 therapy responders in both melanoma and ccRCC patients.

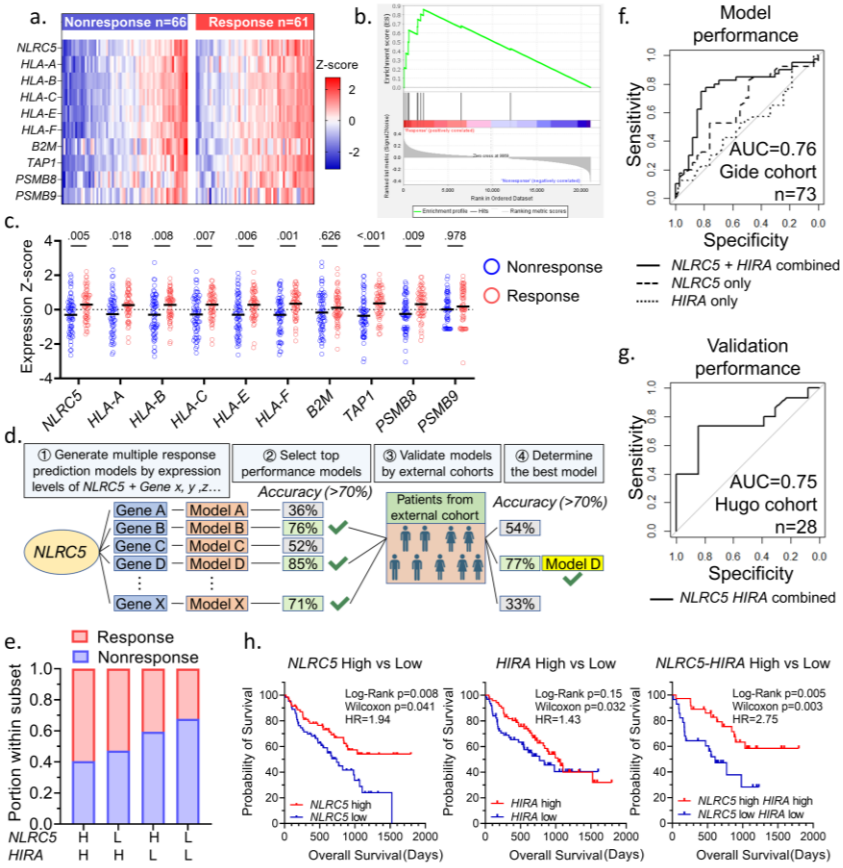

Figure 9 Generation of the prediction model for the response to anti-PD-1 therapy by transcriptional screening in melanoma.

Patient groups with benefit by anti-PD-1 therapy (Response, *n*=61) and without benefit (Nonresponse, *n*=66) from Gide et al., Hugo et al., and Riaz et al., were analyzed for differential gene set enrichment by (a) Heatmap, (b) GSEA and (c) individual gene expression levels of *NLRC5* and related MHC class I genes. (d) Schematic illustration of screening strategy to identify the best prediction model for response to anti-PD-1 therapy. (e) Classification of response and nonresponse patients based on *NLRC5* and *HIRA* expression level. H indicates expression levels of indicated genes are higher than mean and L indicates lower than mean. (f) ROC curve for response prediction model using the expression of *NLRC5* alone, *HIRA* alone or combination of *NLRC5* and *HIRA* in z-score in the model training cohort. (g) ROC curve prediction model using combination of *NLRC5* and *HIRA* expression in z-score in the independent validation cohort. (h) Kaplan-Meier survival curves of melanoma patients with high and low *NLRC5* expression (left), with high and low *HIRA* expression (middle), and with $NLRC5_{high}$ / $HIRA_{high}$ and $NLRC5_{low}$ / $HIRA_{low}$ expression (right) in tumors before anti-PD-1 therapy. Patients were divided based

on *NLRC5* and *HIRA* expression: Patients with higher expression than mean were defined as “high” and patients with lower expression than mean were defined as “low”. Points on curve indicate censored samples. Statistical significance was tested by unpaired two-sided student’s *t*-test (for c.), log-rank and Wilcoxon test (for h.). AUC: area under the curve. ROC: receiver operating characteristic.

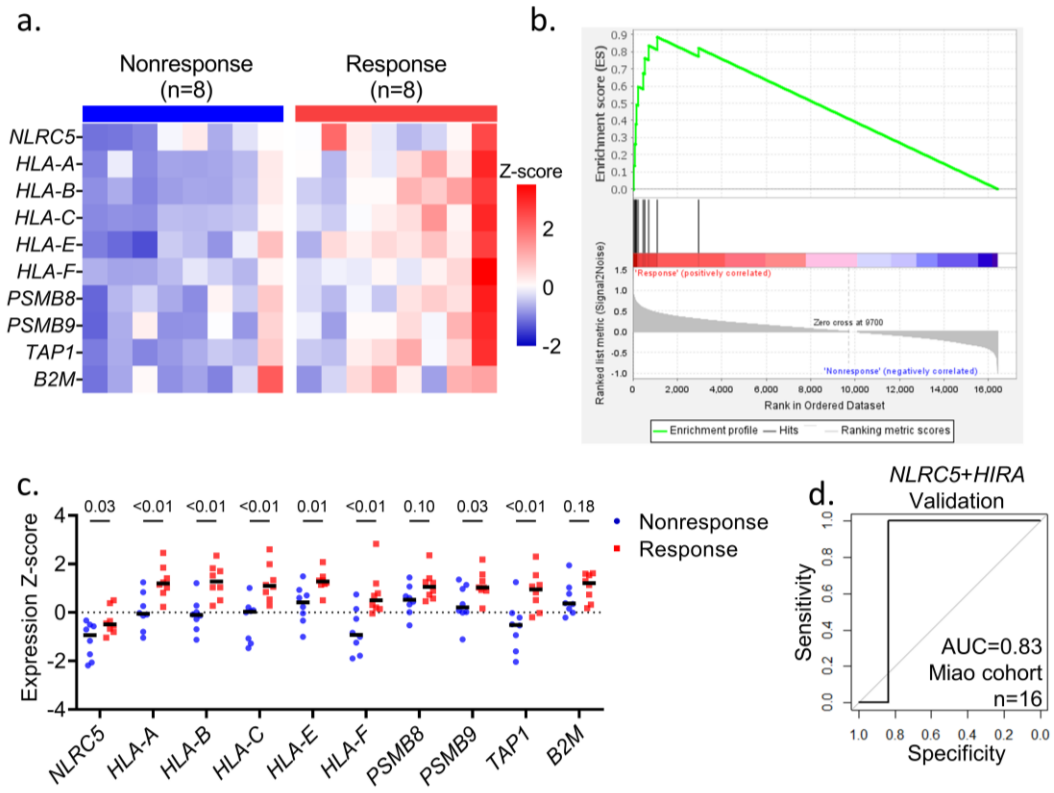

Figure 10 The prediction model for the response to anti-PD-1 therapy by the combination of *NLRC5* and *HIRA* expression can be applied for clear cell renal cell carcinoma.

Patient groups who benefitted from anti-PD-1 therapy (Response, *n*=8) and who did not (Nonresponse, *n*=8) from Miao et al. ccRCC cohort were analyzed for the differential gene set enrichment by (a) heatmap, (b) GSEA as well as (c) individual gene expression levels. (d) ROC curve in predicting patients' response of ccRCC in Miao et al. cohort. The prediction model with *NLRC5* + *HIRA* expression generated by the data of the Gide et al cohort for the response to anti-PD-1 therapy was used. Statistical significance was examined by unpaired two-sided student's *t*-test for c.

- **Combined *NLRC5* and *HIRA* model efficiently predict patients' response to anti-PD-1 therapy.**

NLRC5 is reported to have a better response prediction efficacy to ICB therapy when combined with other genes (Yoshihama *et al.*, 2021). However, further optimization of prediction model and validation by independent external cohort are needed to simulate the application of prediction model in new patients. Therefore, we sought to screen for candidate gene that show the highest prediction accuracy when combined with *NLRC5* using RF algorithm. Prediction models that utilize the expression levels of *NLRC5* and another candidate gene were generated from Gide et al. cohort and then validated in Hugo et al. cohort (Hugo *et al.*, 2016, Gide *et al.*, 2019b) (Figure 9d). Among candidate genes, *HIRA*, a composition of histone chaperone complex that deposits histone variant H3.3 onto chromatin (Ray-Gallet *et al.*, 2018), was identified as the most effective co-biomarker to predict anti-PD-1 therapy outcome in melanoma when combined with *NLRC5*. Pathway enrichment analysis showed that expression of *HIRA* was positively associated with pathways of metabolism and skin differentiation, and negatively associated with humoral immunity pathway (Figure 11a). Combination analysis of *NLRC5* and *HIRA* expression showed positive correlation with proportion of responders (Figure 9e).

In Gide et al. cohort, an area under the curve (AUC) of *NLRC5+HIRA* RF model was 0.76 while *NLRC5* or *HIRA* alone showed AUC of 0.66 and 0.52 respectively (Gide *et al.*, 2019a) (Figure 9f). Validation of *NLRC5+HIRA* RF model in melanoma Hugo et al. cohort or ccRCC Miao et al. cohort showed AUC of 0.75 or 0.83 (Figure 9g, Figure 10d) (Hugo *et al.*, 2016, Miao *et al.*, 2018). These results suggest that *NLRC5+HIRA* RF model is effective in melanoma and ccRCC.

Because *NLRC5+HIRA* RF model could predict patients' response to anti-PD-1 therapy, correlation of *NLRC5* and *HIRA* expression levels with overall survival was analyzed in melanoma patients. Patients were classified into "High" or "Low", or "High-High" or "Low-Low" groups based on expression levels of *NLRC5* and/or *HIRA*. Multivariate analysis using both *NLRC5* and *HIRA* showed more significantly improved prognosis in "High-High" against "Low-Low" group compared with single variable analysis by *NLRC5* or *HIRA* (Hazard ratio, HR (NLRC5 and HIRA) = 2.75, (NLRC5) 1.94, (HIRA) 1.43; Figure 9h), indicating that multivariate analysis using *NLRC5* and *HIRA* expression is superior to single variable analysis.

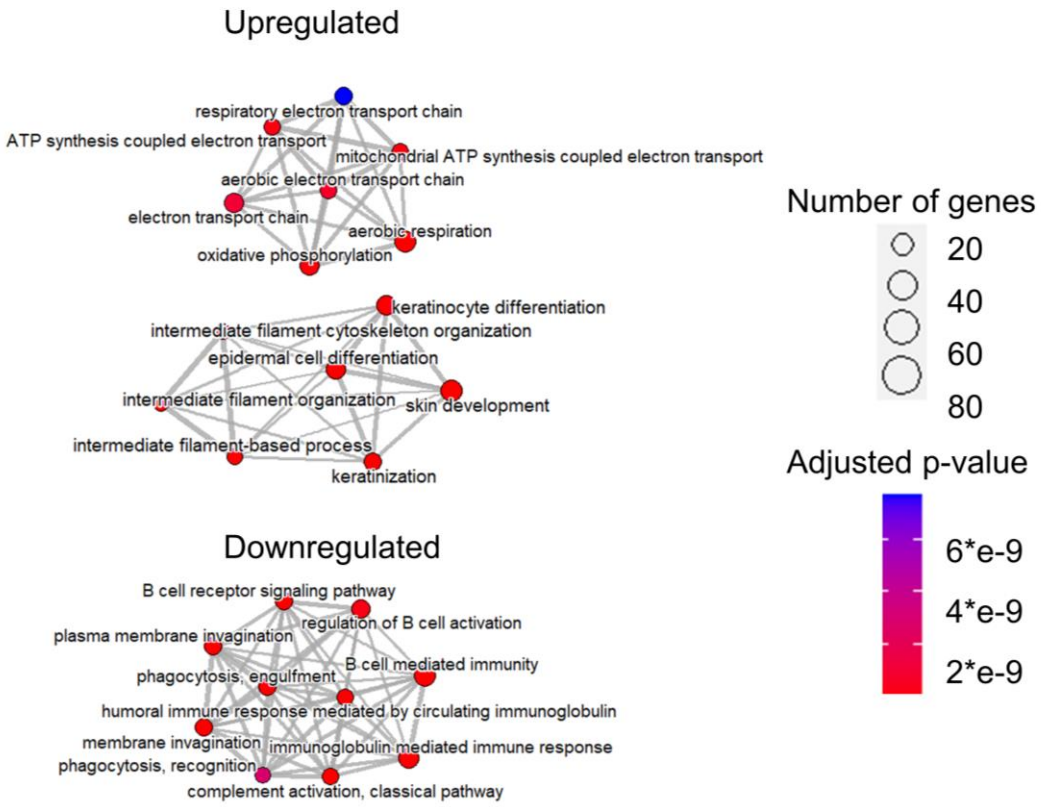

Figure 11 The expression level of *HIRA* is correlated with metabolic pathway in melanoma.

Enrichment map of representative pathways either enriched (upper panel) or decreased (lower panel) together with *HIRA*. Transcriptome profile from TCGA SKCM cohort was divided into two groups, either higher or lower *HIRA* expression groups than average *HIRA* expression level. Representative enriched/decreased pathways in *HIRA* high group were identified and presented.

Chapter 1: Discussion

In this study, we induced genomic deletion of *Nlrc5* in E0771 and B16F10 cell lines. We show that genomic deletion of *Nlrc5* reduced expression of baseline and IFN-γ induced MHC class I and related genes in E0771 and B16F10 cell lines. The effect of *Nlrc5* knockout on MHC class I antigen presentation pathway in normal tissues and cells is well demonstrated as *Nlrc5* deficient mouse express reduced levels of MHC class I and related genes (Biswas *et al.*, 2012, Robbins *et al.*, 2012, Staehli *et al.*, 2012, Yao *et al.*, 2012). Accordingly, analysis of transcriptome profiles in human cancers reveled that *NLRC5* expression is correlated with MHC class I and related genes (Yoshihama *et al.*, 2016). But validation in *Nlrc5* knockout cancer cell lines were limited in evaluation of surface MHC class I levels (Freeman *et al.*, 2019, Kalbasi *et al.*, 2020b, Dersh *et al.*, 2021). Our results confirmed that *NLRC5* not only controls transcription of MHC class I and related gene in immune cells but also function as transcription activator of MHC class I and related genes in cancer, implying the critical role of NLRC5 in anti-cancer immunity.

Loss of MHC class I is correlated with increase in malignant tumor growth (Garcia-Lora *et al.*, 2001, Del Campo *et al.*, 2014). We showed that *Nlrc5* deletion in E0771 model induce immune evasion by impairing tumor antigen presentation to CD8+ T cells through MHC class I. Our results in E0771 model were further verified in B16F10 model. Although *Nlrc5* deletion alone was insufficient to change tumor growth in B16F10 model, we observed that *Nlrc5*+/+ B16F10 tumors responded to anti-PD-1 treatment, but not in *Nlrc5*−/− B16F10 tumors. We showed that loss of response was associated with reduced CD8+ T cell infiltration, activation, and MHC class I levels on B16F10 by *Nlrc5* deletion. Indeed, impairment of MHC class I antigen presentation pathway is correlated with resistance to immune checkpoint blockade therapy (Zaretsky *et al.*, 2016, Gettinger *et al.*, 2017, Le *et al.*, 2017, Sade-Feldman *et al.*, 2017, Chowell *et al.*, 2018, Rodig *et al.*, 2018, Liu *et al.*, 2019). Moreover, tumor infiltrating CD8+ T cells are correlated with clinical benefit of ICB therapy and better cancer prognosis (Bruni *et al.*, 2020, Li *et al.*, 2021). Additionally, *NLRC5* expression is enriched in responders of ICB therapy, and it is positively correlated with expression levels of CD8+ T cell cytotoxic markers (Yoshihama *et al.*, 2016, Yoshihama *et al.*, 2021). These results suggest that *NLRC5* is required for response to anti-PD-1 treatment in B16F10 model by providing sufficient antigen presentation through MHC class I pathway for recognition and killing by cytotoxic CD8+ T cell.

Given the important role of *Nlrc5* in response to anti-PD-1 treatment, we generated anti-PD-1 therapy response prediction model using combined cohort based on the

expression level of *NLRC5*. We performed transcriptome screening and identified that combination of *NLRC5* + *HIRA* generates prediction model with the highest accuracy. Our strategy is superior compared with previous study that utilized expression level of *NLRC5* in three primary ways (Yoshihama *et al.*, 2021). First, we included validation by independent external cohort. Second, we utilized larger cohorts. Third, we performed transcriptome screening to identify the best combination for prediction model. Most importantly, inclusion of validation process by independent cohorts mimics the process of predicting new patients, which highlight the value of using the prediction model in clinical application. Although we sought to identify combination of biomarker with the highest accuracy when combined with *NLRC5*, prediction models do not have to be based on *NLRC5* expression level. Our strategy can be applied to any markers or cohorts, which provide rooms for improvement and clinical application.

In this study, our focus was limited on characterization of TILs. On the other hand, MHC class I levels are associated with natural killer (NK) cells mediated immunity against B16F10 (Freeman *et al.*, 2019). Although not statistically significant, we observed that the volume of *Nlrc5*−/− B16F10 tumors tended to be decreased compared with *Nlrc5*+/+ B16F10 tumors under PBS control treatment. It is possible that NK cell mediated killing is enhanced by *Nlrc5* deletion as *Nlrc5*−/− B16F10 tumors lack expression of MHC class I, the inhibitory ligand for NK cell activation (Moretta *et al.*, 2004). Additionally, MHC-I and related gene levels on cancer cells may influence T cell cross priming in tumor draining lymph nodes (TDLNs) by dendritic cells through antigen uptake or MHC cross dressing (Fu *et al.*, 2018, Duong *et al.*, 2022, MacNabb *et al.*, 2022). It would contribute to further understanding of the role of *NLRC5* in anti-cancer immunity to investigate whether cancer derived *NLRC5* plays a role in NK cell activation and T cell priming in TDLNs. Furthermore, our study on anti-PD-1 treatment was limited to B16F10 model. E0771 and B16F10 cells showed different extent of MHC class I reduction after *Nlrc5* deletion. Therefore, *Nlrc5* may play different role in response to anti-PD-1 treatment of E0771 model. Additional study would contribute to further understanding of how *NLRC5* modulate response to anti-PD-1 treatment.

Title of Chapter 2: Enhancing the immunogenicity of cancer by targeted demethylation and activation of *Nlrc5*.

Chapter 2: Introduction

NLRC5 expression is important to regulate the expression of MHC class I and related genes and immunogenicity to CD8+ T cell immunity. *Nlrc5* deficiency reduced the expression of MHC class I and related genes and CD8+ T cell specific killing in mice (Biswas *et al.*, 2012, Robbins *et al.*, 2012, Staehli *et al.*, 2012, Yao *et al.*, 2012), and *NLRC5* has been identified as one of the top positive regulators of MHC class I expression by CRISPR knockout screening in cancer (Freeman *et al.*, 2019, Kalbasi *et al.*, 2020b, Dersh *et al.*, 2021, Gu *et al.*, 2021). Furthermore, in Chapter 1, we induced genomic deletion of *Nlrc5* in B16F10 and E0771, which led to reduction of MHC class I expression levels and weakened anti-cancer immune response. These phenotypes were observed in the absence of *Nlrc5*, therefore, we next sought to investigate whether it is possible to increase cancer immunogenicity and host anti-cancer response by inducing *Nlrc5* expression.

Aberrant changes in DNA methylation have a well-established role in cancer pathogenesis (Banerjee *et al.*, 2022). Particularly, *NLRC5* promoter is hypermethylated in cancers and *NLRC5* methylation level is negatively correlated with expression levels of *NLRC5*, which downregulates antigen presentation through MHC class I, leading to a poor prognosis (Yoshihama *et al.*, 2016). Therefore, hypermethylation of *NLRC5* promoter in cancer is associated with immune evasion. Accordingly, overexpression of *Nlrc5* in mouse melanoma increased cancer immunogenicity specifically to CD8+ T cells and inhibited tumor growth *in vivo* (Rodriguez *et al.*, 2016). Therefore, targeted demethylation of *NLRC5* promoter is a potentially viable therapeutic approach to enhance cancer immunogenicity by recovering the expression of *NLRC5*, and dependent MHC class I and related genes.

DNA demethylating agents have arisen as a therapeutic tool for the treatment of cancer. Azacytidine, a DNA methyltransferases inhibitor, is used as chemotherapy for subtypes of leukemia and shown to be effective in the treatment of solid tumors in mouse models(Noguchi *et al.*, 2015, Luo *et al.*, 2018). But azacytidine, along with other types of DNA demethylating agents, has severe side effects and unable to induce DNA demethylation in site specific manner, which limit their clinical applications. Recent advance in clustered regularly interspaced short palindromic repeats/deactivated endonuclease Cas9 fused with ten eleven translocation 1 catalytic domain (CRISPR/dCas9-TET1cd) technology is enabling targeted DNA demethylation *in vitro* and *in vivo* (Choudhury *et al.*, 2016, Liu *et al.*, 2016, Xu *et al.*, 2016, Liu *et al.*, 2018). To induce targeted demethylation, dCas9-TET1cd is recruited to single guide RNA (sgRNA) target site in genomic DNA, where TET1cd oxidize methyl groups to induce

DNA demethylation. TET1cd is fused with sgRNA binding protein MS2 to recruit more copies of TET1cd to sgRNA target site(Xu *et al.*, 2016). The CRISPR/dCas9-TET1cd system has been shown to induce targeted demethylation in cancer (Choudhury *et al.*, 2016, Wang *et al.*, 2019). However, currently available strategies lack satisfactory efficacy of gene expression induction and suitable target to specifically eliminate cancer cells. Therefore, targeted demethylation of *NLRC5* promoter by CRISPR/dCas9-TET1cd could induce *NLRC5* expression and dependent MHC class I and related genes, which could activate host anti-cancer immunity to induce specific elimination of cancer cells by enhancing immunogenicity. Furthermore, coupling dCas9-TET1cd system with transcription activators, such as P65-HSF1 and VP64, is shown to increase its gene activation efficacy (Morita *et al.*, 2020, Nunez *et al.*, 2021, Chan *et al.*, 2022). Targeting *NLRC5* with TET1cd and transcription activators is expected to have improved efficacy compared with dCas9/TET1cd system.

Immune checkpoint blockade (ICB) therapy, such as anti-PD-1 therapy, has emerged as effective therapeutic method against various kinds of cancers. But a portion of patients do not benefit from ICB therapy. Factors that determine ICB therapy benefit are under investigation, however, previous studies identified that the expression of MHC class I genes and *NLRC5* is enriched in patients with efficient response to ICB therapy (Liu *et al.*, 2019, Yoshihama *et al.*, 2021). Since overexpression of *NLRC5* increase host anti-cancer response, targeted demethylation and activation of *NLRC5* in cancer may enhance the efficacy of ICB therapy by facilitating the elimination of cancer cells to CD8+ T cell mediated killing (Rodriguez *et al.*, 2016).

In this study, we showed that targeted demethylation and activation of *NLRC5* specifically upregulated the expression of MHC class I and related genes in mouse melanoma cell line B16F10 and human breast cancer cell line MCF7. Targeted demethylation of *Nlrc5* promoter alone induced *Nlrc5* expression but was insufficient to significantly increase cancer immunogenicity. We enhanced the efficacy of gene expression induction by fusing transcription activators to induce targeted demethylation and activation and referred to as TDMa system. This strategy significantly increased MHC class I levels and immunogenicity in B16F10. *In vivo* implantation of B16F10-TDMa cells showed that targeted demethylation and activation of *Nlrc5* suppressed tumor growth by activating host anti-cancer immunity and preferentially aggregated CD8+ T cells to tumor center. Interestingly, we found that targeted demethylation and activation of *Nlrc5* sensitized B16F10 to anti-PD-1 treatment. CD8+ T cell, but not CD4+ T cell immunity, was preferentially induced by anti-PD-1 treatment. Our results highlight *NLRC5* and TDMa system as a vaiable approach to develop novel immune therapy. Alternatively, *NLRC5* and TDMa system can be targeted as simultaneously

with ICB therapy to enhance its efficacy.

Chapter 2: Methods

Mice

C57BL/6JJcl (B6; RRID:MGI:3055581) and BALB/cAJcl-Foxn1nu (NUDE; RRID:MGI:3806503) mice were purchased from CLEA Japan, Inc. (Tokyo, Japan). C57BL/6-Tg (TcraTcrb) 1100Mjb/J (OT-I; RRID:IMSR_JAX:003831) mice were purchased from The Jackson Laboratory (Bar Harbor, ME, USA). Mice were bred and maintained in the Institution for Animal Experimentation at Hokkaido University Graduate School of Medicine in specific pathogen-free (SPF) conditions. Male and female mice at the age of 7–10 weeks-old were used in the subsequent experiments. All animal experiments were conducted according to the guidelines of the Hokkaido University Animal Experiment Implementation Manual and were approved by the Institutional Animal Care and Use Committee of Hokkaido University Graduate School of Medicine (Approval No. 19-0134).

Cell lines

Mouse melanoma B16F10 and human breast adenocarcinoma MCF7 cell lines were from RIKEN Bio BRC, Japan (Tsukuba, Japan, cat. RCB2630, RRID:CVCL_0159; cat. RCB1904, RRID:CVCL_0031). Human Lenti-X 293T cell line was from Takara Bio (Kasatsu, Japan. cat. 632180, RRID:CVCL_4401). MCF7, Lenti-X 293T, and B16F10 cell lines were cultured in Dulbecco's Modified Eagle Medium (DMEM, Nacalai, Kyoto, Japan, cat. 08458-16). For OT-I CD8+ T cell primary culture, cells were kept in Roswell Park Memorial Institute (RPMI) 1640 (Nacalai, cat. 30264-56) medium supplied with 50 μM of 2-mercaptoethanol (Life Technologies, Carlsbad, CA, cat. 21985023) and 2 mM of L-Glutamine (Life Technologies, cat. 25030081). All cell culture mediums were supplemented with 10% heat-inactivated fetal bovine serum (FBS; Nichirei, Kyoto, Japan, cat. 175012) and kept in 37 °C with 5% CO_2 in a humidified incubator. All the cell lines were tested negative for mycoplasma contamination.

Plasmids

Lenti dCAS-VP64 Blast (Addgene, Watertown, NY, USA, cat. #61425), lenti MS2-P65-HSF1 Hygro (Addgene, cat. #61426) and lenti sgRNA (MS2) zeo backbone (Addgene, cat. #61427) were gifts from Feng Zhang. To accommodate insertion of TET1cd, additional restriction sites, *Xba*I and *BstB*I, were inserted between *BamH*I and *BsrG*I in Lenti dCAS-VP64 Blast and lenti MS2-P65-HSF1 Hygro by restriction digestion and ligation cloning. Human TET1cd was amplified by PCR from pPlatTet-

grna2 (Addgene, cat. #82559, a gift from Izuho Hatada) with either *BamH*I-*Xba*I or *BamH*I-*BstB*I as restriction sites and ligated into lenti dCAS-VP64 Blast and lenti MS2-P65-HSF1 Hygro. As a result, lenti dCAS9-TET1CD, lenti MS2-TET1CD (using *BamH*I, *Xba*I, flanking VP64 in lenti dCAS-VP64 Blast and P65-HSF1 in lenti MS2-P65-HSF1 Hygro) and lenti dCAS9-TET1CD-VP64, lenti MS2-TET1CD-P65-HSF1 (using *BamH*I, *BstB*I) were generated. For cloning of sgRNA, oligonucleotides encoding sgRNA target sites were custom ordered (Life Technologies), phosphorylated by T4 polynucleotide kinase (NEB, Ipswich, MA, USA, cat. M0201), denatured, annealed, and inserted into *BsmB*I by golden gate assembly of lenti sgRNA (MS2) zeo (Addgene, cat. #61427, a gift from Feng Zhang) as described previously(Konermann *et al.*, 2015). Unmodified lenti sgRNA (MS2) zeo was used to express scrambled control sgRNA. All experiments involving recombinant DNA and lentiviral vectors were approved by Hokkaido University Safety Committee on Genetic Recombination Experiments (Approval number: 2018-037).

Generation of stable cell lines

All the lentiviral vectors were generated using Lenti-X 293T cell line. Specifically, 5×10^5 Lenti-X 293T cells were seeded in 6-well plate and incubated overnight. Total 3 μg of target lentiviral plasmids, pCMV-VSV-G and psPAX2 plasmids (Addgene, #8454 a gift from Bob Weinberg; cat. #12260, a gift from Didier Trono) were at 1 μg:1 μg:1 μg ratio, subsequently, the plasmids mixture was incubated with 15 μg of Polyethylenimine max (PEI MAX, Polysciences, Warrington, PA, USA, cat. 24765-1) for 15 min. DNA-PEI mixture was added dropwise into 6-well plate and incubated for 6 h before the culture medium was replaced with refresh medium and cells were incubated for additional 42 h. The lentiviral vector containing media was centrifuged at 500× g for 3 min to remove cells and debris and supernatant was filtered through 0.45 μM filter (Sartorius stedim, Göttingen, Germany, cat. S7598-FXOSK). Next, 1.5 ml of lentiviral vector containing media was added to the target cells in 6-well plate with 8 μg ml^{-1} of polybrene (Nacalai Tesque, cat. 12996-81) and incubated for 48 h. Subsequently, stably transduced cells were selected by corresponding antibiotics.

For B16F10, cells were co-transduced by lenti dCAS9-TET1CD and lenti MS2-TET1CD (B16F10-TDM) or lenti dCAS9-TET1CD-VP64 and lenti MS2-TET1CD-P65-HSF1 (B16F10-TDMa). Subsequently, stably transduced cells were co-selected by 1.25 μg ml^{-1} of blasticidin (KAKEN PHARMACEUTICAL, Tokyo, Japan, cat. KK-400) and 125 μg ml^{-1} of hygromycin (InvivoGen, San Diego, CA, USA, cat. ant-hg-1) for 6 d. For B16F10-TDM, single cell clones were generated before sgRNA transduction. Subsequently, lenti sgRNA (MS2) zeo expressing various sgRNAs were

transduced into B16F10-TDM and B16F10-TDMa and stably transduced cells were selected by 120 μg ml^{-1} of zeocin (Life Technologies, cat. R25001) for 10 d.

For MCF7, cells were sequentially transduced with lenti dCAS9-TET1CD-VP64, lenti MS2-TET1CD-P65-HSF1, and lenti sgRNA (MS2) zeo to generate MCF7-TDMa cells. After each transduction, stably transduced cells were sequentially selected by 25 μg ml^{-1} of blasticidin, 250 μg ml^{-1} of hygromycin for 7 d, and 500 μg ml^{-1} of zeocin for 10 d, respectively.

Successful integration of lentiviral vector construct was confirmed by qRT-PCR quantification of lentiviral transfer vector gene expression and resistance to corresponding antibiotics. Antibiotics were removed from culture medium after confirmation of successful integration. The sequence of sgRNAs used in this study is described in Table 2.

Quantitative reverse transcription PCR (qRT-PCR)

To quantify mRNA expression levels, approximate 1×10^5 B16F10-TDM, B16F10 TDMa, or 1.5×10^5 MCF7-TDMa cells were seeded in 12 well plate on day 0. From day 1, cells were stimulated with 20ng ml^{-1} of mouse interferon-γ (mIFN-γ) (BioLegend, San Diego, CA, USA, cat. 575302) or left unstimulated for 24 h. Subsequently, cells were homogenized in Sepasol (Nacalai, cat. 09379-55) and total RNA was extracted according to manufacturer's instructions. RNA was reverse transcribed into cDNA using ReverTra Ace qPCR RT Master Mix (Toyobo, Osaka, Japan, cat. FSQ-301), and qRT-PCR was performed using THUNDERBIRDTM SYBR qPCR Mix reagent (Toyobo, cat. QPS-201) in StepOne qRT-PCR instrument (Life Technologies). Mouse or human *Nlrc5/NLRC5, H2-K^b, H2-D^b, HLA-A, HLA-B, HLA-C, Lmp2/LMP2, Tap1/TAP1, B2m/B2M, Ciita/CIITA, Mx1/MX1* and *Gapdh/GAPDH* were amplified by specific primers. *Gapdh/GAPDH* was used to normalize the value and relative gene expression level was calculated as fold change compared with the control samples using 2^(ΔΔCt) method. The sequence of primers used for qRT-PCR in this study is described in Table 2.

Flow cytometry

To evaluate surface MHC class I expression levels *in vitro*, 5×10^4 B16F10-TDM, B16F10-TDMa or 1×10^5 MCF7-TDMa cells were seeded in 12-well plates and incubated for 48 h with or without 20 ng ml-1 of mIFN-γ stimulation. Subsequently, cells were detached by trypsinization and resuspended in FACS buffer (2% FBS in PBS). Next, cells were stained by FITC H2-K^b/D^b antibody (BioLegend, cat. 114605,

RRID:AB_313596) and MCF7 was stained by PE HLA-A,B,C (BioLegend, cat. 311405, RRID:AB_314874) for 30 min on ice. Stained cells were washed twice and resuspended in FACS buffer and acquired by FACSCanto II.

To characterize tumor-infiltrating lymphocytes (TILs) and cancer cells *in vivo*, tumors were fragmented by scissors and filtered through a 70 μm cell strainer (AS ONE, Osaka, Japan, cat. VCS-70) to generate single cell suspension. Red blood cells were lysed for 5 min on ice in 1 ml ammonium-chloride-potassium (ACK) lysis buffer (Life Technologies, cat. A1049201).

To distinguish alive cells, 3×10^6 dissociated tumor cells were stained by 100 μl Zombie Violet Fixable Viability dye (1:1000 dilution in PBS; BioLegend, cat. 423113) at 25℃ for 15 min. Subsequently, tumor cells were aliquoted into two tubes for characterization of TILs (2×10^6) or tumor cells (1×10^6).

To characterize TILs, Zombie dye-stained cells were further stained with the following antibodies (all from BioLegend, 1:100 dilution): APC-Cy7 CD45.2 (cat. 109824, RRID:AB_830789), FITC CD4 (cat. 100405, RRID:AB_312690), APC CD8a (cat. 100712, RRID:AB_312751), PE IFN-γ (cat. 505808, RRID:AB_315402), and PerCP-cy5.5 CD44 (cat. 103032, RRID:AB_2076204). Cells were incubated with antibodies for surface markers in 100 μl FACS buffer on ice for 30 min. Subsequently, cells were fixed by incubating with 4% PFA for 15 min on ice, and then permeabilized with 1× intracellular staining permeabilization wash buffer (BioLegend, cat. 420801) according to manufacturer's instructions. Subsequently, cells were incubated with PE IFN-γ antibody in 100 μl 1× intracellular staining buffer for 30 min on ice.

To quantify MHC class I and PD-L1 levels in tumor cells *in vivo*, 1×10^6 Zombie dye-stained cells were further stained with APC-Cy7 CD45.2, FITC H-2K^b/D^b, and PE PD-L1 (cat. 124308, RRID:AB_2073556), in the same manner as TILs surface marker staining.

Samples were acquired using an BD FACS Canto II flow cytometer. Specific antibody binding was ensured by staining with corresponding isotype antibodies. Collected data were analyzed using FlowJo v10.6.2. (BD).

Assessment of DNA methylation level

Cells were digested by proteinase K (Fujifilm Wako Pure Chemical Corp, Osaka, Japan, cat.161-28701) overnight, subsequently, genomic DNA was extracted by ethanol precipitation and residual RNA was removed by incubating with RNase A (10 μg ml^{-1}, NIPPON GENE, Tokyo, Japan, cat. 313-01461) for 30 min at 37℃. Bisulfite conversion and purification was performed using 500 ng of genomic DNA with EZ DNA Methylation Kit (Zymo Research, Irvine, CA, USA, cat. D5001) according to

manufacturer's instructions. Fragment of human and mouse *NLRC5* promotor region in the converted genomic DNA was amplified by PCR using AmpliTaq Gold 360 Master Mix (Life Technologies, cat. 4398876) and specific primers. PCR products were either sequenced directly or cloned into pBlueScript II SK(+) by SLiCE method (Zhang *et al.*, 2012) before sanger sequencing. For direct sanger sequencing of PCR product, percentage of methylated cytosine was calculated by (fluorescence intensity of guanine)/(fluorescence intensity of guanine + thymine) in the cytosine of CpG dinucleotides. The sequence of primers used to amplify bisulfite converted DNA by PCR in this study is described in Table 2.

Isolation of OT-I CD8+ T cells from spleen

Spleen from 7-10 weeks old OT-I transgenic mice were dissociated by slide glass. Single cell suspension was generated by passing cells through 48 μm mesh (San-web, Tokyo, Japan, cat. 91-1189). Red blood cells (RBCs) were lysed by incubation in ACK lysing buffer for 5 min on ice. Subsequently, OT-I CD8+ T cells were isolated by positive selection using BD IMag system (BD, Franklin Lakes, NJ, USA, magnet: cat. 552311; CD8a Particles: cat. 551516) according to manufacturer's instruction and used for co-culture experiments.

OT-I T cell activation assay

B16F10-TDM sgScramble and sg*Nlrc5* or B16F10-TDMa sgScramble or sg*Nlrc5* cells were seeded at 3×10^4 or 6×10^4 cells per well in 48-well plate and loaded with 0, 1, and 2 or 0, 0.0625, 0.125, 0.25, 0.5, and 1 μg ml^{-1} of Ovalbumin (OVA) peptide (257-264) SIINFEKL (PEPTIDE INSTITUTE, Osaka, Japan, cat. POV-3659-PI) overnight. Unbound OVA peptides were washed away with PBS the next day. Isolated OT-I CD8+ T cells were added at 2×10^5 or 3×10^5 per well to each well and co-cultured with B16F10 cells for 26 h in total. Monensin (Life Technologies, cat. 00-4505-51) was treated to each well at concentration of 2 μM to accumulate intracellular cytokine for 6 h before harvest. Cells were resuspended in PBS and stained by 1:1000 Zombie violet viability dye (BioLegend, cat. 423113) for 15 min at room temperature followed by surface marker staining by APC CD8 and FITC CD69 (Life Technologies, cat. 11-0691-82) for 30 min on ice. Subsequently, cells were fixed by 4% paraformaldehyde phosphate buffer (PFA, Nacalai, cat. 09154-85) on ice for 15 min. Next, cells were permeabilized by 1x permeabilization buffer (BioLegend, cat. 421002) according to manufacturer's instruction. Finally, cells were stained by PE IFN-γ for 30 min in 1x permeabilization buffer on ice. After washing, samples were acquired by FACSCanto II.

OT-I T cell killing assay

B16F10-TDMa sgScramble and sg*Nlrc5* cells were stained by 5 μM carboxyfluorescein diacetate succinimidyl ester (CFSE, Tonbo Biosciences, 13-0850-U500) for 10 min in the dark and seeded at 2.5×10^4 cells per well in 48-well plate. Cells were loaded with 0.5 μg ml^{-1} of OVA peptide overnight. Unbound OVA peptides were washed away with PBS. Purified OT-I CD8+ T cells were added to the media at OT-I:B16 ratio of 10:1, 5:1, 2.5:1, and 1.25:1 and co-cultured for additional 48 h. Cells were detached by trypsinization and stained by 1:1000 PBS diluted Zombie Violet for 15 min at room temperature. After washing, samples were acquired by FACSCanto II.

Subcutaneous B16F10 melanoma model

To investigate the effect of targeted demethylation and activation of *Nlrc5* on tumor growth *in vivo*, female and male C57BL/6 or NUDE mice were subcutaneously injected with 3×10^5 or 5×10^5 of B16F10-TDMa sgScramble and sg*Nlrc5* cells in 100uL PBS in the left flank using 26G needle and 1 ml syringe. Tumor volume was estimated daily or every 2 d by digital caliper after tumors were visually apparent and tumor volume was calculated by Tumor Volume (mm3) = length × width × width /2 (Tomayko *et al.*, 1989). Mice were euthanized on day 18 for C57BL/6 or day 15 for NUDE mice and tumor was harvested and used for flow cytometry, RNA-seq, and immunohistochemistry analysis.

To investigate the effect of targeted demethylation and activation of *Nlrc5* on efficacy of anti-PD-1 treatment *in vivo*, female and male C57BL/6 mice were implanted with 6×10^5 of B16F10-TDMa sgScramble and sgNlrc5 cells similarly as described above. Subsequently, mice were randomly divided into isotype and PD-1 groups. Each group was intraperitoneally injected with 250 μg/100uL of isotype control (leinco, Fenton, MO, USA, cat. I-1177, RRID:AB 2737530) or anti-PD-1 antibody (leinco, cat. P362, RRID:AB_2737557) every 2 days from day 3, for total of 5 times. Tumor volume was estimated every 2 days from day 3 similarly as described above. Mice were euthanized on day 15 in sgScramble and day 18 in sg*Nlrc5* group and tumors were harvested for flow cytometry analysis.

Immunohistochemistry (IHC)

B16F10-TDMa sgScramble and sg*Nlrc5* tumors were snap frozen by liquid nitrogen immediately after harvest and kept until IHC analysis. Tumors were fixed in 10% formalin, dehydrated with increasing concentrations of ethanol, and then impregnated with and embedded in paraffin. Tissue blocks were sectioned and deparaffinized in xylene, washed in PBS (pH 7.4), and rehydrated in a graded series of ethanol solutions for hematoxylin and eosin (H&E) staining with a standard protocol. For IHC, heat-

mediated antigen retrieval was performed in Tris/EDTA buffer (pH 9.0) at 97 °C for 20 min. The sections were treated with 0.3% hydrogen peroxidase for 5 min to quench endogenous peroxidase activity. After saturation with serum, primary antibody of anti-CD8 (1:300 dilution, 4℃ overnight incubations; Cell Signaling, Danvers, MA, USA, cat. 98941, RRID:AB_2756376) and anti-CD3 (1:75 dilution, 25℃ 60 min incubations; GeneTex, Irvine, CA, USA, cat. GTX16669, RRID:AB_425123) were used for staining. After washing in PBS, slides were incubated with biotinylated goat anti-rabbit immunoglobulin antibody for 30 min at room temperature. Visualization of antibody specific binding were performed with freshly prepared 3,3′-diaminobenzidine tetrahydrochloride. The intensity of the staining was analyzed by HistoQuest software (TissueGnostics, Vienna, Austria). Sites with representative staining were selected in the tumor center and invasive margin of tumors and staining intensity was calculated by ImageJ (Schneider *et al.*, 2012).

Analysis of methylation status of the *NLRC5* promoter in human melanoma

DNA methylation profile of human nonmalignant skin tissue and breast tissue were accessed through Gene Expression Omnibus (GEO; Accession number: GSE51954, GSE88883) (Barrett *et al.*, 2012, Vandiver *et al.*, 2015, Johnson *et al.*, 2017). DNA methylation and transcriptome profiles of melanoma tissue from the Cancer Genome Atlas skin cutaneous melanoma (TCGA SKCM) cohort and breast invasive carcinoma (TCGA BRCA) cohort were obtained from UCSC XENA (Cancer Genome Atlas, 2012, Cancer Genome Atlas, 2015, Goldman *et al.*, 2020). Immune cell infiltration estimation of TCGA SKCM and BRCA cohorts was from TIMER (Li *et al.*, 2016). CpG sites of cg08159663, cg07839457, and cg16411857 in *NLRC5* promoter from HumanMethylation450 BeadChip (illumina, San Diego, CA, USA) were methylated in melanoma and breast cancer tissues, therefore, their β values were averaged to represent *NLRC5* promoter methylation levels. The mean *NLRC5* methylation level was used in the correlation analysis with *NLRC5* expression and estimated immune cells infiltration levels.

RNA sequencing

Total RNA was extracted using Sepasol according to the manufacturer's instructions and assessed for RNA Integrity Number using Agilent 2100 Bioanalyzer (Agilent Technologies, Santa Clara, CA, USA). Poly(A)-tailed mRNA was selected with beads using the NEBNext Poly(A) mRNA Magnetic Isolation Module (NEB, cat. E7490). RNA-seq libraries were prepared using the NEBNext Ultra II Directional RNA Library Prep Kit (NEB, cat. E7760) according to the manufacturer's instructions. Sequencing

of 150 nucleotide-long paired-end reads was performed on the NovaSeq 6000 (illumina).

The sequencing data were aligned to mouse genome (GRCm39/mm39) using STAR aligner (v2.7.10a) (Dobin *et al.*, 2013). Raw gene counts were obtained by STAR --quantMode GeneCounts option and loaded into R (v4.2.1) for data normalization and differential expression analysis by DESeq2 (v1.36)(Love *et al.*, 2014). Genes with adjusted $p < 0.05$ (Benjamini–Hochberg method) and $|\text{Fold change}| > 2$ were considered significantly differentially expressed. Gene ontology (GO) enrichment analysis was performed using clusterProfiler (Yu *et al.*, 2012). The false discovery rate (FDR) < 0.001 and the normalized enrichment score $|\text{NES}| > 2$ was considered as significantly altered pathway.

Statistical analysis

For *in vivo* tumor growth analysis, significance was analyzed using 2-way ANOVA test. For others, significance was analyzed using either Fisher's LSD test or two-tailed unpaired Student's t-test. A *p*-value of less than 0.05 was regarded as statistically significant. Error bars represents mean values ±SEM in tumor growth curve and ±SD in others. All statistical analyses were performed using GraphPad Prism software (v9.3.1).

Data availability statement

DNA methylation and RNA-Seq gene expression data from TCGA SKCM and BRCA were accessed through UNSC XENA at https://xenabrowser.net/datapages/(Cancer Genome Atlas, 2012, Cancer Genome Atlas, 2015, Goldman *et al.*, 2020). Codes used for RNA-Seq data process and part of figures were deposited to GitHub at https://github.com/firemanzzzz/Demethylation_Nlrc5.

Table 2 Sequence of PCR primers and sgRNAs used in Chapter 2. Bold and underbar sgRNAs were selected as sg*NLRC5*s or sg*Nlrc*5.

Names	Purpose	Sequence (5'-3', without NGG)
Scramble	Scramble control sgRNA	GGAGACGGGATACCGTCTCT
mNlrc5 #1	Mouse *Nlrc5* targeting sgRNA	GAACTTTCCAGGGCTGACGC
mNlrc5 #2	Mouse *Nlrc5* targeting sgRNA	CCTAGGCAACCCTTGCACCC
mNlrc5 #3	Mouse *Nlrc5* targeting sgRNA	CCTGGAGGCCGCGCTTGTCC
mNlrc5 #4	Mouse *Nlrc5* targeting sgRNA	CTTCATCCTACATCGTCTCT
mNlrc5 #5	Mouse *Nlrc5* targeting sgRNA	CTGCGATCTCCAAGCCGCGG
mNlrc5 #6	Mouse *Nlrc5* targeting sgRNA	TCAGTTTCCACAGAGCGCGG
mNlrc5 #7	Mouse *Nlrc5* targeting sgRNA	GATAGACAAACGGACTGAG
hNLRC5 #1	Human *NLRC5* targeting sgRNA	CACCGGATGAGTATGTCCAG
hNLRC5 #2	Human *NLRC5* targeting sgRNA	ATCCAACCCAGTCCCCACTG
hNLRC5 #3	Human *NLRC5* targeting sgRNA	TCGGACCCAAGGACAGTCCC
hNLRC5 #4	Human *NLRC5* targeting sgRNA	CAGGCATCACCCTATGTTCC
hNLRC5 #5	Human *NLRC5* targeting sgRNA	GGTGAAGGTCGGCTCACATG
hNLRC5 #6	Human *NLRC5* targeting sgRNA	CAGTTTCCCGTCCACGAAAG
BSP_*mNlrc5*_SLiCE_Fw	Cloning based bisulfite sequencing	CGGTATCGATAAGCTTGATATCTTGTATTTAGGGATTA GTAGAGAT
BSP_*mNlrc5*_SLiCE_Re	Cloning based bisulfite sequencing	CGGGCTGCAGGAATTCGATATCCATACCTCTCTAACTA CTAAAACTAAAT
BSP_m*Nlrc5* _Fw	Direct bisulfite sequencing	TGTAGAATTTGGAATAGAGATAGGAATT
BSP_m*Nlrc5* _Re	Direct bisulfite sequencing	CATACCTCTCTAACTACTAAAACTAAAT
BSP_h*NLRC5*_ SLiCE_Fw	Cloning based bisulfite sequencing	ATAAGCTTGATATCGAATTCAGGTATTGAGATAGGGTT TTGG
BSP_h*NLRC5*_ SLiCE_Re	Cloning based bisulfite sequencing	CCCCCGGGCTGCAGGAATTCCTCCRCCAATACATAAA ACTAA
BSP_h*NLRC5*_ Fw	Direct bisulfite sequencing	AGGTATTGAGATAGGGTTTTGG
BSP_h*NLRC5*_Re	Direct bisulfite sequencing	CTCCRCCAATACATAAAACTAA
*Nlrc5*_Fw	qRT-PCR; Mouse	CTTCCCGCCTCTCCTTCCACAAT
*Nlrc5*_Re	qRT-PCR; Mouse	CTCCACCTGCCCACATCCTACCA
*H2-K^b*_Fw	qRT-PCR; Mouse	GGCAATGAGCAGAGTTTCCGAG
*H2-K^b*_Re	qRT-PCR; Mouse	CCACTTCACAGCCAGAGATCAC
*H2-D^b*_Fw	qRT-PCR; Mouse	CCCTGTGAGCTTGGGTTCAG
*H2-D^b*_Re	qRT-PCR; Mouse	ACAGGGCAGTGCAGGGATAG

*Psmb9*_Fw	qRT-PCR; Mouse	CATGAACCGAGATGGCTCTAGT
*Psmb9*_Re	qRT-PCR; Mouse	TCATCGTAGAATTTTGGCAGCTC
*Tap1*_Fw	qRT-PCR; Mouse	GACTCCTTGCTCTCCACTCAGT
*Tap1*_Re	qRT-PCR; Mouse	AACGCTGTCACCGTTCCAGGAT
*B2m*_Fw	qRT-PCR; Mouse	ACAGTTCCACCCGCCTCACATT
*B2m*_Re	qRT-PCR; Mouse	TAGAAAGACCAGTCCTTGCTGAAG
*Ciita*_Fw	qRT-PCR; Mouse	CCCTGCGTGTGATGGATGTC
*Ciita*_Re	qRT-PCR; Mouse	ATCTCAGACTGATCCTGGCAT
*Mx1*_Fw	qRT-PCR; Mouse	CCAAAAACAAGAGACCATCAACCT
*Mx1*_Re	qRT-PCR; Mouse	CTCAGAGCCTCTGTGGTAGCAA
*NLRC5*_Fw	qRT-PCR; Human	CTGGCCAGTCTCACCGCACAA
*NLRC5*_Re	qRT-PCR; Human	CCAGGGGACAGCCATCAAAATC
*HLA-A*_Fw	qRT-PCR; Human	AAAAGGAGGGAGTTACACTCAGG
*HLA-A*_Re	qRT-PCR; Human	GCTGTGAGGGACACATCAGAG
*HLA-B*_Fw	qRT-PCR; Human	CTACCCTGCGGAGATCA
*HLA-B*_Re	qRT-PCR; Human	ACAGCCAGGCCAGCAACA
*HLA-C*_Fw	qRT-PCR; Human	GGAGACACAGAAGTACAAGCGC
*HLA-C*_Re	qRT-PCR; Human	ACATCCTCTGGAGGGTGTGAGA
*PSMB9*_Fw	qRT-PCR; Human	CGTTGTGATGGGTTCTGATTCC
*PSMB9*_Re	qRT-PCR; Human	GACAGCTTGTCAAACACTCGGTT
*TAP1*_Fw	qRT-PCR; Human	AGGGCTGGCTGGCTGCTTTGA
*TAP1*_Re	qRT-PCR; Human	ACGTGGCCCATGGTGTTGTTAT
*B2M*_Fw	qRT-PCR; Human	TGCTGTCTCCATGTTTGATGTATCT
*B2M*_Re	qRT-PCR; Human	TCTCTGCTCCCCACCTCTAAGT
*CIITA*_Fw	qRT-PCR; Human	ACAGAGCACCAAGACAGAGC
*CIITA*_Re	qRT-PCR; Human	CTCTGAGAGCTGGCACACTG
*dCas9*_Fw	qRT-PCR, Transduction validation	AACCTATGCCCACCTGTTCG
*dCas9*_Re	qRT-PCR, Transduction validation	AGGATTGTCTTGCCGGACTG
*MS2*_Fw	qRT-PCR, Transduction validation	TGGATCAGCTCCAACTCACG
*MS2*_Re	qRT-PCR, Transduction validation	TGTCTGGGTAGCCACTTTGG
*TET1*_Fw	qRT-PCR, Transduction validation	AGAAAGAAGCAGCACTCCCC
*TET1*_Re	qRT-PCR, Transduction validation	TTCGCCAAGCTGTGAAATGC

Chapter 2: Results

- **Hypermethylation of *NLRC5* promoter correlates with less inflamed tumor microenvironment.**

NLRC5 transactivates the expression of MHC class I and related genes and *NLRC5* promoter hypermethylation is correlated with reduced expression of MHC class I and related genes in melanoma and breast cancer patients (Meissner *et al.*, 2010, Yoshihama *et al.*, 2016). We compared *NLRC5* promoter methylation levels between normal tissues in skin and breast and cancer tissues in melanoma and breast cancer. We found that CpG sites of cg08159663, cg16411857, and cg07839457 in *NLRC5* promoter is hypermethylated in melanoma and breast cancer compared with normal tissues (Figure 12a). We took the mean β value of these CpG sites to represent *NLRC5* promoter methylation levels and performed correlation analysis with *NLRC5* expression levels. We found that *NLRC5* methylation levels negatively correlated with *NLRC5* expression levels (Figure 12b). Since antigen presentation through MHC class I in cancer is essential for specific killing by cytotoxic T cells (Jhunjhunwala *et al.*, 2021), we wondered whether *NLRC5* methylation levels is associated with the abundance of tumor infiltrating immune cells. We performed correlation analysis between mean *NLRC5* methylation levels and estimated immune cell infiltration scores generated by TIMER (Li *et al.*, 2016). We found that *NLRC5* methylation levels negatively correlated with immune cell infiltration scores, while *NLRC5* expression levels are positively correlated with estimated immune cell infiltration scores in melanoma and breast cancer (Figure 12c). These results indicate that *NLRC5* promoter is hypermethylated and *NLRC5* methylation levels are correlated with host cell infiltration in melanoma and breast cancer.

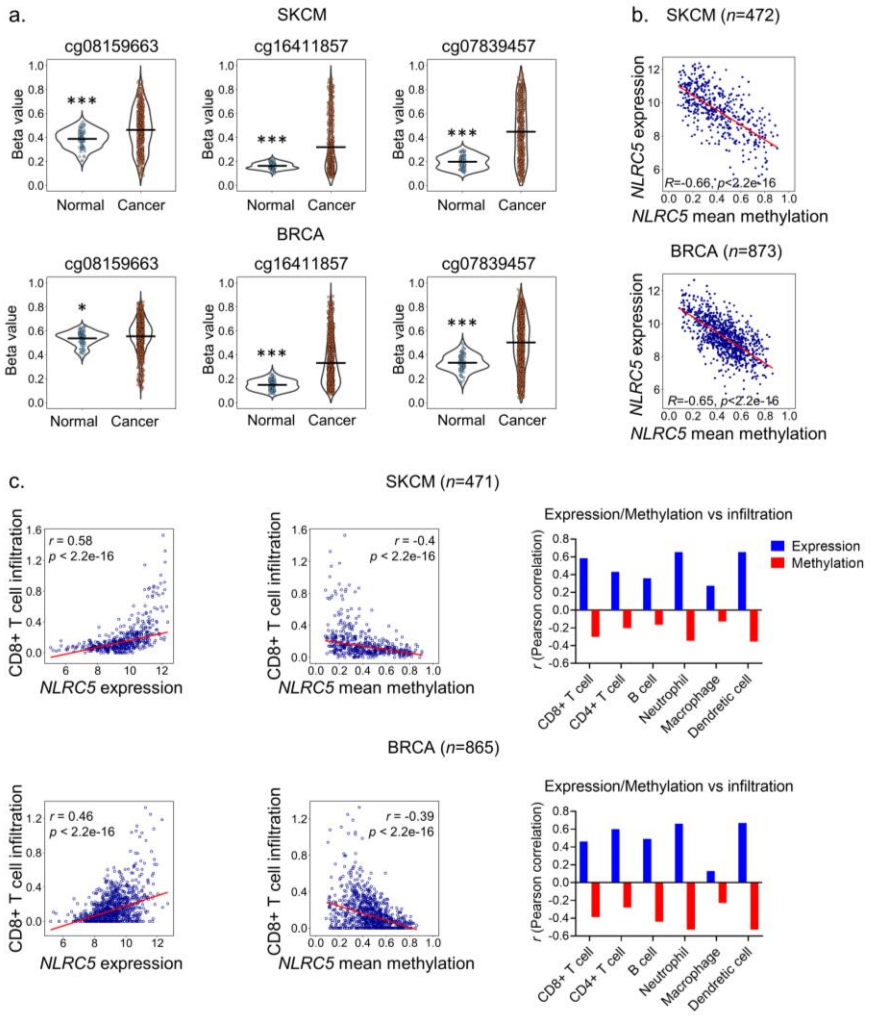

Figure 12 Hypermethylation of the NLRC5 promoter negatively correlates with NLRC5 expression and immune cell infiltration.

(a.) The DNA methylation status of *NLRC5* promoter was compared between normal skin (*n*=78) and melanoma tissues (SKCM) (*n*=475), or normal breast (*n*=100) and breast adenocarcinoma tissues (BRCA) (*n*=888) using representative CpG sites (cg08159663, cg16411857, and cg07839457) of *NLRC5* promoter.

(b.) Scatter plot showing the correlation between mean methylation level of *NLRC5* promoter (cg08159663, cg16411857, and cg07839457) and *NLRC5* expression levels in melanoma and breast adenocarcinoma tissue.

(c.) Correlations analysis was performed between *NLRC5* expression levels or mean *NLRC5* methylation levels and estimated immune cell infiltration scores in melanoma and breast adenocarcinoma tissue. (Left) The correlation of *NLRC5* expression or methylation levels with estimated CD8+ T cell infiltration scores. (Right) *r* (Pearson correlation coefficient) value of *NLRC5* expression or

methylation levels with estimated immune cell infiltration scores.
'*n*' stands for number of patients. Statistical significance was determined by unpaired two-sided student's *t*-test in (a.). * $p < 0.05$; *** $p < 0.001$. Pairwise correlations in (b, c) were calculated using the Pearson correlation test.

- **Targeted demethylation of *Nlrc5* promoter in B16F10 increased *Nlrc5* expression but failed to significantly enhance immunogenicity.**

NLRC5 promoter methylation status is correlated with the amount of tumor infiltrating immune cells. Therefore, we hypothesized that demethylation of *NLRC5* promoter in cancer is a potential therapeutic approach that promote immune cell infiltration by increasing the expression of *NLRC5* and dependent MHC class I and related genes. To test, we selected poorly immunogenic mouse melanoma B16F10 cell line with low MHC class I expression levels (Wang *et al.*, 1998). We evaluated the methylation status of *Nlrc5* promoter and shown that *Nlrc5* promoter is methylated in B16F10 (Figure 13a). To induce targeted demethylation in *Nlrc5* promoter, we replaced transcription activators in CRISPR/dCas9 based SAM system (Konermann *et al.*, 2015) with a methylcytosine dioxygenase TET1cd, which is referred to as TDM (targeted demethylation) system (Figure 13b). Previous similar approaches successfully induced targeted demethylation (Choudhury *et al.*, 2016, Liu *et al.*, 2016, Xu *et al.*, 2016, Liu *et al.*, 2018). We stably transduced TDM system into wild type B16F10 and named the stable cell line as B16F10-TDM. We optimized *Nlrc5*-targeting sgRNA by quantifying *Nlrc5* mRNA induction by each sgRNA. Non-targeting scramble sgRNA was transduced as control, which is referred to as sgScramble. SgRNA #4 shown the highest *Nlrc5* mRNA induction and was referred to as sg*Nlrc5* (Figure 13c). Quantification of mRNA levels by qRT-PCR showed that TDM-sg*Nlrc5* expressed higher levels of *Nlrc5* and dependent MHC class I and related genes, including *H2-K^b, H2-D^b, Psmb9, Tap1*, and *B2m*, but not in unrelated gene *Ciita* with or without IFN-γ stimulation (Figure 13d). To characterize the transcriptome profile, we performed RNA-Seq analysis on TDM-sgScramble and TDM-sg*Nlrc5* cells without IFN-γ stimulation. *Nlrc5* was identified as one of the significantly upregulated genes, but not in *Nlrc5* dependent MHC class I and related genes in TDM-sg*Nlrc5* (Figure 13e). Surface MHC class I levels were increased in TDM-sg*Nlrc5* with or without IFN-γ stimulation (Figure 13f, Figure 14a). We confirmed successful demethylation of *Nlrc5* promoter as methylated cytosine were completely removed in TDM-sg*Nlrc5* (Figure 13g).

Next, we investigated whether tumor immunogenicity was increased in TDM-sg*Nlrc5*. OVA peptide was loaded at 0-2 μg ml^{-1} in B16F10-TDM cells and co-cultured with OVA-specific OT-I CD8+ T cells. TDM-sg*Nlrc5* cells showed higher proportion of activated IFN-γ+ and CD69+ OT-I T cells only when loaded with high dose (2 μg ml^{-1}) of OVA peptide loading (Figure 13h; Figure 14b; Figure 15a). These results indicate that demethylation of *Nlrc5* promoter can increase MHC class I expression but unable to significantly enhance tumor immunogenicity towards CD8+ T cells in

B16F10.

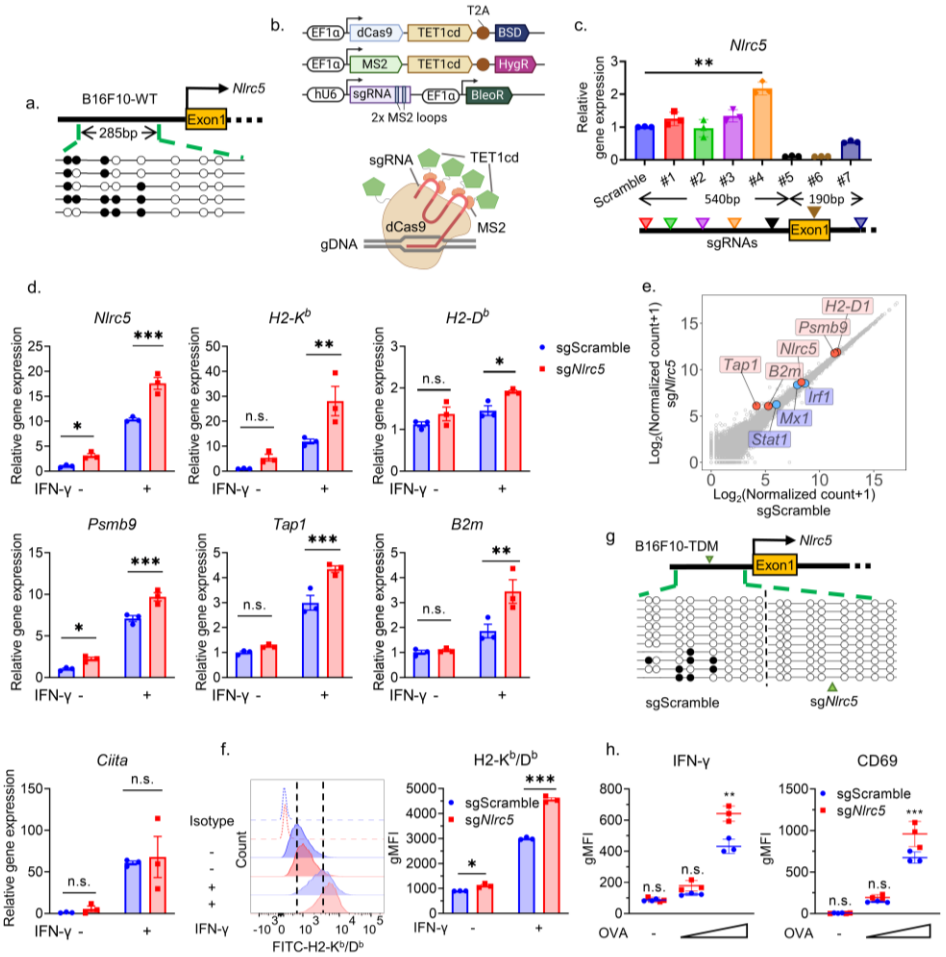

Figure 13 Demethylation of the *Nlrc5* promoter by the TDM system induced MHC class I expression in B16F10.

(a) DNA methylation status of the *Nlrc5* promoter in B16F10 cells was determined by bisulfite PCR analysis. CpG dinucleotides are shown as white or black circles to represent unmethylated or methylated CpG dinucleotides. Each row represents an individual plasmid clone of total 5 clones.

(b) Schematic illustrations of (Upper) main components in the lentiviral vectors of the TDM system, and (Lower) assembled components of the TDM system at the *Nlrc5* promoter.

(c) (Upper) Scramble or *Nlrc5* promoter targeting sgRNA was stably transduced in B16F10-TDM cells and the mRNA expression level of *Nlrc5* was quantified by qRT-PCR. Relative gene expression levels were determined by 2^(–ΔΔCT) method using *Gapdh* as a reference gene. (Lower) A schematic diagram of sgRNA targeting sites at *Nlrc5* promoter, with colored triangular signs indicating each sgRNA target site corresponding to the upper plot.

(d) The mRNA expression levels of *Nlrc5*, *H2-K*^{b}, *H2-D*^{b}, *Psmb9*, *Tap1*, *B2m,* and

Ciita in B16F10-TDM sgScramble and sg*Nlrc5* cells were quantified by qRT-PCR with or without IFN-γ stimulation. Relative gene expression levels were determined by 2^(–ΔΔCT) method using *Gapdh* as a reference gene.

(e) The mRNA gene expression levels by RNA-Seq in $\log_2$(Normalized Count+1) values of B16F10-TDM sgScramble were compared with sg*Nlrc5* cells. Marked genes are *Nlrc5* and dependent MHC class I and related genes (in red), and *Nlrc5* transcription activator *Stat1*, *Irf1*, and unrelated control *Mx1* (in blue). The average from $n = 2$ is shown.

(f) Surface H2-K^b/D^b expression levels in B16F10-TDM sgScramble and sg*Nlrc5* cells were quantified by flow cytometry with or without IFN-γ stimulation. (Left) Representative histogram. (Right) Geometric MFI.

(g) DNA methylation status of the *Nlrc5* promoter in B16F10-TDM sgScramble and sg*Nlrc5* cells was determined by bisulfite PCR analysis. Ten clones were analyzed per group. Triangle sign indicates *sgNlrc5* targeting site.

(h) B16F10-TDM sgScramble and sg*Nlrc5* cells were pulsed with 0, 1, or 2μg ml^{-1} of OVA peptide overnight and co-cultured with OT-I T cells for 24 h. Intracellular IFN-γ and surface CD69 expression levels in OT-I T cells were quantified by flow cytometry.

Values in bar plots are mean ±SD. For (c, d, f, h), $n = 3$, for (e) $n = 2$ in each group; '*n*' stands for number of biological replicates. Statistical significance was determined by unpaired two-sided student's t-test (c) or Fisher's LSD test (d, f, h). n.s., not significant; * $p < 0.05$; ** $p < 0.01$; *** $p < 0.001$.

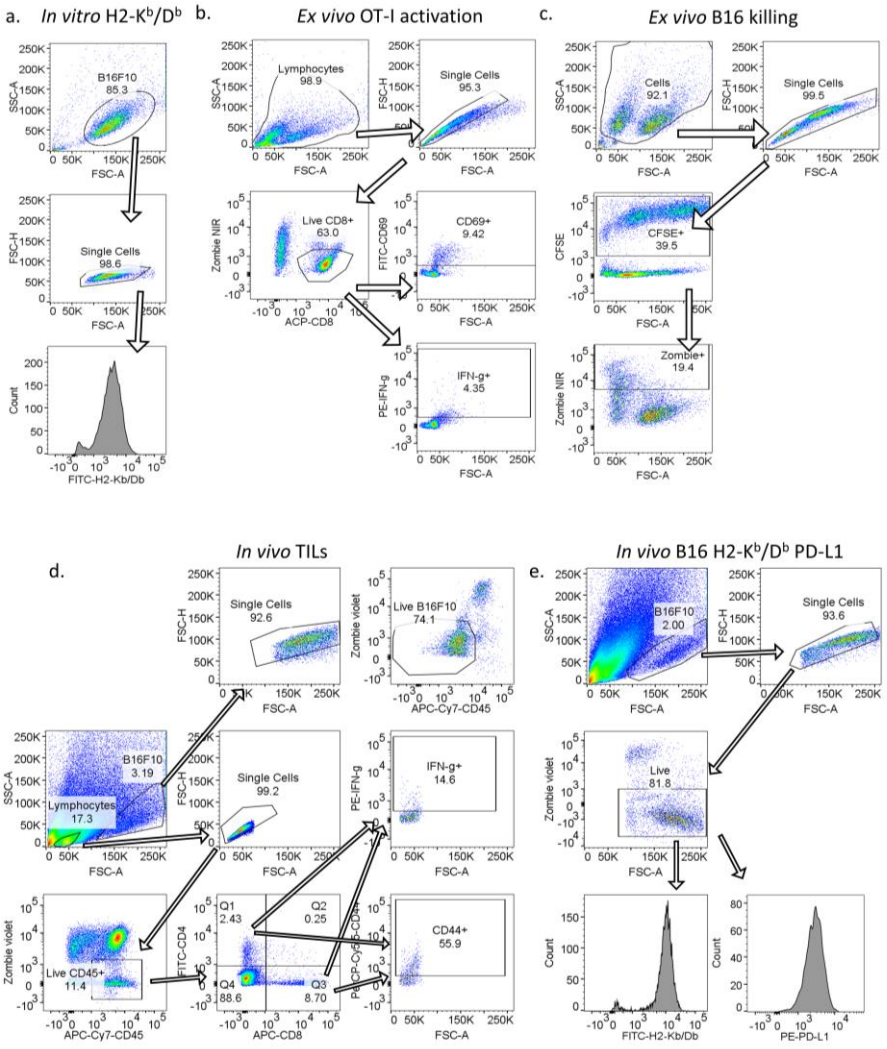

Figure 14 Gating strategy for flow cytometry analysis.

(a.) Quantification of MHC class I levels on B16F10 and MCF7 cell lines *in vitro*. Corresponding to Figure 13f, Figure 16d, and Figure 24e. Cultured cells were gated by size using FSC-A and SSC-A and singlets were gated by FSC-A and FSC-H.

(b.) Characterization of OT-I T cells activation status in co-culture *ex vivo*. Corresponding to Figure 13h, Figure 16f, and Figure 15a, Figure 15b. Live OT-I T cells were gated by FSC-A, SSC-A, FSC-H, Zombie NIR–, and CD8+. Activated OT-I T cells were gated as IFN-γ+ and CD69+.

(c.) Quantification of dead B16F10-TDMa cells in co-culture with OT-I T cells *ex vivo*. Corresponding to Figure 16g and Figure 15c. CSFE labeled B16F10-TDMa cells were gated as FITC+. Dead cells were gated as Zombie NIR+.

(d.) Characterization of tumor infiltrating lymphocytes and quantification of viable B16F10 cells *in vivo*. Corresponding to Figure 17e, Figure 22d, and Figure 18,

Figure 23. Single live nucleated hematopoietic cells were gated based on FSC-A, SSC-A, SSC-H, Zombie NIR–, and CD45+ signals. Subsequently, CD4+ or CD8+ T cells were gated by CD4+ or CD8+, followed by gating IFN-γ+ and CD44+ cells to identify activated/memory lymphocytes. Single B16F10-TDMa cells were determined by FSC-A, SSC-A, SSC-H, and viable B16F10-TDMa cells were determined as Zombie NIR– and CD45–.

(e.) Quantification of H2-K^b/D^b and PD-L1 levels on B16F10 cells *in vivo*. Corresponding to Figure 17f and Figure 22e. Single live B16F10 cells were gated by FSC-A, SSC-A, SSC-H, Zombie NIR–, and CD45–.

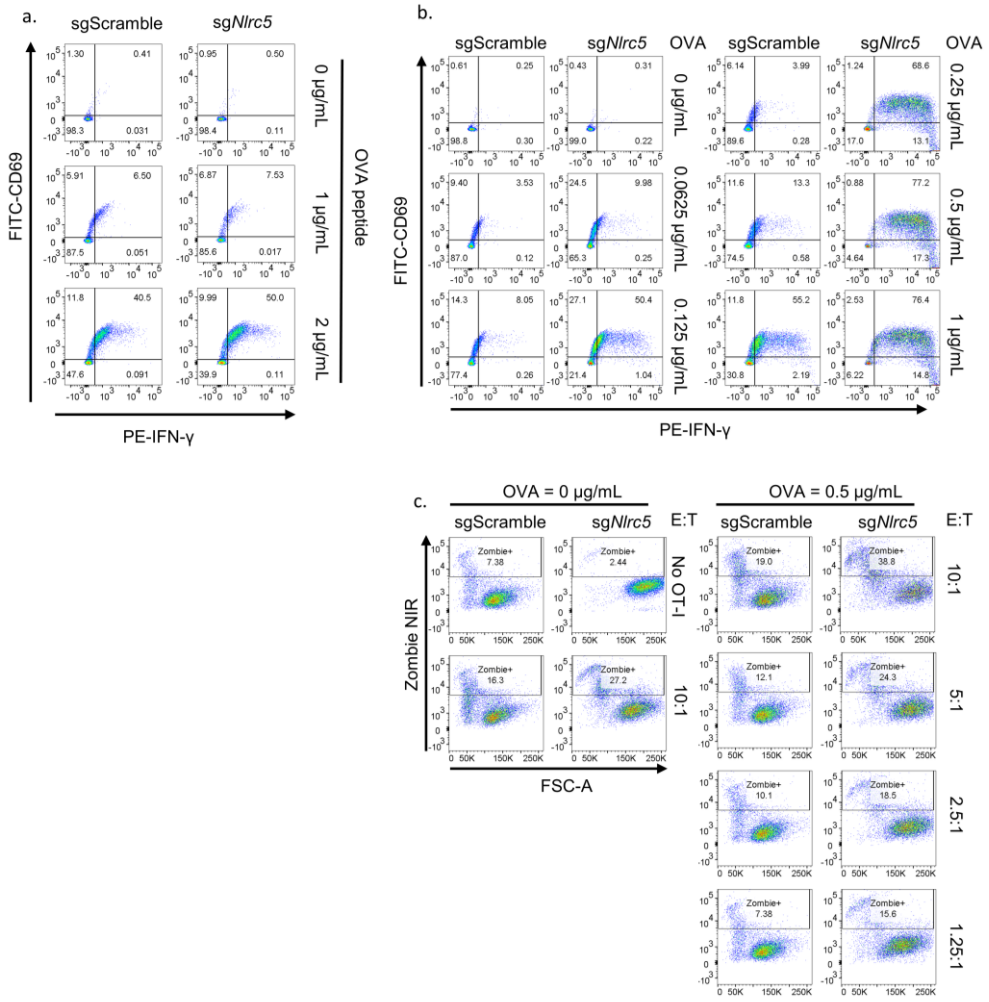

Figure 15 Representative scatter plots by flow cytometry analysis in ex vivo co-culture experiments.

OT-I CD8+ T cells were co-cultured with B16F10-TDM and B16F10-TDMa cells stably transduced with sgScramble or sg*Nlrc5*. IFN-γ and CD69 expression levels of OT-I T cells was evaluated by flow cytometry when co-cultured with (a) B16F10-TDM, and (b) B16F10-TDMa cells, corresponding to Figure 13h, Figure 16f. (c) CFSE labeled B16F10-TDMa sgScramble or sg*Nlrc5* cells were co-cultured with OT-I T cells and dead B16F10-TDMa cells were quantified by CFSE+ Zombie NIR+, corresponding to Figure 16g.

- **Targeted demethylation and activation of *Nlrc5* enhanced B16F10 immunogenicity.**

Since demethylation of *Nlrc5* promoter in B16F10 was insufficient to significantly increase tumor immunogenicity, we sought to improve *Nlrc5* activation efficacy by adding activators to TDM system. To do that, we directly inserted TET1cd in the SAM system without removing activation motifs, VP64, P65, and HSF1 (Figure 16a). The modified system is referred as TDMa (Targeted demethylation and activation) system. We stably transduced TDMa system into B16F10 and generated B16F10-TDMa cell line. Next, non-targeting control sgRNA, sgScramble and *Nlrc5* targeting sgRNA, sg*Nlrc5* were stably transduced into B16F10-TDMa. QRT-PCR analysis of mRNA levels showed that the expression of *Nlrc5* and dependent MHC class I and related genes, including *H2-K^b, H2-D^b, Psmb9, Tap1*, and *B2m* was upregulated, but not the expression of an unrelated gene, *Mx1* in TDMa-sg*Nlrc5* (Figure 16b). RNA-seq analysis showed that Nlrc5 and dependent MHC class I and related genes consisted most of the significantly highly expressed genes in TDMa-sg*Nlrc5*, emphasizing the specificity of TDMa system (Figure 16c). Whereas the expression of *Mx1*, and *Nlrc5*-inducing transcription factors, *Stat1, Irf1* (Yoo *et al.*, 2021) was tended to be downregulated in TDMa-sg*Nlrc5* (Figure 16c). In addition to its role as CITA, *Nlrc5* is also reported to negatively regulate NF-κB pathway (Cui *et al.*, 2010), which could explain multiple downregulated genes identified in TDMa-sg*Nlrc5* (Figure 16c). Surface H2-K^b/D^b levels were evaluated by flow cytometry and TDMa-sg*Nlrc5* showed an upregulated expression MHC class I (Figure 16d; Figure 14a). Furthermore, we evaluated the methylation status of *Nlrc5* promoter in B16F10-TDMa. The proportion of methylated cytosine was reduced in CpG sites adjacent to the sg*Nlrc5* targeting site, but not in CpG sites at distant site (Figure 16e). These results indicate that sg*Nlrc5* in B16F10-TDMa induced targeted demethylation and robust transcription activation of *Nlrc5*, which upregulated the expression of downstream MHC class I and related genes.

Next, we investigated whether tumor immunogenicity was increased in TDMa-sg*Nlrc5*. B16F10-TDMa cells were loaded with OVA peptide (0-1 μg ml^{-1}) and co-cultured with OT-I CD8+ T cells. OT-I CD8+ T cells showed higher proportion of IFN-γ+ and CD69+ cells starting at low dose (0.125 μg ml^{-1}) of OVA peptide loaded in TDMa-sg*Nlrc5* (Figure 16f; Figure 14c; Figure 15b). We evaluated whether specific killing by OT-I CD8+ T cells was increased in TDMa-sg*Nlrc5* cells. OT-I CD8+ T cells induced cell death more efficiently in TDMa-sg*Nlrc5* cells in an OT-I CD8+ T cells and OVA peptide dependent manner (Figure 16g; Figure 14c; Figure 15c). Altogether, these results demonstrate that TDMa system enhanced B16F10 immunogenicity though

MHC class I by induction of targeted demethylation and activation of *Nlrc5*.

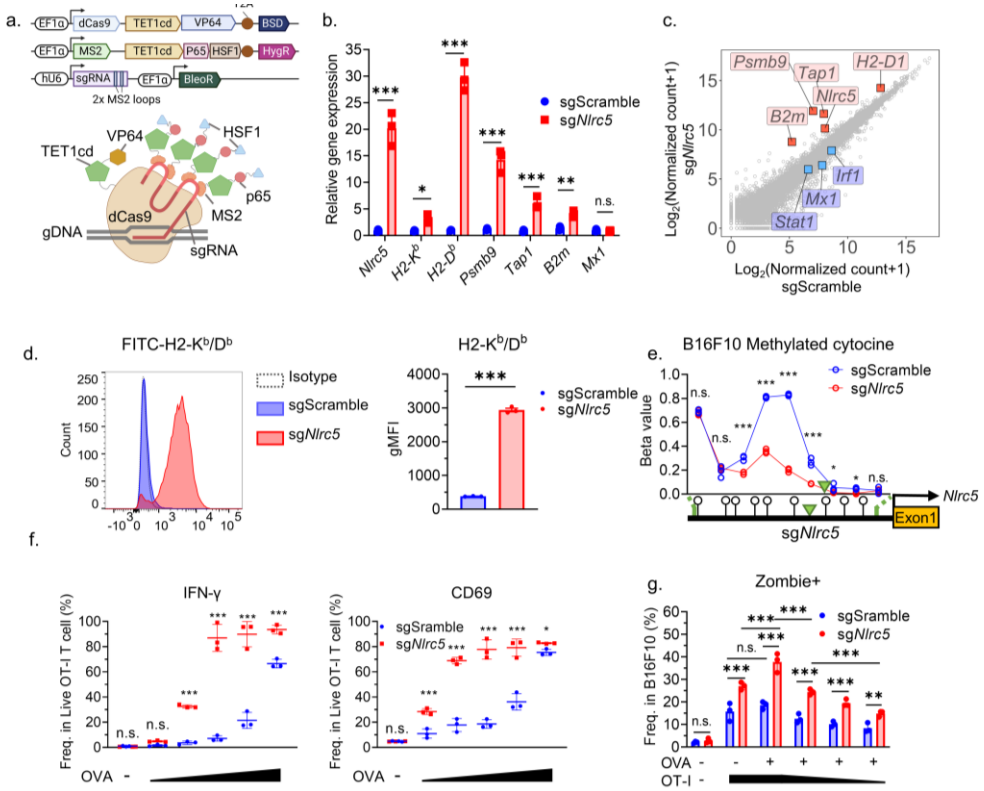

Figure 16 Targeted demethylation and activation of *Nlrc5* increased immunogenicity to CD8+ T cells in B16F10.

(a) A schematic illustration of main components in the lentiviral vectors of the TDMa system(Upper) and assembled components of the TDMa system at *Nlrc5* promoter(Lower).

(b) B16F10-TDMa cells were stably transduced with lentiviral vectors expressing sgScramble and sg*Nlrc5*. The mRNA expression levels of *Nlrc5*, *H2-K*^{b}, *H2-D*^{b}, *Psmb9*, *B2m,* and *Mx1* in B16F10-TDMa sgScramble and sg*Nlrc5* cells were quantified by qRT-PCR. Relative gene expression levels were determined by 2^(–ΔΔCT) method using *Gapdh* as a reference gene.

(c) The mRNA gene expression levels in $\log_2$(Normalized Count+1) values of all detected genes in RNA-seq analysis of B16F10-TDMa sgScramble cells were compared with sg*Nlrc5* cells. Marked genes are *Nlrc5* and dependent MHC class I and related genes (in red), and *Nlrc5* transcription activator *Stat1*, *Irf1*, and unrelated control *Mx1* (in blue). The average from $n = 2$ is shown.

(d) Surface H2-K^b/D^b expression levels in B16F10-TDMa sgScramble and sg*Nlrc5* cells were quantified by flow cytometry. (Left) Representative histogram. (Right) Geometric MFI.

(e) DNA methylation status of *Nlrc5* promoter in B16F10-TDMa sgScramble and sg*Nlrc5* cells were determined by direct sanger sequencing of bisulfite PCR

product. (Upper) Methylation levels of CpG dinucleotides. (Lower) A schematic diagram of sgRNA targeting sites (green triangles) and locations of CpG dinucleotides (white circles) at *Nlrc5* promoter, corresponding to upper plot.

(f) B16F10-TDMa sgScramble and sg*Nlrc5* cells were pulsed with 0, 0.0625, 0.125, 0.25, 0.5, or 1 μg ml^{-1} of OVA peptide overnight and co-cultured with OT-I T cells for 24 h. Intracellular IFN-γ and surface CD69 expression levels on OT-I T cells were quantified by flow cytometry.

(g) CFSE-labeled B16F10-TDMa sgScramble and sg*Nlrc5* cells were pulsed with 0 or 0.5μg ml^{-1} of OVA peptide overnight and co-cultured with OT-I T cells at OT-I:B16F10 ratio of 0:1, 1.25:1, 2.5:1, 5:1, and 10:1 for 48 h. Dead B16F10-TDMa cells were quantified as CFSE+ Zombie dye+ by flow cytometry.

Values shown are mean ±SD. For (b, d, e, f, g), $n = 3$; for (c) $n = 2$ in each group; '*n*' stands for number of biological replicates. Statistical significance was determined by Fisher's LSD test in (b, e, f, g), unpaired two-sided student's *t*-test in (d). n.s., not significant; * $p < 0.05$; ** $p < 0.01$; *** $p < 0.001$.

- **CD8+ T cell mediated anti-cancer immunity is enhanced by targeted demethylation and activation of *Nlrc5***

Since TDMa-sg*Nlrc5* cells showed enhanced immunogenicity, we wondered whether TDMa-sg*Nlrc5* cells can augment host anti-cancer immunity *in vivo*. Therefore, we subcutaneously implanted B16F10-TDMa sgScramble and sg*Nlrc5* cells into the wild type C57BL/6 mouse and monitored tumor growth. Tumor volume of TDMa-sg*Nlrc5* was significantly reduced compared with sgScramble control (Figure 17a, b). To identify whether the transcription of *Nlrc5*, MHC class I and related gene is upregulated in TDMa-sg*Nlrc5* tumors *in vivo*, total RNA was extracted from dissociated tumors to perform RNA-Seq analysis. Differentially expressed gene analysis identified that genes involved in MHC class I antigen presentation pathway, including *Nlrc5, H2-D1, Psmb9, Tap1, B2m,* key transcription factor in IFN pathway *Stat1*, and cytotoxic T cell activation marker *Gzmb* were significantly upregulated in TDMa-sg*Nlrc5* tumors. While proliferation marker *Mki67* were significantly downregulated in TDMa-sg*Nlrc5* tumors (Figure 17c). Gene ontology (GO) pathway enrichment analysis showed that pathways related to antigen presentation and adaptive immune response were among top upregulated pathways in TDMa-sg*Nlrc5* tumors (Figure 17d).

Next, to characterize tumor cells and infiltrating lymphocytes at cellular level, flow cytometry were performed in the dissociated tumors (Figure 14d,e). We observed increased CD45+ cell infiltration in TDMa-sg*Nlrc5* tumors (Figure 17e; Figure 18a). Further characterization on TILs showed that the infiltration of CD8+, but not CD4+ T cells were increased in TDMa-sg*Nlrc5* tumors (Figure 17e; Figure 18b). Expression of IFN-γ and CD44 in T cells are the markers for cytotoxicity and memory (Baaten *et al.*, 2012, Topham *et al.*, 2018, Nicolet *et al.*, 2020). We observed elevated proportion of IFN-γ+ and CD44+ CD8+ T cells, but not that of CD4+ T cell in TDMa-sg*Nlrc5* tumors (Figure 17e; Figure 18c). Moreover, we observed reduced amount of viable B16F10 cells in TDMa-sg*Nlrc5* tumors (Figure 17e; Figure 18d). These results showed that CD8+ T cell mediated anti-cancer immunity is increased in TDMa-sg*Nlrc5* tumors. Furthermore, we evaluated surface H2-K^b/D^b levels on B16F10 tumor cells *in vivo* and found that H2-K^b/D^b levels were elevated in TDMa-sg*Nlrc5* tumors (Figure 17f). Next, to determine whether adoptive immune system is required to inhibit tumor growth in sg*Nlrc5* tumors, we subcutaneously implanted B16F10-TDMa sgScramble and sg*Nlrc5* tumors in NUDE mice, which lacks mature T cells. Tumor growth was not significantly changed between B16F10-TDMa sgScramble and sg*Nlrc5* tumors in NUDE mice (Figure 17g,h). Altogether, these results indicate that targeted demethylation and activation of *Nlrc5* inhibited tumor growth by promoting CD8+ T cell infiltration and

activation via augmentation of immunogenicity of cancer cells though MHC class I.

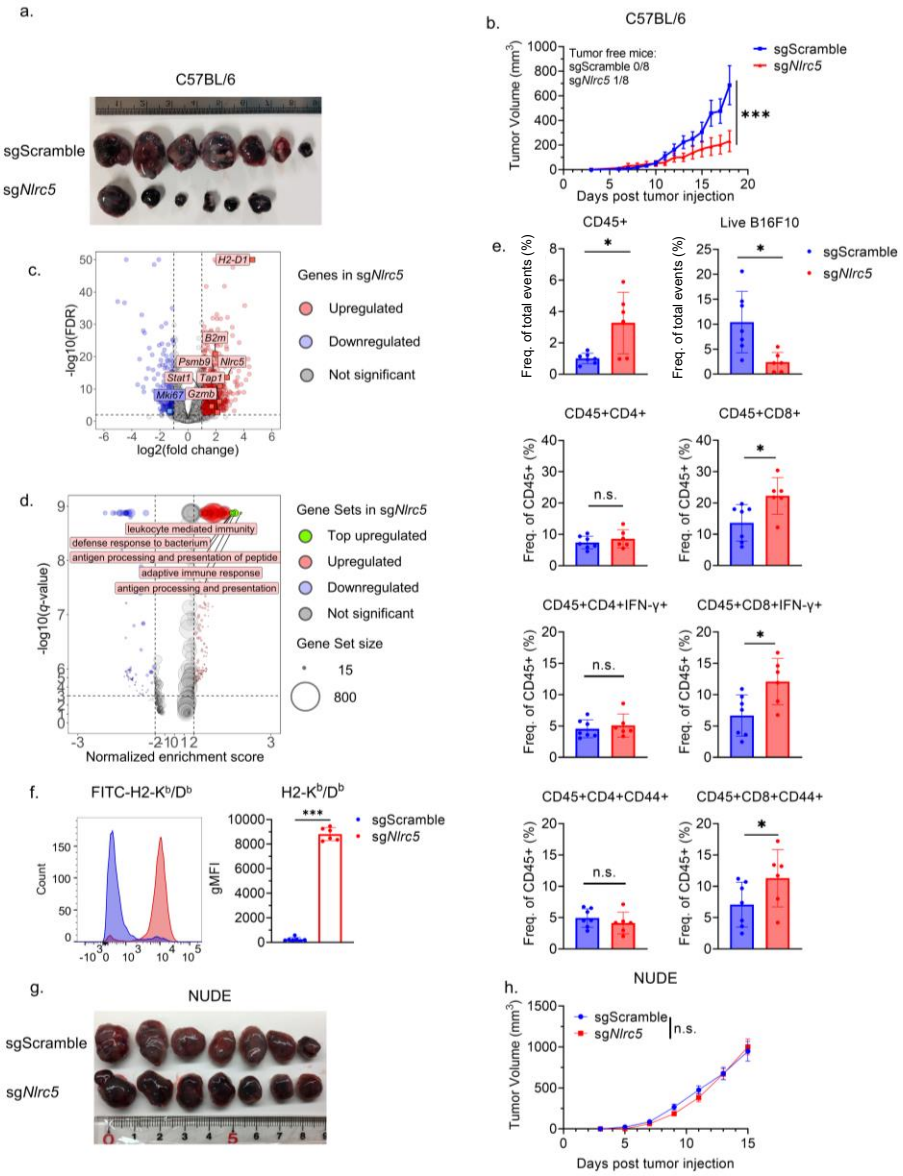

Figure 17 Targeted demethylation and activation of *Nlrc5* enhanced CD8+ T cell mediated anti-cancer immunity *in vivo*.

(a.) Three hundred thousand of B16F10-TDMa sgScramble and sg*Nlrc5* cells were subcutaneously implanted into left flank of C57BL/6 mice on day 0. An image of tumors on day 18 was obtained, with one mouse in the sg*Nlrc5* group that did not show tumor growth.

(b.) Volumes of B16F10-TDMa sgScramble and sg*Nlrc5* tumors were estimated daily by digital caliper since day 6 using visible tumor area and the following formula: volume (mm^3) = length * width * width / 2.

(c.) RNA-Seq and differentially expressed gene analysis between B16F10-TDMa sgScramble and sg*Nlrc5* tumors were performed. Red signs indicate significantly upregulated genes and blue signs indicate significantly downregulated genes in

TDMa-sg*Nlrc5* tumors. FDR, false discovery rate.

(d.) Gene Ontology (GO) pathway enrichment analysis between B16F10-TDMa sgScramble and sg*Nlrc5* tumors *in vivo* using RNA-seq data. Green circles represent the top significantly upregulated pathways in sg*Nlrc5* tumors. Size of circle indicates the number of genes included in the gene set.

(e.) Quantification of tumor infiltrating CD45+, and CD4+ or CD8+ T cells, IFN-γ+ or CD44+ T cells, and viable tumor cells from B16F10-TDMa sgScramble and sg*Nlrc5* tumors by flow cytometry.

(f.) Quantification of surface H2-K^b/D^b levels on viable tumor cells from B16F10-TDMa sgScramble and sg*Nlrc5* tumors by flow cytometry. (Left) Representative histogram. (Right) Geometric MFI of live B16F10 cells.

(g.) Five hundred thousand of B16F10-TDMa sgScramble and sg*Nlrc5* cells were subcutaneously implanted into left flank of NUDE mice on day 0. An image of tumors on day 15 was obtained.

(h.) Volumes of B16F10-TDMa sgScramble and sg*Nlrc5* tumors from NUDE mice were estimated every 2 days since day 4 by digital caliper using visible tumor area and the following formula: volume (mm^3) = length * width * width / 2.

Values shown are mean ±SEM in (a, g), and mean ±SD in (e, f). For (a, e, f, g), n=7 (TDMa-sgScramble tumors), n=6 (TDMa-sg*Nlrc5* tumors); for (c, d) n=4 in each group; 'n' stands for number of biological replicates. Statistical significance was determined by two-way ANOVA test in (a, g), and unpaired two-sided student's t-test in (e, f). n.s., not significant; * $p < 0.05$; *** $p < 0.001$.

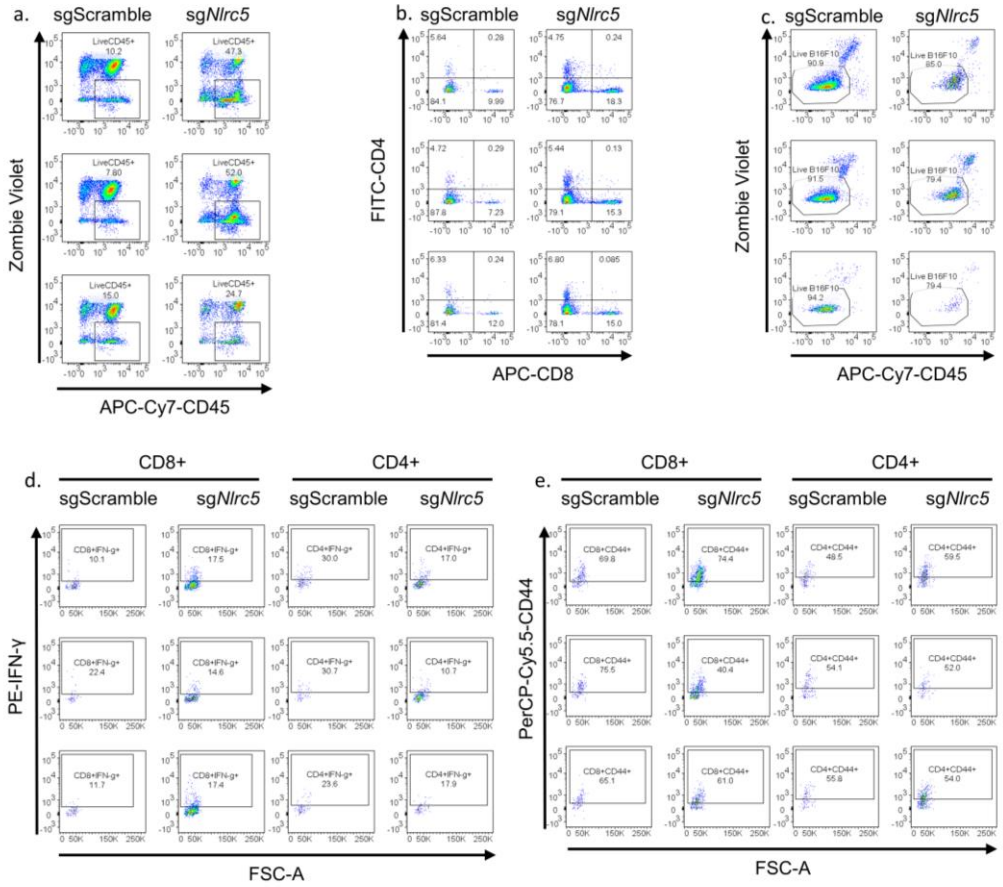

Figure 18 Representative scatter plots by flow cytometry analysis of B16F10-TDMa tumors implanted in C57BL/6 mice.

The B16F10-TDMa sgScramble and sg*Nlrc5* cells were implanted in C57BL/6 mice on day 0, and tumors were harvested on day 18. TILs and B16F10 cells were characterized by (a) Zombie violet– CD45+ live leucocytes, (b) CD4+ or CD8+ T cells, (c) Zombie violet– CD45– live B16F10-TDMa cells, (d) IFN-γ+ activated CD4+ and CD8+ T cells, and (e) CD44+ effector/memory CD4+ and CD8+ T cells. Corresponding to Figure 17d.

- **Targeted demethylation and activation of *Nlrc5* promoted infiltration of CD8+ T cells into tumor center.**

Localization of TILs in the tumor center correlates with a better cancer patients' prognosis and response to immune checkpoint blockade therapy (Galon *et al.*, 2012, Nie *et al.*, 2019). Since TDMa-sg*Nlrc5* tumors showed an increased tumor immunogenicity and amount of tumor infiltrating CD8+ T cells, we wondered whether the distribution of tumor infiltrating CD8+ T cells were altered in TDMa-sg*Nlrc5* tumors. To this end, we examined the localization of CD3+ and CD8+ cells by immunohistochemistry on B16F10-TDMa sgScramble and sg*Nlrc5* tumors. H&E staining showed abundant immune cell infiltration in TDMa-sg*Nlrc5* tumors (Figure 19a). Immunohistochemistry staining of CD3+ and CD8+ T cells showed an significantly increased infiltration in invasive margin, and tendency of increment in the tumor center of TDMa-sg*Nlrc5* tumors (Figure 19a,b; Figure 20a; Figure 21a). To quantify whether CD8+ T cells were preferentially recruited into the center of TDMa-sg*Nlrc5* tumors, we calculated the ratio of CD3+ or CD8+ stained area between tumor center and invasive margin within the same tumor. Interestingly, we found that CD8+ T cell infiltration were more concentrated in the center of TDMa-sg*Nlrc5* tumors compared with sgScramble tumors, but not for CD3+ T cell infiltration (Figure 19c). These results indicate that targeted demethylation and activation of *Nlrc5* not only increased the number of TILs, but also boosted infiltration of CD8+ cells into tumor center.

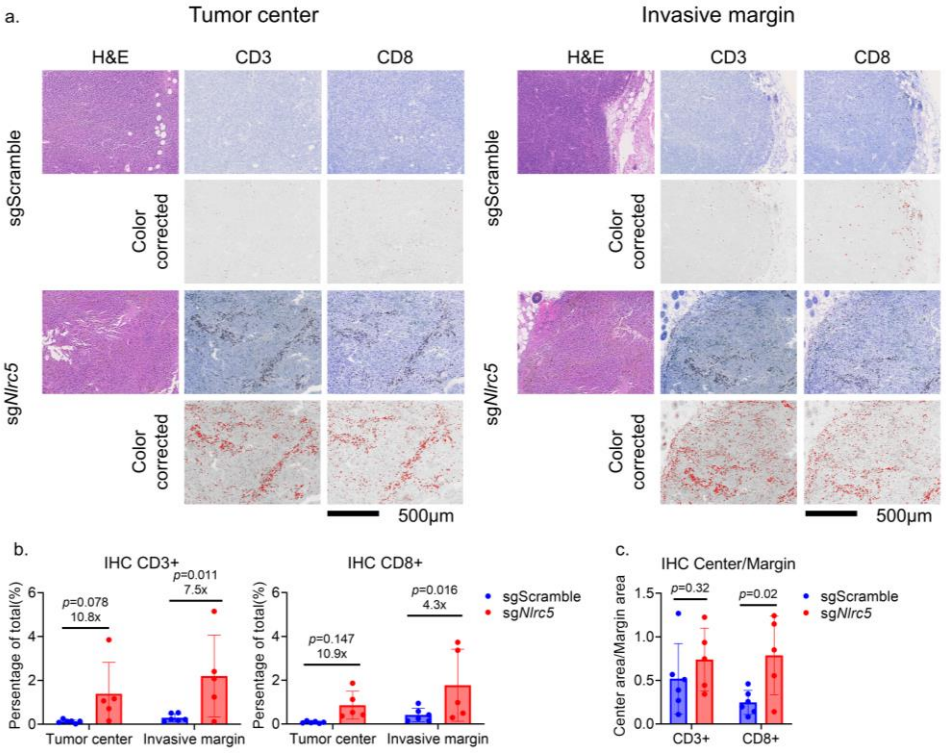

Figure 19 Targeted demethylation and activation of *Nlrc5* preferentially promoted the infiltration of CD8+ T cells into center of tumors.

(a.) Representative immunohistochemistry images of tumor center and invasive margin of B16F10-TDMa sgScramble and sg*Nlrc5* tumors implanted in C57BL/6 mice. (Upper) H&E, anti-CD3, and anti-CD8+ staining in TDMa-sgScramble or sg*Nlrc5* tumors; (Lower) Colors of anti-CD3+ and anti-CD8+ staining in images of TDMa-sgScramble or sg*Nlrc5* tumors were corrected to red to highlight CD3+ and CD8+ signals.

(b.) Comparison of CD3+ and CD8+ stained area between B16F10-TDMa sgScramble and sg*Nlrc5* tumors in the tumor center and invasive margin. Antibody-stained area was calculated as the percentage of CD3+ and CD8+ stained area of the whole tumor area (%). The numbers show are *p*-values and fold induction of antibody-stained area in TDMa-sg*Nlrc5* tumors compared with sgScramble tumors.

(c.) The ratio of CD3+ and CD8+ stained area between tumor center and invasive margin within each tumor was calculated and compared between TDMa-sgScramble and sg*Nlrc5* tumors. The numbers show are *p*-values.

Bar plots in (b, c) are mean ±SD. For (a, b, c), *n*=6 (sgScramble tumors), *n*=5 (sg*Nlrc5* tumors); '*n*' stands for number of biological replicates. Statistical significance was determined by Fisher's LSD test.

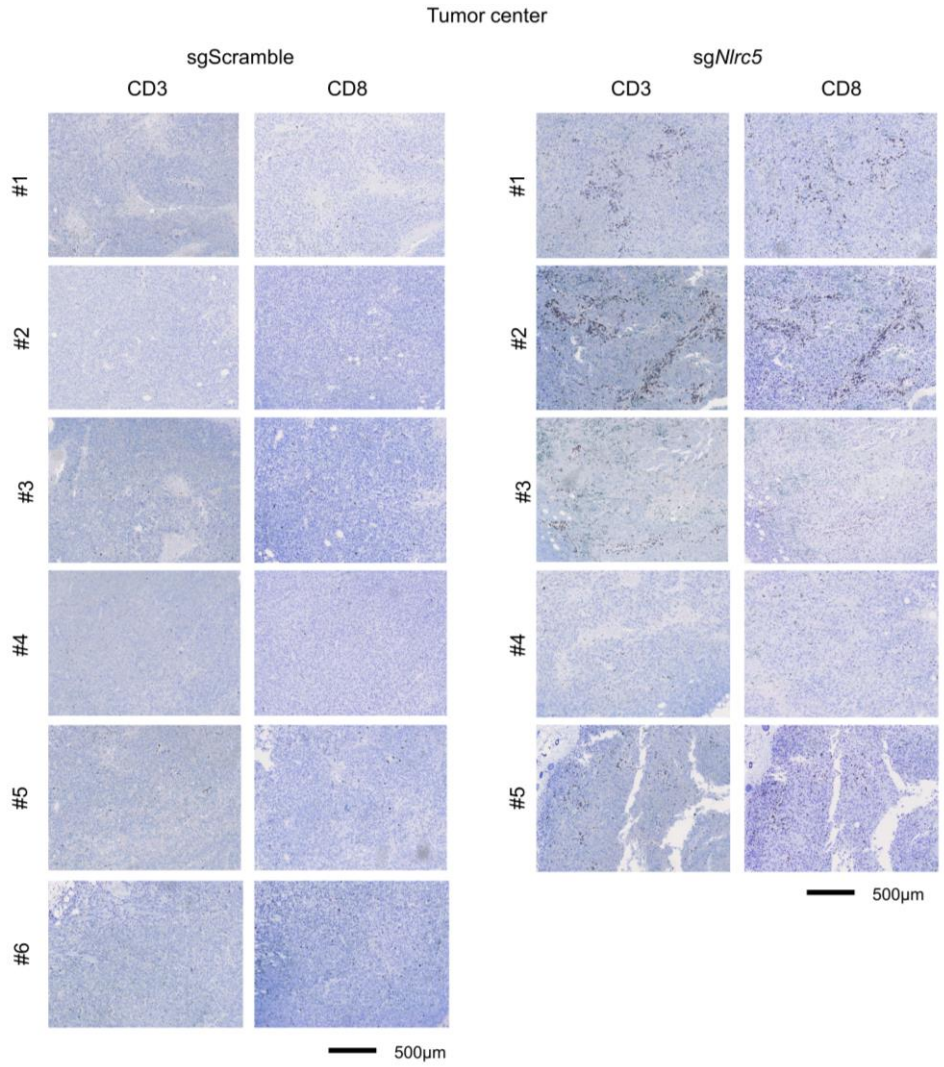

Figure 20 Immunohistochemistry for CD3+ and CD8+ infiltrating cells in the center of sgScramble and sg*Nlrc5* tumors, corresponding to Figure 19.

B16F10-TDMa sgScramble and sg*Nlrc5* cells were subcutaneously implanted into C57BL/6 mice on day 0 and tumors were harvested on day 18. Immunohistochemistry was performed using tumors with sufficient volume, *n*=6 for sgScramble; *n*=5 for sg*Nlrc5* tumors. '*n*' stands for number of mice used in the experiment. Tumor infiltrating cells were stained with anti-CD3 and -CD8 antibodies and images in the tumor center were obtained for sgScramble and sg*Nlrc5* tumors.

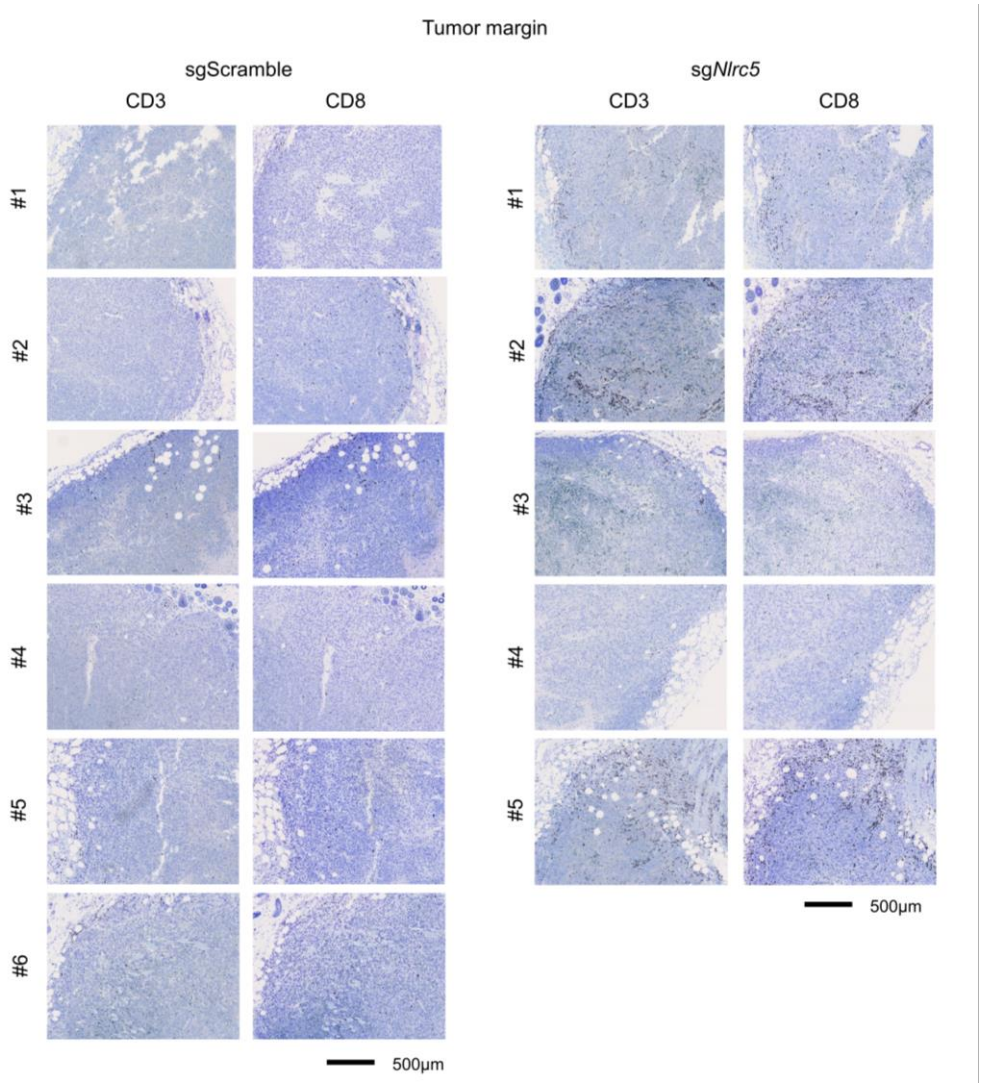

Figure 21 Immunohistochemistry staining for CD3+ and CD8+ infiltrating cells in the invasive margin of sgScramble and sg*Nlrc5* tumors *in vivo*, corresponding to Figure 19.

B16F10-TDMa sgScramble and sg*Nlrc5* cells were subcutaneously implanted into C57BL/6 mice on day 0 and tumors were harvested on day 18. Immunohistochemistry was performed on tumors with sufficient volume, *n*=6 for sgScramble; *n*=5 for sg*Nlrc5* tumors. '*n*' stands for number of mice used in the experiment. Tumor infiltrating cells were stained with anti-CD3 and -CD8 antibodies and images in the invasive margin were obtained for sgScramble and sg*Nlrc5* tumors.

- **Targeted demethylation and activation of *Nlrc5* sensitized B16F10 to anti-PD-1 treatment through MHC class I.**

The expression of *NLRC5* is enriched in melanoma patients who benefited from anti-PD-1 therapy (Yoshihama *et al.*, 2021). Since TDMa system robustly activated *Nlrc5* expression, we hypothesized that TDMa-sg*Nlrc5* tumors are more sensitive to anti-PD-1 treatment. To this end, we subcutaneously implanted B16F10-TDMa sgScramble and sg*Nlrc5* tumors into the mice and treated with anti-PD-1 and isotype control antibodies. Although anti-PD-1 treatment significantly reduced tumor volume of both TDMa-sgScramble and sg*Nlrc5* tumors, we observed the lowest tumor volume in TDMa-sg*Nlrc5* tumors with anti-PD-1 treatment (Figure 22a,b). We harvested TDMa sgScramble tumors at day 15 and sg*Nlrc5* tumors at day 18 when their tumor volumes were approximately the same in isotype control treated tumors. (Figure 22b). While weight of TDMa-sgScramble and sg*Nlrc5* tumors were not significantly different with isotype control treatment at these time points, weight of TDMa-sg*Nlrc5* tumors were significantly reduced compared with sgScramble tumors with anti-PD-1 treatment (Figure 22c). These results suggest that B16F10-TDMa sg*Nlrc5* tumors respond more sensitively to anti-PD-1 treatment.

We hypothesized that the sensitized response to anti-PD-1 treatment in sg*Nlrc5* tumors were contributed by its enhanced immunogenicity via MHC class I. Therefore, we characterized TILs and tumor cells by flow cytometry (Figure 14d,e). We observed a more inflamed tumor microenvironment by anti-PD-1 treatment in TDMa-sg*Nlrc5* tumors as CD45+ leucocytes infiltration was significantly upregulated by anti-PD-1 treatment (Figure 22d; Figure 23a). However, upregulation of CD45+ leucocytes infiltration by anti-PD-1 treatment was not observed in sgScramble tumors (Figure 22d; Figure 23a). The infiltration of CD8+ T cells were upregulated in both TDMa-sgScramble and sg*Nlrc5* tumors upon anti-PD-1 treatment (Figure 22d; Figure 23b). Anti-PD-1 treatment increased the proportion of IFN-γ+ and CD44+ CD8+ T cells only in TDMa-sg*Nlrc5* tumors, but not in TDMa-sgScramble tumors (Figure 22d; Figure 23c,d). We observed that TDMa-sg*Nlrc5* tumors treated by anti-PD-1 had the highest proportion of CD45+ leucocytes, CD8+ T cells and activated IFN-γ+ and CD44+ CD8+ T cells among other groups (Figure 22d; Figure 23c). CD4+ T cell infiltration and activation were not significantly changed by anti-PD-1 treatment, except for the proportion of CD44+CD4+ T cells, where it was slightly induced by anti-PD-1 treatment in TDMa-sg*Nlrc5* tumors (Figure 22d; Figure 23c). These results indicate that anti-PD-1 treatment preferentially activated CD8+ T cell mediated anti-cancer immunity in sg*Nlrc5* tumors.

To test whether elevated MHC class I levels in TDMa-sg*Nlrc5* tumors were associated with sensitized response to anti-PD-1 treatment and increased CD8+ T cell activity, we evaluated surface H2-K^b/D^b of B16F10-TDMa cells *in vivo* (Figure 14e). Anti-PD-1 treatment induced surface H2-K^b/D^b levels in TDMa-sg*Nlrc5* but not in sgScramble tumors (Figure 22e). Anti-PD-1 treatment elevated PD-L1 levels in both TDMa-sgScramble and sg*Nlrc5* tumors (Figure 22e). But we did not observe significant difference in surface PD-L1 levels between TDMa-sgScramble and sg*Nlrc5* tumors treated by either anti-PD-1 or isotype control (Figure 22e). Taken together, our results indicate that targeted demethylation and activation of *Nlrc5* enhanced the response to anti-PD-1 treatment by upregulation of cancer immunogenicity to CD8+ T cells through MHC class I.

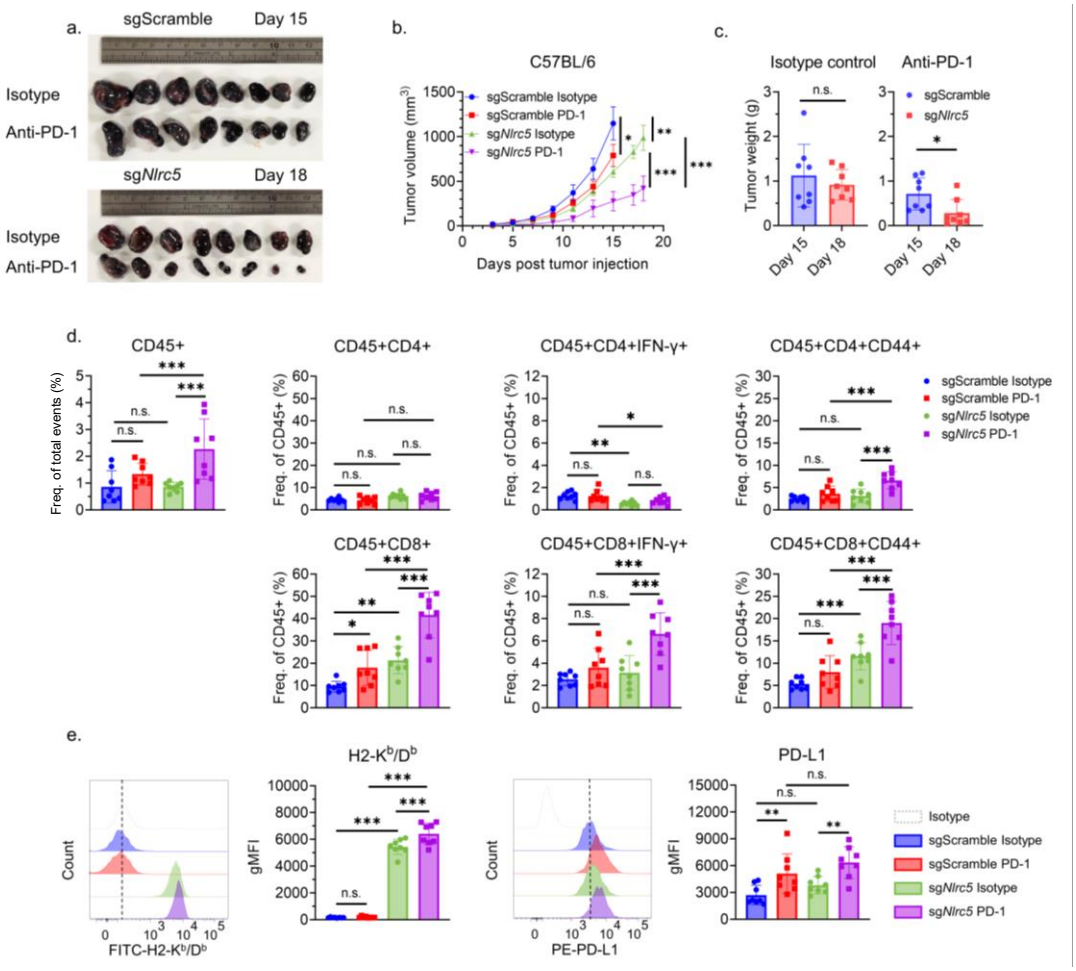

Figure 22 Targeted demethylation and activation of *Nlrc5* sensitized B16F10-TDMa tumors to anti-PD-1 treatment.

(a.) Six hundred thousand of B16F10-TDMa sgScramble and sg*Nlrc5* cells were subcutaneously implanted into left flank of C57BL/6 mice on day 0. Isotype control or anti-PD-1 antibodies were intraperitoneally injected every 2 days from day 3 at 250μg/mouse for 5 times in total. Image of B16F10-TDMa sgScramble and sg*Nlrc5* tumors harvested on day 15 and day 18 respectively were obtained.

(b.) Tumor volumes of B16F10-TDMa sgScramble and sg*Nlrc5* tumors treated by isotype control or anti-PD-1 antibodies were estimated every 2 days since day 3 by digital caliper using visible tumor area and the following formula: volume (mm^3) = length * width * width / 2.

(c.) Tumor weight was measured and compared between day 15 for sgScramble tumors and day 18 for sg*Nlrc5* tumors treated by isotype control or anti-PD-1.

(d.) Quantification of tumor infiltrating CD45+, and CD4+ or CD8+ T cells, and activated/effector/memory IFN-γ+ or CD44+ T cells from B16F10-TDMa sgScramble and sg*Nlrc5* tumors by flow cytometry.

(e.) Quantification of H2-K^b/D^b and PD-L1 levels on viable tumor cells from B16F10-TDMa sgScramble and sg*Nlrc5* tumors treated by isotype control or anti-PD-1 by flow cytometry. (Left) Mean gMFI of live B16F10 cells. (Right) Representative histogram.

Values shown in (a) are mean ±SEM, and in (c, d, e) are mean ±SD. n=8 in each group; 'n' stands for number of biological replicates. Statistical significance was determined by two-way ANOVA test in (a.), unpaired two-sided student's t-test in (c.), and Fisher's LSD test in (d, e). n.s., not significant; * $p < 0.05$; ** $p < 0.01$; *** $p < 0.001$.

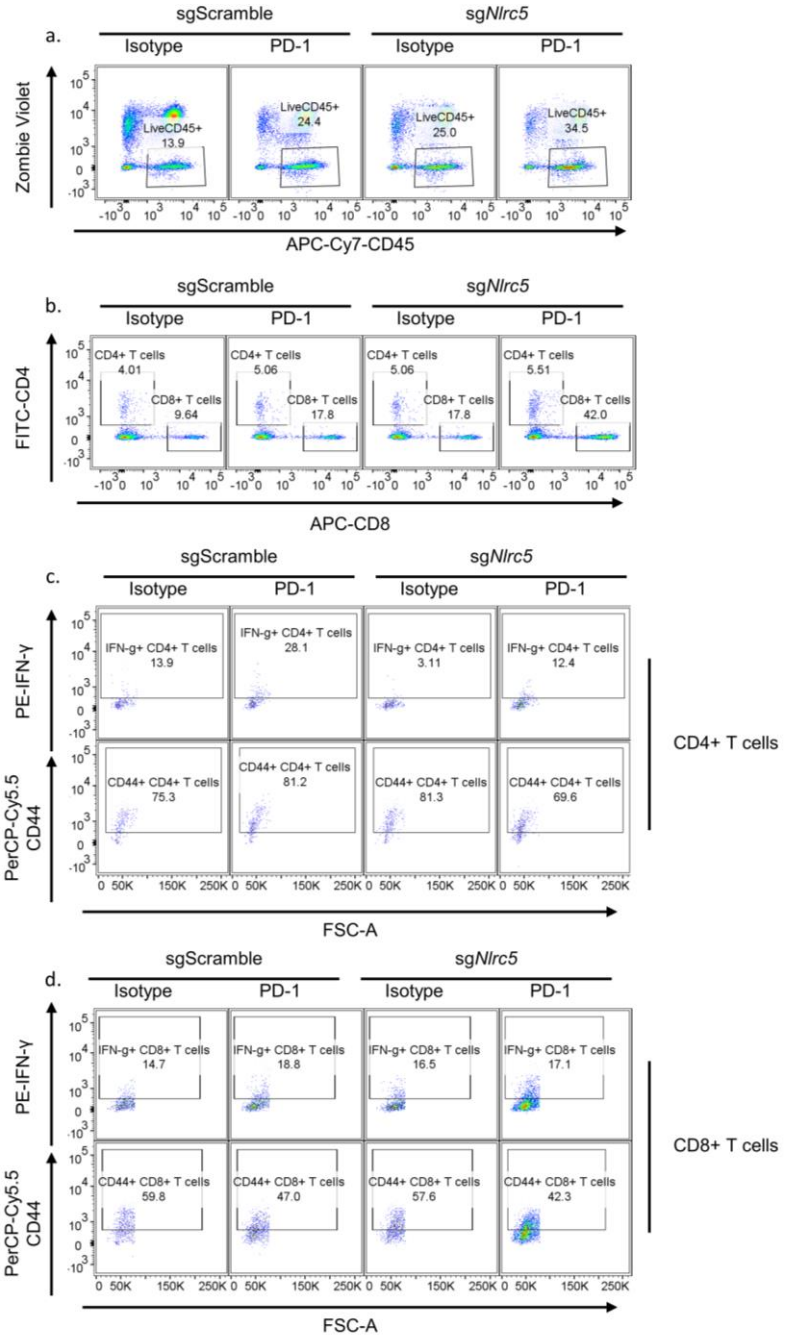

Figure 23 Representative scatter plots by flow cytometry analysis of from B16F10-TDMa tumors implanted in C57BL/6 mice treated with isotype control or anti-PD-1 antibodies.

The B16F10-TDMa sgScramble and sg*Nlrc5* cells were implanted in C57BL/6 mice on day 0. The mice received either isotype control or anti-PD-1 antibody treatment. TDMa-sgScramble tumors were harvested on day 15 and TDMa-sg*Nlrc5* tumors were harvested on day 18. TILs were characterized by (a) Zombie violet– CD45+ live leucocytes, (b) CD4+ or CD8+ T cells, (c) IFN-γ+ activated CD4+ and CD8+ T cells, and (d) CD44+ effector/memory CD4+ and CD8+ T cells. Corresponding to

Figure 22d.

- **Targeted demethylation and activation of *NLRC5* increased MHC class I expression levels in human breast cancer cell line MCF7.**

We showed that in B16F10, targeted demethylation and activation of *Nlrc5* enhanced its immunogenicity, host anti-cancer immunity, and sensitized to anti-PD-1 treatment. Next, we wondered whether similar strategy can be applied to human cancer cell lines. We used human breast cancer cell line MCF7 as it has low *NLRC5* expression level and high methylation level according to NCI60 database (Shoemaker, 2006). We evaluated the methylation level of *NLRC5* promoter in MCF7 by bisulfite sequencing and identified that MCF7 contains highly methylated region in *NLRC5* promoter (Figure 24a). Therefore, we transduced TDMa system into MCF7 cell line and generated MCF7-TDMa cell line. Next, we optimized targeting sgRNA on human *NLRC5* promoter by quantifying *NLRC5* induction. All 6 candidate sgRNAs were able to induce *NLRC5* expression at low level (Figure 24b). To enhance the efficacy of *NLRC5* activation, we transduced combinations of multiple sgRNAs into MCF7-TDMa. Among the combinations tested, combination #1 showed the highest *NLRC5* induction (Figure 24c), which is referred to as MCF7-TDMa sg*NLRC5*s. Non-targeting scramble sgRNA was used as control, referred to as MCF7-TDMa sgScramble. The mRNA expression levels of *NLRC5* and dependent MHC class I and related gene, including *HLA-A, B, C, PSMB9, TAP1*, and *B2M* were induced by sg*NLRC5*s, but not in an unrelated gene *CIITA* (Figure 24d). Surface MHC class I levels were increased in TDMa-sg*NLRC5*s cells (Figure 24e). And the methylation levels of *NLRC5* promoter were decreased in sg*NLRC5*s cells (Figure 24f). These results show that TDMa system can induce targeted demethylation and activation of *NLRC5* and increase the expression MHC class I gene on human breast cancer MCF7 cell line.

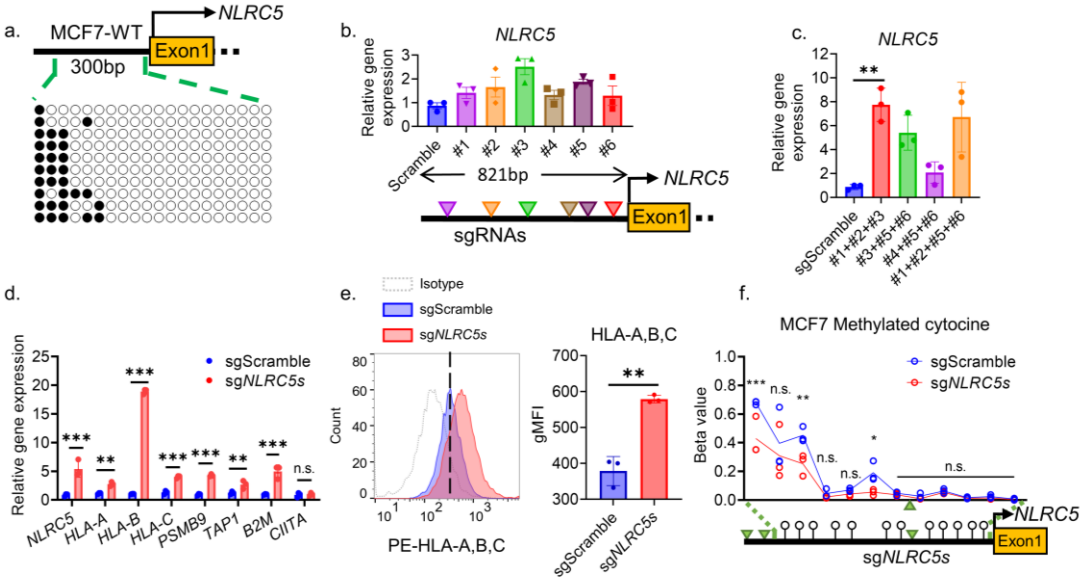

Figure 24 Targeted demethylation and activation of NLRC5 increase the expression of MHC class I in MCF7.

(a.) DNA methylation status of *NLRC5* promoter in MCF7 cells were determined by bisulfite PCR analysis. CpG dinucleotides are shown as white or black circles to represent unmethylated or methylated CpG dinucleotides. Each row represents an individual plasmid clone of total 10 clones.

(b.) (Upper) Scramble and *NLRC5* promoter targeting sgRNA were stably transduced in MCF7-TDMa cells and the mRNA expression level of *NLRC5* was quantified by qRT-PCR. (Lower) A schematic of sgRNA targeting sites at *NLRC5* promoter, with colored triangular signs indicating each sgRNA target site corresponding to the upper plot.

(c.) Lentiviral vectors expressing scramble gRNA or multiple combinations of *NLRC5* promoter targeting sgRNAs were stably transduced in MCF7-TDMa cells and the mRNA expression level of *NLRC5* was quantified by RT-qPCR.

(d.) The mRNA expression levels of *NLRC5*, *HLA-A*, *HLA-B*, *HLA-C*, *PSMB9, TAP1*, *B2M* and *CIITA* in MCF7-TDMa sgScramble and sg*NLRC5s* cells were quantified by qRT-PCR.

(e.) Surface HLA-A/B/C expression levels in MCF7-TDMa sgScramble and sg*NLRC5s* cells were quantified by flow cytometry. (Left) Representative histograms. (Right) Mean gMFI.

(f.) (Upper) DNA methylation status of *NLRC5* promoter in MCF7-TDMa sgScramble and sg*NLRC5s* cells were determined by direct sanger sequencing of bisulfite PCR product. (Lower) A schematic diagram of sgRNA targeting sites

(green triangles) and locations of CpG dinucleotides (white circles) at the *NLRC5* promoter, corresponding to upper plot.

Relative gene expression levels in qRT-PCR analysis were determined by 2^(–ΔΔCT) method using *GAPDH* as a reference gene. Values in bar plots shown are mean ±SD. n=3 in each group; 'n' stands for number of biological replicates. Statistical significance was determined by unpaired two-sided student's t-test in (c, e), Fisher's LSD test in (d, f). n.s., not significant; * $p < 0.05$; ** $p < 0.01$; *** $p < 0.001$.

Chapter 2: Discussion

In this study, we first aimed to increase cancer immunogenicity by targeted demethylation of *Nlrc5* promoter in B16F10 using TDM system. We observed demethylation of *Nlrc5* promoter and increased *Nlrc5* and MHC class I expression levels. However, MHC class I induction was insufficient to display significantly enhanced immunogenicity in the OT-I co-culture system. Studies aimed to increase gene expression levels by targeted demethylation using dCas9 fused with TET1cd alone often exhibit unsatisfactory efficacy for potential downstream therapeutic applications *in vivo* (Choudhury *et al.*, 2016, Wang *et al.*, 2019, Hanzawa *et al.*, 2020, Nunez *et al.*, 2021). On the contrary, one study achieved successful therapeutic effect *in vivo* by targeting CGG repeats in the promoter of *FMR1* gene (Liu *et al.*, 2018). The presence of CGG repeats enabled recruitment of multiple copies of dCas9-Tet1 complex by one sgRNA to the heavily methylated *FMR1* promoter. However, promoter CGG repeats are mainly present in genes associated with neuron development (Annear *et al.*, 2021). Therefore, application of targeted demethylation for novel therapy development in cancers should require careful selection of target genes.

To increase the induction of *Nlrc5* expression levels, we fused additional transcription activators to generate TDMa system. TDMa system is composed by the combination of TET1cd and activation motifs to induces both targeted demethylation and activation, which has been shown to induce higher target gene expression compared with TET1cd or activators alone (Chan *et al.*, 2022). Integration of TDMa into B16F10 induced specific demethylation and activation of *Nlrc5*, which robustly enhanced its immunogenicity *ex vivo* and host CD8+ T cells mediated anti-cancer immunity *in vivo* though MHC class I. TDMa system targeting human *NLRC5* in MCF7 cell line also showed increased expression of MHC class I, highlighting its application in human cancers. These results are consistent with previous study that utilized *Nlrc5* overexpression system (Rodriguez *et al.*, 2016). The majority of approaches to develop novel immunotherapy are targeted at immune system, while little attention has been paid to augment cancer cell immunogenicity (Taefehshokr *et al.*, 2020). Our results present *Nlrc5* and TDMa system as novel therapeutic approaches to increase cancer cell immunogenicity.

The aggregation of TILs in tumor center correlates with improved prognosis in cancers (Galon *et al.*, 2006, Fridman *et al.*, 2012, Mlecnik *et al.*, 2016, Pages *et al.*, 2018, Bruni *et al.*, 2020, Qi *et al.*, 2021). Although MHC class I levels on cancer cells correlate with abundance of TILs (Yoshihama *et al.*, 2016), it is not clear whether MHC class I levels affects the localization of TILs. Our results indicated that TILs in both

invasive margin and center of the tumors were enriched in TDMa-sgNlrc5 tumors. Interestingly, we found that CD8+ cells, but not CD3+ cells, were preferentially concentrated into the tumor center in TDMa-sgNlrc5 tumors. The underlying mechanisms for such phenotypes are unclear, however, reasonable speculations can be made. Firstly, primed CD8+ T cells receive its activation signal through TCR-MHC class I interaction to exert its cytotoxic effect (Curtsinger *et al.*, 2003). Cytotoxic T cells secretes cytokines such as IFN-γ to facilitates killing, which also provides additional signals to recruit more CD8+ T cells. This positive feedback loop may have been enhanced in TDMa-sg*Nlrc5* tumors that facilitated CD8+ T cell redistribution. Secondly, dendritic cells (DCs) uptake antigens for cross presentation to prime CD8+ T cells through MHC class I by either antigen presentation pathway or MHC class I cross dressing (Duong *et al.*, 2022, MacNabb *et al.*, 2022). DCs are also able to restimulate CD8+ T cells within the tumor to recruit more CD8+ T cells (Zagorulya *et al.*, 2023). Both processes may be enhanced by abundant MHC class I level in TDMa-sg*Nlrc5* tumors, resulting in preferential recruitment of CD8+ T cells. It would contribute to further understanding of anti-cancer immunity to investigate the underlying mechanisms of the effect of MHC class I on distribution of TILs.

Subcutaneous B16F10 model shows poor or no response to anti-PD-1 treatment (Iwai *et al.*, 2005, De Henau *et al.*, 2016, Meng *et al.*, 2018, Gao *et al.*, 2019, Albershardt *et al.*, 2020, Pi *et al.*, 2022). It could partially attributes to low expression levels of surface MHC class I in B16F10 as loss of surface MHC class I is one of the mechanisms that cause resistance to immune checkpoint blockade (ICB) therapy (Zaretsky *et al.*, 2016, Gettinger *et al.*, 2017, Le *et al.*, 2017, Sade-Feldman *et al.*, 2017, Chowell *et al.*, 2018, Rodig *et al.*, 2018, Kalbasi *et al.*, 2020a). Accordingly, downregulation of NLRC5 expression may contribute the resistance to ICB therapy because *NLRC5* transactivates the expression of MHC class I and related genes. This is supported by the findings that Nlrc5 deletion promoted cancer cell survival against anti-PD-1 treatment *in vivo* (Manguso *et al.*, 2017), and the expression of *Nlrc5* is decreased in patients who failed to respond to anti-PD-1 therapy (Yoshihama *et al.*, 2021). Here, we showed that targeted demethylation and activation of *Nlrc5* on B16F10-TDMa sg*Nlrc5* sensitized its response to anti-PD-1 treatment. We found that CD8+ T cell, but not CD4+ T cell mediated immune response was synergistically augmented by anti-PD-1 treatment with demethylation and activation of *Nlrc5*. This is consistent with finding that CD8+ T cell infiltration and activation were exclusively induced by anti-PD-1 treatment (Curran *et al.*, 2010). It is possible that CD8+ T cells play major roles in anti-cancer immune response induced by anti-PD-1 treatment in B16F10 model. Therefore, enhanced CD8+ T cells activity may have worked in synergy with the high expression

levels of MHC class I in TDMa-sg*Nlrc5* tumors, which sensitized the response to anti-PD-1. Taken together, we showed that augmentation of *Nlrc5* expression by targeted demethylation and activation is a viable approach to increase sensitivity to anti-PD-1 treatment in cancer.

Although we showed that integration of TDMa system in B16F10 and MCF7 targeting *Nlrc5* robustly increased MHC class I expression levels, the delivery of TDMa system was performed *in vitro* through lentiviral vectors. TDMa system is consisted by 3 lentiviral vectors and stably transduced cells were selected by antibiotics of blasticidin, hygromycin, and zeocine, which makes the delivery of TDMa system cumbersome and inefficient. Thus, even though the direct delivery of TDMa system as drug *in vivo* to enhance *NLRC5* expression in cancer cells is the most favorable therapeutic approach for TDMa system, direct delivery of lentiviral vectors of TDMa system as therapeutic method *in vivo* may have limited viability. Success of delivery using lipid nanoparticles or virus like particles enabled delivery of complex mRNA and proteins molecules *in vivo* (Banskota *et al.*, 2022). Therefore, further optimization of TDMa system for direct *in vivo* delivery could occur through lipid nanoparticles or virus like particles containing mRNA that encodes TDMa system or proteins of TDMa system with sgRNA. Furthermore, injection of liquid nitrogen snap frozen cancer cells *in vivo* were shown to increase host anti-cancer immune response (Ci *et al.*, 2020, Zhao *et al.*, 2022). As a potential therapeutic approach, TDMa system edited cancer cells can be generated *in vitro*, followed by snap freeze and injection *in vivo*, where enhanced MHC class I expression levels by TDMa system are expected to induce stronger anti-cancer response.

Conclusion

New findings from this study

- Genomic deletion of *Nlrc5* downregulated the expression of MHC class I in B16F10 and E0771 cell lines.
- Genomic deletion of *Nlrc5* dampened host CD8+ T cell mediated anti-cancer immunity and promoted tumor growth in E0771 model.
- *Nlrc5* is required for response to anti-PD-1 treatment in B16F10 model.
- Established a biomarker screening strategy by transcriptional screening and validation by external cohort
- Newly established a CRISPR/dCas9-MS2-TET1cd based system (TDMa) that induce targeted demethylation and activation.
- TDMa system specifically increased the expression of *Nlrc5/NLRC5* and dependent MHC class I and related genes in B16F10 and MCF7 cells.
- Targeted demethylation and activation of *Nlrc5* by TDMa system is viable approach to increase cancer immunogenicity through MHC class I in B16F10 and MCF7 cell lines.
- Targeted demethylation and activation of *Nlrc5* by TDMa system specifically activated host CD8+ T cell mediated anti-cancer immunity.
- MHC class I in cancer specifically concentrated CD8+ T cell infiltration into tumor center in B16F10 model.
- Targeted demethylation and activation of *Nlrc5* sensitized response to anti-PD-1 treatment in B16F10 model.

Significance of new findings

- Advances our understanding of mechanisms underlying cancer immune evasion caused by *NLRC5* silencing.
- Provided a novel method for development and validation of prediction models applicable for multiple independent cohorts, which has potential clinical applications.
- Deepened our understanding of how MHC class I expression in cancer modulates host anti-cancer immunity and response to immunotherapy.
- Provided the rational and viable approaches for future immunotherapy development that aim increase cancer immunogenicity.

Future research plans

- We performed transcriptome screening to identify the biomarkers that show the

highest prediction efficacy when combined with *NLRC5*. Currently, we identified combinations of 2 markers. I addition, application of up to 3 or 4 markers is expected to have improved prediction efficacy and stability.

- We observed that CD8+ T cells are preferentially concentrated into tumor center by targeted demethylation and activation of *Nlrc5* in B16F10 model. The underlying mechanisms remain unknown and it is not clear whether similar phenotype can be observed in other types of cancers.

Future research tasks

- TDMa system targeting *Nlrc5* induced robust augmentation in expression of *Nlrc5* and dependent MHC class I related genes in B16F10, however, we did not achieve similar efficacy in MCF7. Further optimization of TDMa system targeting at human cell lines is required to translate into clinical application.
- TDMa system is consist by 3 separate lentiviral vectors. To stably transduce these vectors into cells, tedious process of antibodies selections is required. Therefore, it is unlikely that TDMa system can be applied *in vivo* in current formality. Optimization of efficient delivery method is critical for *in vivo* application.

Acknowledgment

The authors thank C. Matsukawa and K. Ogawa for secretarial assistance, and all members of the Department of Immunology of the Graduate School of Medicine at Hokkaido university for their support. We are grateful to staffs of the Institute for Animal Experimentation of the Graduate School of Medicine at Hokkaido University and Central Research Institute Hokkaido University Graduate School of medicine Graduate School of Dental Medicine for their help with the mouse experiment. This work was supported by JSPS KAKEN [JP18H06135] and [JP20K21511]; the Japan Agency for Medical Research and Development (AMED) [JP223fa627005]; Takeda Science Foundation, Bristol Myers Squibb, SENSHIN Medical Research Foundation, Hitachi Global Foundation, Kobayashi Foundation, and Hokkaido University DX Doctoral Fellowship [PH6R210009] and [PH8D220001].

Disclosure of Conflict of interest

The author declares no conflict of interest.

List of References

Albershardt, T. C., Parsons, A. J., Reeves, R. S., Flynn, P. A., Campbell, D. J., Ter Meulen, J. & Berglund, P. 2020. Therapeutic efficacy of PD1/PDL1 blockade in B16 melanoma is greatly enhanced by immunization with dendritic cell-targeting lentiviral vector and protein vaccine. *Vaccine,* 38**,** 3369-3377.

Annear, D. J., Vandeweyer, G., Elinck, E., Sanchis-Juan, A., French, C. E., Raymond, L. & Kooy, R. F. 2021. Abundancy of polymorphic CGG repeats in the human genome suggest a broad involvement in neurological disease. *Sci Rep,* 11**,** 2515.

Baaten, B. J., Tinoco, R., Chen, A. T. & Bradley, L. M. 2012. Regulation of Antigen-Experienced T Cells: Lessons from the Quintessential Memory Marker CD44. *Front Immunol,* 3**,** 23.

Banerjee, R., Smith, J., Eccles, M. R., Weeks, R. J. & Chatterjee, A. 2022. Epigenetic basis and targeting of cancer metastasis. *Trends Cancer,* 8**,** 226-241.

Banskota, S., Raguram, A., Suh, S., Du, S. W., Davis, J. R., Choi, E. H., Wang, X., Nielsen, S. C., Newby, G. A., Randolph, P. B.*, et al.* 2022. Engineered virus-like particles for efficient in vivo delivery of therapeutic proteins. *Cell,* 185**,** 250-265 e16.

Barrett, T., Wilhite, S. E., Ledoux, P., Evangelista, C., Kim, I. F., Tomashevsky, M., Marshall, K. A., Phillippy, K. H., Sherman, P. M. & Holko, M. 2012. NCBI GEO: archive for functional genomics data sets—update. *Nucleic Acids Res,* 41**,** D991-D995.

Biswas, A., Meissner, T. B., Kawai, T. & Kobayashi, K. S. 2012. Cutting edge: impaired MHC class I expression in mice deficient for Nlrc5/class I transactivator. *J Immunol,* 189**,** 516-20.

Bruni, D., Angell, H. K. & Galon, J. 2020. The immune contexture and Immunoscore in cancer prognosis and therapeutic efficacy. *Nat Rev Cancer,* 20**,** 662-680.

Cancer Genome Atlas, N. 2012. Comprehensive molecular portraits of human breast tumours. *Nature,* 490**,** 61-70.

Cancer Genome Atlas, N. 2015. Genomic Classification of Cutaneous Melanoma. *Cell,* 161**,** 1681-96.

Canver, M. C., Bauer, D. E., Dass, A., Yien, Y. Y., Chung, J., Masuda, T., Maeda, T., Paw, B. H. & Orkin, S. H. 2014. Characterization of genomic deletion efficiency mediated by clustered regularly interspaced short palindromic repeats (CRISPR)/Cas9 nuclease system in mammalian cells. *J Biol Chem*, 289, 21312-24.

Chan, W. F., Coughlan, H. D., Chen, Y., Keenan, C. R., Smyth, G. K., Perkins, A. C., Johanson, T. M. & Allan, R. S. 2022. Activation of stably silenced genes by recruitment of a synthetic de-methylating module. *Nat Commun,* 13**,** 5582.

Chen, S., Lee, L. F., Fisher, T. S., Jessen, B., Elliott, M., Evering, W., Logronio, K., Tu, G. H., Tsaparikos, K., Li, X.*, et al.* 2015. Combination of 4-1BB agonist and PD-1 antagonist promotes antitumor effector/memory CD8 T cells in a poorly

immunogenic tumor model. *Cancer Immunol Res,* 3**,** 149-60.

Chen, S., Zhou, Y., Chen, Y. & Gu, J. 2018. fastp: an ultra-fast all-in-one FASTQ preprocessor. *Bioinformatics,* 34**,** i884-i890.

Choudhury, S. R., Cui, Y., Lubecka, K., Stefanska, B. & Irudayaraj, J. 2016. CRISPR-dCas9 mediated TET1 targeting for selective DNA demethylation at BRCA1 promoter. *Oncotarget,* 7**,** 46545-46556.

Chowell, D., Morris, L. G. T., Grigg, C. M., Weber, J. K., Samstein, R. M., Makarov, V., Kuo, F., Kendall, S. M., Requena, D., Riaz, N.*, et al.* 2018. Patient HLA class I genotype influences cancer response to checkpoint blockade immunotherapy. *Science,* 359**,** 582-587.

Ci, T., Li, H., Chen, G., Wang, Z., Wang, J., Abdou, P., Tu, Y., Dotti, G. & Gu, Z. 2020. Cryo-shocked cancer cells for targeted drug delivery and vaccination. *Sci Adv,* 6**,** eabc3013.

Cui, J., Zhu, L., Xia, X., Wang, H. Y., Legras, X., Hong, J., Ji, J., Shen, P., Zheng, S., Chen, Z. J.*, et al.* 2010. NLRC5 negatively regulates the NF-kappaB and type I interferon signaling pathways. *Cell,* 141**,** 483-96.

Curran, M. A., Montalvo, W., Yagita, H. & Allison, J. P. 2010. PD-1 and CTLA-4 combination blockade expands infiltrating T cells and reduces regulatory T and myeloid cells within B16 melanoma tumors. *Proc Natl Acad Sci U S A,* 107**,** 4275-80.

Curtsinger, J. M., Lins, D. C. & Mescher, M. F. 2003. Signal 3 determines tolerance versus full activation of naive CD8 T cells: dissociating proliferation and development of effector function. *J Exp Med*, 197, 1141-51.

De Henau, O., Rausch, M., Winkler, D., Campesato, L. F., Liu, C., Cymerman, D. H., Budhu, S., Ghosh, A., Pink, M., Tchaicha, J.*, et al.* 2016. Overcoming resistance to checkpoint blockade therapy by targeting PI3Kgamma in myeloid cells. *Nature,* 539**,** 443-447.

Del Campo, A. B., Kyte, J. A., Carretero, J., Zinchencko, S., Méndez, R., González-Aseguinolaza, G., Ruiz-Cabello, F., Aamdal, S., Gaudernack, G. & Garrido, F. 2014. Immune escape of cancer cells with beta2-microglobulin loss over the course of metastatic melanoma. *Int J Cancer.*, 134, 102-113.

Dersh, D., Phelan, J. D., Gumina, M. E., Wang, B., Arbuckle, J. H., Holly, J., Kishton, R. J., Markowitz, T. E., Seedhom, M. O., Fridlyand, N.*, et al.* 2021. Genome-wide Screens Identify Lineage- and Tumor-Specific Genes Modulating MHC-I- and MHC-II-Restricted Immunosurveillance of Human Lymphomas. *Immunity,* 54**,** 116-131 e10.

Dobin, A., Davis, C. A., Schlesinger, F., Drenkow, J., Zaleski, C., Jha, S., Batut, P., Chaisson, M. & Gingeras, T. R. 2013. STAR: ultrafast universal RNA-seq aligner. *Bioinformatics*, 29, 15-21.

Duong, E., Fessenden, T. B., Lutz, E., Dinter, T., Yim, L., Blatt, S., Bhutkar, A., Wittrup, K. D. & Spranger, S. 2022. Type I interferon activates MHC class I-dressed CD11b(+) conventional dendritic cells to promote protective anti-tumor CD8(+)

T cell immunity. *Immunity*, 55, 308-323 e9.

Faustino-Rocha, A., Oliveira, P. A., Pinho-Oliveira, J., Teixeira-Guedes, C., Soares-Maia, R., Da Costa, R. G., Colaco, B., Pires, M. J., Colaco, J., Ferreira, R., et al. 2013. Estimation of rat mammary tumor volume using caliper and ultrasonography measurements. *Lab Anim (NY)*, 42, 217-24.

Freeman, A. J., Vervoort, S. J., Ramsbottom, K. M., Kelly, M. J., Michie, J., Pijpers, L., Johnstone, R. W., Kearney, C. J. & Oliaro, J. 2019. Natural Killer Cells Suppress T Cell-Associated Tumor Immune Evasion. *Cell Rep,* 28, 2784-2794 e5.

Fridman, W. H., Pages, F., Sautes-Fridman, C. & Galon, J. 2012. The immune contexture in human tumours: impact on clinical outcome. *Nat Rev Cancer,* 12**,** 298-306.

Fu, C. & Jiang, A. 2018. Dendritic Cells and CD8 T Cell Immunity in Tumor Microenvironment. *Front Immunol,* 9**,** 3059.

Fu, J., Li, K., Zhang, W., Wan, C., Zhang, J., Jiang, P. & Liu, X. S. 2020. Large-scale public data reuse to model immunotherapy response and resistance. *Genome Med*, 12, 21.

Galon, J., Costes, A., Sanchez-Cabo, F., Kirilovsky, A., Mlecnik, B., Lagorce-Pages, C., Tosolini, M., Camus, M., Berger, A., Wind, P., et al. 2006. Type, density, and location of immune cells within human colorectal tumors predict clinical outcome. *Science*, 313, 1960-4.

Galon, J., Pages, F., Marincola, F. M., Angell, H. K., Thurin, M., Lugli, A., Zlobec, I., Berger, A., Bifulco, C., Botti, G.*, et al.* 2012. Cancer classification using the Immunoscore: a worldwide task force. *J Transl Med,* 10**,** 205.

Gao, W., Zhang, X., Yang, W., Dou, D., Zhang, H., Tang, Y., Zhong, W., Meng, J., Bai, Y., Liu, Y.*, et al.* 2019. Prim-O-glucosylcimifugin enhances the antitumour effect of PD-1 inhibition by targeting myeloid-derived suppressor cells. *J Immunother Cancer,* 7**,** 231.

Garcia‐Lora, A., Algarra, I., Gaforio, J. J., Ruiz‐Cabello, F. & Garrido, F. 2001. Immunoselection by T lymphocytes generates repeated MHC class I‐deficient metastatic tumor variants. *Int J Cancer.*, 91, 109-119.

Gettinger, S., Choi, J., Hastings, K., Truini, A., Datar, I., Sowell, R., Wurtz, A., Dong, W., Cai, G. & Melnick, M. 2017. Impaired HLA Class I Antigen Processing and Presentation as a Mechanism of Acquired Resistance to Immune Checkpoint Inhibitors in Lung CancerAntigen-Processing Defects and Resistance to PD-1 Blockade. *Cancer Discov.*, 7, 1420-1435.

Gide, T. N., Quek, C., Menzies, A. M., Tasker, A. T., Shang, P., Holst, J., Madore, J., Lim, S. Y., Velickovic, R., Wongchenko, M.*, et al.* 2019a. Distinct Immune Cell Populations Define Response to Anti-PD-1 Monotherapy and Anti-PD-1/Anti-CTLA-4 Combined Therapy. *Cancer Cell,* 35**,** 238-255 e6.

Gide, T. N., Quek, C., Menzies, A. M., Tasker, A. T., Shang, P., Holst, J., Madore, J., Lim, S. Y., Velickovic, R., Wongchenko, M.*, et al.* 2019b. Distinct Immune Cell Populations Define Response to Anti-PD-1 Monotherapy and Anti-PD-1/Anti-

CTLA-4 Combined Therapy. *Cancer Cell,* 35**,** 238-255.e6.

Goldman, M. J., Craft, B., Hastie, M., Repecka, K., Mcdade, F., Kamath, A., Banerjee, A., Luo, Y., Rogers, D., Brooks, A. N.*, et al.* 2020. Visualizing and interpreting cancer genomics data via the Xena platform. *Nat Biotechnol,* 38**,** 675-678.

Gu, S. S., Zhang, W., Wang, X., Jiang, P., Traugh, N., Li, Z., Meyer, C., Stewig, B., Xie, Y., Bu, X.*, et al.* 2021. Therapeutically Increasing MHC-I Expression Potentiates Immune Checkpoint Blockade. *Cancer Discov,* 11**,** 1524-1541.

Hanzawa, N., Hashimoto, K., Yuan, X., Kawahori, K., Tsujimoto, K., Hamaguchi, M., Tanaka, T., Nagaoka, Y., Nishina, H., Morita, S.*, et al.* 2020. Targeted DNA demethylation of the Fgf21 promoter by CRISPR/dCas9-mediated epigenome editing. *Sci Rep,* 10**,** 5181.

Hugo, W., Zaretsky, J. M., Sun, L., Song, C., Moreno, B. H., Hu-Lieskovan, S., Berent-Maoz, B., Pang, J., Chmielowski, B., Cherry, G.*, et al.* 2016. Genomic and Transcriptomic Features of Response to Anti-PD-1 Therapy in Metastatic Melanoma. *Cell,* 165**,** 35-44.

Iwai, Y., Terawaki, S. & Honjo, T. 2005. PD-1 blockade inhibits hematogenous spread of poorly immunogenic tumor cells by enhanced recruitment of effector T cells. *Int Immunol,* 17**,** 133-44.

Jhunjhunwala, S., Hammer, C. & Delamarre, L. 2021. Antigen presentation in cancer: insights into tumour immunogenicity and immune evasion. *Nat Rev Cancer,* 21**,** 298-312.

Johnson, K. C., Houseman, E. A., King, J. E. & Christensen, B. C. 2017. Normal breast tissue DNA methylation differences at regulatory elements are associated with the cancer risk factor age. *Breast Cancer Res,* 19**,** 81.

Jorgovanovic, D., Song, M. J., Wang, L. P. & Zhang, Y. 2020. Roles of IFN-gamma in tumor progression and regression: a review. *Biomarker Research,* 8**,** 1-16.

Kalbasi, A. & Ribas, A. 2020a. Tumour-intrinsic resistance to immune checkpoint blockade. *Nat Rev Immunol,* 20**,** 25-39.

Kalbasi, A., Tariveranmoshabad, M., Hakimi, K., Kremer, S., Campbell, K. M., Funes, J. M., Vega-Crespo, A., Parisi, G., Champekar, A., Nguyen, C.*, et al.* 2020b. Uncoupling interferon signaling and antigen presentation to overcome immunotherapy resistance due to JAK1 loss in melanoma. *Sci Transl Med,* 12**,** eabb0152.

Konermann, S., Brigham, M. D., Trevino, A. E., Joung, J., Abudayyeh, O. O., Barcena, C., Hsu, P. D., Habib, N., Gootenberg, J. S., Nishimasu, H.*, et al.* 2015. Genome-scale transcriptional activation by an engineered CRISPR-Cas9 complex. *Nature,* 517**,** 583-8.

Kuhn, M. 2015. Caret: classification and regression training. ascl: 1505.003.

Le, D. T., Durham, J. N., Smith, K. N., Wang, H., Bartlett, B. R., Aulakh, L. K., Lu, S., Kemberling, H., Wilt, C., Luber, B. S.*, et al.* 2017. Mismatch repair deficiency predicts response of solid tumors to PD-1 blockade. *Science,* 357**,** 409-413.

Le Naour, A., Rossary, A. & Vasson, M. P. 2020. EO771, is it a well-characterized cell

line for mouse mammary cancer model? Limit and uncertainty. *Cancer Med,* 9**,** 8074-8085.

Leinonen, R., Sugawara, H., Shumway, M. & International Nucleotide Sequence Database, C. 2011. The sequence read archive. *Nucleic Acids Res,* 39**,** D19-21.

Li, B., Severson, E., Pignon, J. C., Zhao, H., Li, T., Novak, J., Jiang, P., Shen, H., Aster, J. C., Rodig, S.*, et al.* 2016. Comprehensive analyses of tumor immunity: implications for cancer immunotherapy. *Genome Biol,* 17**,** 174.

Li, F., Li, C., Cai, X., Xie, Z., Zhou, L., Cheng, B., Zhong, R., Xiong, S., Li, J., Chen, Z.*, et al.* 2021. The association between CD8+ tumor-infiltrating lymphocytes and the clinical outcome of cancer immunotherapy: A systematic review and meta-analysis. *EClinicalMedicine,* 41**,** 101134.

Liu, D., Schilling, B., Liu, D., Sucker, A., Livingstone, E., Jerby-Arnon, L., Zimmer, L., Gutzmer, R., Satzger, I., Loquai, C.*, et al.* 2019. Integrative molecular and clinical modeling of clinical outcomes to PD1 blockade in patients with metastatic melanoma. *Nat Med,* 25**,** 1916-1927.

Liu, X. S., Wu, H., Ji, X., Stelzer, Y., Wu, X., Czauderna, S., Shu, J., Dadon, D., Young, R. A. & Jaenisch, R. 2016. Editing DNA Methylation in the Mammalian Genome. *Cell,* 167**,** 233-247 e17.

Liu, X. S., Wu, H., Krzisch, M., Wu, X., Graef, J., Muffat, J., Hnisz, D., Li, C. H., Yuan, B., Xu, C.*, et al.* 2018. Rescue of Fragile X Syndrome Neurons by DNA Methylation Editing of the *FMR1* Gene. *Cell,* 172**,** 979-992 e6.

Love, M. I., Huber, W. & Anders, S. 2014. Moderated estimation of fold change and dispersion for RNA-seq data with DESeq2. *Genome Biol,* 15**,** 550.

Luo, N., Nixon, M. J., Gonzalez-Ericsson, P. I., Sanchez, V., Opalenik, S. R., Li, H., Zahnow, C. A., Nickels, M. L., Liu, F., Tantawy, M. N.*, et al.* 2018. DNA methyltransferase inhibition upregulates MHC-I to potentiate cytotoxic T lymphocyte responses in breast cancer. *Nat Commun,* 9**,** 248.

Macnabb, B. W., Tumuluru, S., Chen, X., Godfrey, J., Kasal, D. N., Yu, J., Jongsma, M. L. M., Spaapen, R. M., Kline, D. E. & Kline, J. 2022. Dendritic cells can prime anti-tumor CD8(+) T cell responses through major histocompatibility complex cross-dressing. *Immunity,* 55**,** 982-997 e8.

Manguso, R. T., Pope, H. W., Zimmer, M. D., Brown, F. D., Yates, K. B., Miller, B. C., Collins, N. B., Bi, K., Lafleur, M. W., Juneja, V. R.*, et al.* 2017. In vivo CRISPR screening identifies Ptpn2 as a cancer immunotherapy target. *Nature,* 547**,** 413-418.

Meissner, T. B., Li, A., Biswas, A., Lee, K. H., Liu, Y. J., Bayir, E., Iliopoulos, D., Van Den Elsen, P. J. & Kobayashi, K. S. 2010. NLR family member NLRC5 is a transcriptional regulator of MHC class I genes. *Proc Natl Acad Sci U S A,* 107**,** 13794-9.

Meng, X., Liu, X., Guo, X., Jiang, S., Chen, T., Hu, Z., Liu, H., Bai, Y., Xue, M., Hu, R.*, et al.* 2018. FBXO38 mediates PD-1 ubiquitination and regulates anti-tumour immunity of T cells. *Nature,* 564**,** 130-135.

Miao, D., Margolis, C. A., Gao, W., Voss, M. H., Li, W., Martini, D. J., Norton, C., Bosse, D., Wankowicz, S. M., Cullen, D., *et al.* 2018. Genomic correlates of response to immune checkpoint therapies in clear cell renal cell carcinoma. *Science,* 359**,** 801-806.

Miguel-Escalada, I., Bonas-Guarch, S., Cebola, I., Ponsa-Cobas, J., Mendieta-Esteban, J., Atla, G., Javierre, B. M., Rolando, D. M. Y., Farabella, I., Morgan, C. C., *et al.* 2019. Human pancreatic islet three-dimensional chromatin architecture provides insights into the genetics of type 2 diabetes. *Nat Genet,* 51**,** 1137-1148.

Mlecnik, B., Bindea, G., Angell, H. K., Maby, P., Angelova, M., Tougeron, D., Church, S. E., Lafontaine, L., Fischer, M., Fredriksen, T., *et al.* 2016. Integrative Analyses of Colorectal Cancer Show Immunoscore Is a Stronger Predictor of Patient Survival Than Microsatellite Instability. *Immunity,* 44**,** 698-711.

Moderna. *An Efficacy Study of Adjuvant Treatment With the Personalized Cancer Vaccine mRNA-4157 and Pembrolizumab in Participants With High-Risk Melanoma (KEYNOTE-942)*. https://ClinicalTrials.gov/show/NCT03897881 [Accessed 2023/07/03].

Moretta, L., Bottino, C., Pende, D., Vitale, M., Mingari, M. C. & Moretta, A. 2004. Different checkpoints in human NK-cell activation. *Trends Immunol,* 25**,** 670-6.

Morita, S., Horii, T., Kimura, M. & Hatada, I. 2020. Synergistic Upregulation of Target Genes by TET1 and VP64 in the dCas9–SunTag Platform. *International Journal of Molecular Sciences,* 21**,** 1574.

Nicolet, B. P., Guislain, A., Van Alphen, F. P. J., Gomez-Eerland, R., Schumacher, T. N. M., Van Den Biggelaar, M. & Wolkers, M. C. 2020. CD29 identifies IFN-γ–producing human CD8+ T cells with an increased cytotoxic potential. *Proceedings of the National Academy of Sciences,* 117**,** 6686-6696.

Nie, R. C., Yuan, S. Q., Wang, Y., Chen, Y. B., Cai, Y. Y., Chen, S., Li, S. M., Zhou, J., Chen, G. M., Luo, T. Q., *et al.* 2019. Robust immunoscore model to predict the response to anti-PD1 therapy in melanoma. *Aging (Albany NY),* 11**,** 11576-11590.

Noguchi, S., Mori, T., Igase, M. & Mizuno, T. 2015. A novel apoptosis-inducing mechanism of 5-aza-2'-deoxycitidine in melanoma cells: Demethylation of TNF-alpha and activation of FOXO1. *Cancer Lett,* 369**,** 344-53.

Nunez, J. K., Chen, J., Pommier, G. C., Cogan, J. Z., Replogle, J. M., Adriaens, C., Ramadoss, G. N., Shi, Q., Hung, K. L., Samelson, A. J., *et al.* 2021. Genome-wide programmable transcriptional memory by CRISPR-based epigenome editing. *Cell,* 184**,** 2503-2519 e17.

Pages, F., Mlecnik, B., Marliot, F., Bindea, G., Ou, F. S., Bifulco, C., Lugli, A., Zlobec, I., Rau, T. T., Berger, M. D., *et al.* 2018. International validation of the consensus Immunoscore for the classification of colon cancer: a prognostic and accuracy study. *Lancet,* 391**,** 2128-2139.

Pan, D., Kobayashi, A., Jiang, P., Ferrari De Andrade, L., Tay, R. E., Luoma, A. M., Tsoucas, D., Qiu, X., Lim, K. & Rao, P. J. S. 2018. A major chromatin regulator

determines resistance of tumor cells to T cell–mediated killing. *Science.,* 359**,** 770-775.

Pardoll, D. M. 2012. The blockade of immune checkpoints in cancer immunotherapy. *Nat Rev Cancer,* 12**,** 252-64.

Patro, R., Duggal, G., Love, M. I., Irizarry, R. A. & Kingsford, C. 2017. Salmon provides fast and bias-aware quantification of transcript expression. *Nat Methods,* 14**,** 417-419.

Pi, C., Jing, P., Li, B., Feng, Y., Xu, L., Xie, K., Huang, T., Xu, X., Gu, H. & Fang, J. 2022. Reversing PD-1 Resistance in B16F10 Cells and Recovering Tumour Immunity Using a COX2 Inhibitor. *Cancers (Basel),* 14(17):4134.

Postow, M. A., Callahan, M. K. & Wolchok, J. D. 2015. Immune Checkpoint Blockade in Cancer Therapy. *J Clin Oncol,* 33**,** 1974-82.

Qi, J., Liu, X., Yan, P., He, S., Lin, Y., Huang, Z., Zhang, S., Xie, S., Li, Y., Lu, X.*, et al.* 2021. Analysis of Immune Landscape Reveals Prognostic Significance of Cytotoxic CD4(+) T Cells in the Central Region of pMMR CRC. *Front Oncol,* 11**,** 724232.

Ran, F. A., Hsu, P. D., Wright, J., Agarwala, V., Scott, D. A. & Zhang, F. 2013. Genome engineering using the CRISPR-Cas9 system. *Nat Protoc,* 8**,** 2281-2308.

Ray-Gallet, D., Ricketts, M. D., Sato, Y., Gupta, K., Boyarchuk, E., Senda, T., Marmorstein, R. & Almouzni, G. 2018. Functional activity of the H3.3 histone chaperone complex HIRA requires trimerization of the HIRA subunit. *Nat Commun,* 9**,** 3103.

Riaz, N., Havel, J. J., Makarov, V., Desrichard, A., Urba, W. J., Sims, J. S., Hodi, F. S., Martin-Algarra, S., Mandal, R., Sharfman, W. H.*, et al.* 2017. Tumor and Microenvironment Evolution during Immunotherapy with Nivolumab. *Cell,* 171**,** 934-949 e16.

Robbins, G. R., Truax, A. D., Davis, B. K., Zhang, L., Brickey, W. J. & Ting, J. P. 2012. Regulation of class I major histocompatibility complex (MHC) by nucleotide-binding domain, leucine-rich repeat-containing (NLR) proteins. *J Biol Chem,* 287**,** 24294-303.

Rodig, S. J., Gusenleitner, D., Jackson, D. G., Gjini, E., Giobbie-Hurder, A., Jin, C., Chang, H., Lovitch, S. B., Horak, C., Weber, J. S.*, et al.* 2018. MHC proteins confer differential sensitivity to CTLA-4 and PD-1 blockade in untreated metastatic melanoma. *Sci Transl Med,* 10**,** eaar3342.

Rodriguez, G. M., Bobbala, D., Serrano, D., Mayhue, M., Champagne, A., Saucier, C., Steimle, V., Kufer, T. A., Menendez, A., Ramanathan, S.*, et al.* 2016. NLRC5 elicits antitumor immunity by enhancing processing and presentation of tumor antigens to CD8(+) T lymphocytes. *Oncoimmunology,* 5**,** e1151593.

Sade-Feldman, M., Jiao, Y. J., Chen, J. H., Rooney, M. S., Barzily-Rokni, M., Eliane, J. P., Bjorgaard, S. L., Hammond, M. R., Vitzthum, H., Blackmon, S. M.*, et al.* 2017. Resistance to checkpoint blockade therapy through inactivation of antigen presentation. *Nat Commun,* 8**,** 1136.

Salio, M., Cerundolo, V. & Lanzavecchia, A. 2000. Dendritic cell maturation is induced by mycoplasma infection but not by necrotic cells. *Eur J Immunol,* 30**,** 705-8.

Schneider, C. A., Rasband, W. S. & Eliceiri, K. W. 2012. NIH Image to ImageJ: 25 years of image analysis. *Nat Methods,* 9**,** 671-5.

Sharma, P. & Allison, J. P. 2015. The future of immune checkpoint therapy. *Science,* 348**,** 56-61.

Shoemaker, R. H. 2006. The NCI60 human tumour cell line anticancer drug screen. *Nat Rev Cancer,* 6**,** 813-23.

Soneson, C., Love, M. I. & Robinson, M. D. 2015. Differential analyses for RNA-seq: transcript-level estimates improve gene-level inferences. *F1000Res,* 4**,** 1521.

Staehli, F., Ludigs, K., Heinz, L. X., Seguin-Estevez, Q., Ferrero, I., Braun, M., Schroder, K., Rebsamen, M., Tardivel, A., Mattmann, C*., et al.* 2012. NLRC5 deficiency selectively impairs MHC class I- dependent lymphocyte killing by cytotoxic T cells. *J Immunol,* 188**,** 3820-8.

Subramanian, A., Tamayo, P., Mootha, V. K., Mukherjee, S., Ebert, B. L., Gillette, M. A., Paulovich, A., Pomeroy, S. L., Golub, T. R., Lander, E. S*., et al.* 2005. Gene set enrichment analysis: a knowledge-based approach for interpreting genome-wide expression profiles. *Proc Natl Acad Sci U S A,* 102**,** 15545-50.

Swart, M., Verbrugge, I. & Beltman, J. B. 2016. Combination Approaches with Immune-Checkpoint Blockade in Cancer Therapy. *Front Oncol,* 6**,** 233.

Taefehshokr, N., Baradaran, B., Baghbanzadeh, A. & Taefehshokr, S. 2020. Promising approaches in cancer immunotherapy. *Immunobiology,* 225**,** 151875.

Tin Kam, H. Random decision forests. Proceedings of 3rd International Conference on Document Analysis and Recognition, 14-16 Aug. 1995 1995. 278-282 vol.1.

Tomayko, M. M. & Reynolds, C. P. 1989. Determination of subcutaneous tumor size in athymic (nude) mice. *Cancer Chemother Pharmacol,* 24**,** 148-54.

Topham, D. J. & Reilly, E. C. 2018. Tissue-Resident Memory CD8(+) T Cells: From Phenotype to Function. *Front Immunol,* 9**,** 515.

Vandiver, A. R., Irizarry, R. A., Hansen, K. D., Garza, L. A., Runarsson, A., Li, X., Chien, A. L., Wang, T. S., Leung, S. G., Kang, S*., et al.* 2015. Age and sun exposure-related widespread genomic blocks of hypomethylation in nonmalignant skin. *Genome Biol,* 16**,** 80.

Wang, J., Saffold, S., Cao, X., Krauss, J. & Chen, W. 1998. Eliciting T Cell Immunity Against Poorly Immunogenic Tumors by Immunization with Dendritic Cell-Tumor Fusion Vaccines1. *The Journal of Immunology,* 161**,** 5516-5524.

Wang, Q., Dai, L., Wang, Y., Deng, J., Lin, Y., Wang, Q., Fang, C., Ma, Z., Wang, H., Shi, G*., et al.* 2019. Targeted demethylation of the SARI promotor impairs colon tumour growth. *Cancer Lett,* 448**,** 132-143.

Xu, X., Tao, Y., Gao, X., Zhang, L., Li, X., Zou, W., Ruan, K., Wang, F., Xu, G. L. & Hu, R. 2016. A CRISPR-based approach for targeted DNA demethylation. *Cell Discov,* 2**,** 16009.

Yamazaki, T., Akiba, H., Koyanagi, A., Azuma, M., Yagita, H. & Okumura, K. J. T. J.

O. I. 2005. Blockade of B7-H1 on macrophages suppresses CD4+ T cell proliferation by augmenting IFN-γ-induced nitric oxide production. *J Immunol.,* 175**,** 1586-1592.

Yao, Y., Wang, Y., Chen, F., Huang, Y., Zhu, S., Leng, Q., Wang, H., Shi, Y. & Qian, Y. 2012. NLRC5 regulates MHC class I antigen presentation in host defense against intracellular pathogens. *Cell Res,* 22**,** 836-47.

Yoo, J. S., Sasaki, M., Cho, S. X., Kasuga, Y., Zhu, B., Ouda, R., Orba, Y., De Figueiredo, P., Sawa, H. & Kobayashi, K. S. 2021. SARS-CoV-2 inhibits induction of the MHC class I pathway by targeting the STAT1-IRF1-NLRC5 axis. *Nat Commun,* 12**,** 6602.

Yoshihama, S., Cho, S. X., Yeung, J., Pan, X., Lizee, G., Konganti, K., Johnson, V. E. & Kobayashi, K. S. 2021. NLRC5/CITA expression correlates with efficient response to checkpoint blockade immunotherapy. *Sci Rep,* 11**,** 3258.

Yoshihama, S., Roszik, J., Downs, I., Meissner, T. B., Vijayan, S., Chapuy, B., Sidiq, T., Shipp, M. A., Lizee, G. A. & Kobayashi, K. S. 2016. NLRC5/MHC class I transactivator is a target for immune evasion in cancer. *Proc Natl Acad Sci U S A,* 113**,** 5999-6004.

Yu, G., Wang, L. G., Han, Y. & He, Q. Y. 2012. clusterProfiler: an R package for comparing biological themes among gene clusters. *OMICS,* 16**,** 284-7.

Zagorulya, M. & Spranger, S. 2023. Once upon a prime: DCs shape cancer immunity. *Trends Cancer,* 9**,** 172-184.

Zaretsky, J. M., Garcia-Diaz, A., Shin, D. S., Escuin-Ordinas, H., Hugo, W., Hu-Lieskovan, S., Torrejon, D. Y., Abril-Rodriguez, G., Sandoval, S., Barthly, L., *et al.* 2016. Mutations Associated with Acquired Resistance to PD-1 Blockade in Melanoma. *N Engl J Med,* 375**,** 819-29.

Zhan, L., Zhang, J., Zhang, J., Liu, X., Zhu, S., Shi, Y., He, Y., Wang, W., Fan, Y., Tang, Z., *et al.* 2022. LC3 and NLRC5 interaction inhibits NLRC5-mediated MHC class I antigen presentation pathway in endometrial cancer. *Cancer Lett,* 529**,** 37-52.

Zhang, Y., Werling, U. & Edelmann, W. 2012. SLiCE: a novel bacterial cell extract-based DNA cloning method. *Nucleic Acids Res,* 40**,** e55.

Zhao, Z., Fang, L., Xiao, P., Sun, X., Zhou, L., Liu, X., Wang, J., Wang, G., Cao, H., Zhang, P., *et al.* 2022. Walking Dead Tumor Cells for Targeted Drug Delivery Against Lung Metastasis of Triple-Negative Breast Cancer. *Adv Mater,* 34**,** e2205462.